The Institute of Paper Chemistry

Appleton, Wisconsin

Doctor's Dissertation

Cell Wall Sulfur Distribution in Sulfonated Southern Pine Latewood

Thomas Edward Heazel

January 11, 1988

CELL WALL SULFUR DISTRIBUTION IN SULFONATED SOUTHERN PINE LATEWOOD

A Ph.D. thesis submitted by

Thomas Edward Heazel

B.S. 1981, Virginia Polytechnic Institute and State University

M.S. 1983, Lawrence University

in partial fulfillment of the requirements
of the Institute of Paper Chemistry
for the degree of Doctor of Philosophy
from Lawrence University,
Appleton, Wisconsin

January 11, 1988

CONTENTS

SUMMARY

In recent years, numerous studies have evaluated wood sulfonation and high-yield sulfite pulping. These studies have raised some intriguing questions concerning the distribution of bound sulfite across the fiber (cell) walls in sulfonated wood and the influence the distribution may have on pulp properties. This study has evaluated the influence of treatment variables on cell wall sulfur distribution in sulfonated southern pine.

Latewood chips were sulfonated under a variety of conditions. Sulfonation variables included sodium sulfite concentration, temperature, time at temperature, liquor pH, and type of cook. The two types of cooks tested were conventional liquid-phase cooks at a 10:1 liquor-to-wood ratio and so called vapor-phase cooks. Cell wall sulfur distributions in the sulfonated chips were evaluated by STEM-EDS.

The STEM-EDS data revealed cell wall sulfur distributions with two basic features: a pronounced middle lamella peak, due to higher lignin levels there, and a gradient across the secondary wall. This gradient was characterized by higher sulfur levels toward the lumen and lower levels toward the middle lamella. The results from a statistical analysis of the linescan data suggest this gradient is influenced by liquor pH and sodium sulfite concentration. Mass loss from the samples during the STEM-EDS analysis was also investigated.

An investigation into possible sources of this secondary wall gradient revealed that these gradients could be attributed to lignin distribution and limited diffusion across the cell wall. Lignin distribution in representative samples was evaluated using UV microscopy. As with the sulfur distributions, the lignin distributions had a pronounced peak in the middle lamella. The

observed lignin distributions across the secondary wall were generally flat with frequent peaks in the S3 layer. These higher lignin levels in the S3 layer may account for some of the nonuniformity in secondary wall sulfonation, but certainly cannot account for the observed S2 sulfur gradients. Mathematical modeling of sodium sulfite diffusion across the cell wall produced secondary wall sulfur gradients similar to those observed using STEM-EDS. The diffusivities used for the modeling were derived from current knowledge of cell wall structure and diffusion in porous solids.

INTRODUCTION

In recent years, the pulp and paper industry has been actively evaluating the use of chemical treatments in mechanical pulping. Pulps produced by processes incorporating such treatments are called chemimechanical pulps (CMP) or, if produced in pressurized refiners, chemithermomechanical pulps (CTMP). Their non-treated counterparts are refiner mechanical pulps (RMP) and thermomechanical pulps (TMP), respectively. CMP and CTMP are high yield pulps with properties which lie between those of mechanical and chemical pulps. These unique properties make the pulp a suitable replacement for kraft pulp in a number of paper grades, including newsprint and other printing papers. In addition to enhancing other properties, CMP and CTMP can often provide adequate strength properties while the higher yields reduce wood requirements.

The chemical treatment in CMP and CTMP production can be performed at several different stages in a number of different forms. The treatment can be applied to the refined fibers, the chips, or the fiberized chips between refining stages. The choices for chemical treatment cover the entire pH scale and include alkaline peroxide, kraft liquor, cold soda, ozone, sodium chlorite, sodium bisulfite, and sodium sulfite. Among the choices for timing and type of chemical treatment, pretreatment of chips with neutral to alkaline sodium sulfite is the most popular.

The effectiveness of sulfite pretreatment does not depend on its ability to delignify the wood, but rather on the manner in which it modifies the lignin that remains in the fiber walls. During sulfite treatment, the lignin is sulfonated, resulting in the formation of lignosulfonic acid groups and in some lignin fragmentation. The sulfonated lignin is more hydrophilic and the lignin structure is looser, so the fibers swell and conform more readily than in

refiner mechanical pulps (RMP). The fibers are also less damaged than those in RMP.

These effects on pulp properties can be controlled by varying the degree of sulfonation, or sulfur content, of the pulp. Numerous studies have investigated the effects of sulfur content and the process variables which influence sulfur content on pulp properties. One intriguing question which has arisen from this work is the possibility of manipulating pulp properties through control of the bound sulfur (sulfite or sulfonic acid group) distribution across the cell wall. The intent of this thesis has been to pursue this question by evaluating the effects of various sulfonation variables on cell wall sulfur distribution.

BACKGROUND

The following discussion reviews current knowledge on sulfonation and sulfur distribution. Although this thesis is primarily concerned with cell wall sulfur distribution, an understanding of sulfonation in general can serve as a foundation on which an understanding of the sources and effects of cell wall sulfur distribution can be built. For the purposes of this work, the term, sulfur distribution, will refer to the distribution of bound sulfite or sulfonic acid groups across the cell walls or fiber walls in sulfonated wood or pulp.

In addition to sulfonation and cell wall sulfur distribution, this discussion reviews vapor-phase cooks, STEM-EDS operating principles, and the determination of lignin distribution by UV microscopy.

SULFONATION REACTIONS

In sulfite pulping, the reactive species varies with pH. Under alkaline conditions, the sulfite ion ($SO_3^=$) predominates. Under mildly acidic conditions, the bisulfite ion (HSO_3^-) predominates, and as the liquor becomes extremely acidic, the bisulfite ion begins to take the form of dissolved SO_2. In sulfite pulping, two of these species are generally present at once. In order to simplify the discussions in this thesis, these species will be referred to as sulfite under alkaline conditions, bisulfite under acidic conditions, and sulfite in a general context.

The reactions of sulfite with lignin have been reviewed by several workers (1,2). The reactions that occur are numerous due to the variety of linkages between lignin monomeric units. The linkages which are most important

in pulping reactions and their relative occurrences are shown in Figure 1. Among these, the α-aryl ether structures (A) are the most common.

In α-aryl ether structures, sulfonation at neutral and alkaline pH levels involves cleavage of an α-hydroxyl or α-ether group to form a quinone methide. This scheme is shown in Figure 2. The α-carbon then undergoes nucleophilic attack by the sulfite or bisulfite ion to form an α-sulfonic acid group. Because a quinone methide intermediate is required, sulfonation of most lignin units under neutral conditions will only occur on phenolic units. At pH levels below or equal pH 7, these α-sulfonic acids are the primary sulfonation

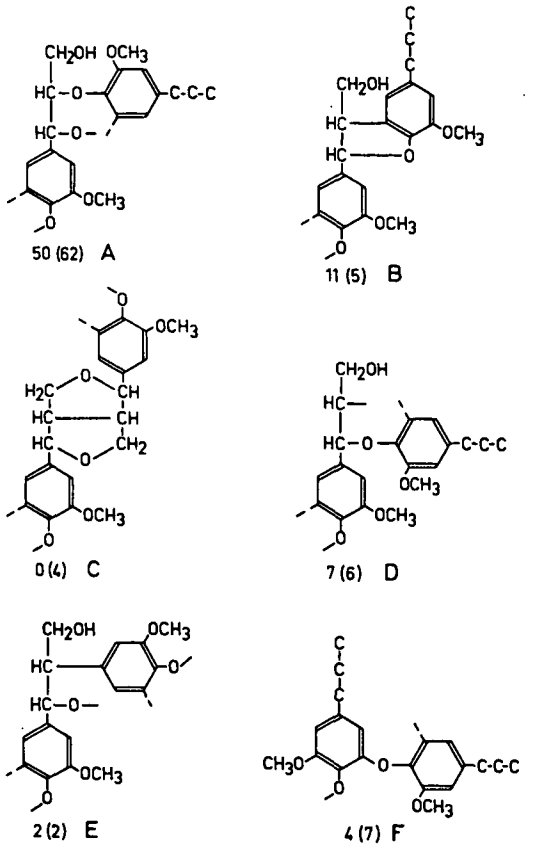

Figure 1. Linkages important in pulping reactions and their relative occurrences in the lignin. Numbers outside ( ) are for spruce. Numbers inside ( ) are for birch. From reference (1).

products obtained from α-aryl ether structures (3). At these pH levels, these α-sulfonic acids undergo β-aryl ether cleavage at a very slow rate. This will result in the formation of α-β-disulfonic acids. The mechanism for α-ether cleavage is believed to be a sulfitolytic cleavage (S_N2 mechanism) facilitated by electron-withdrawal by the α-sulfonic acid (3); however, other mechanisms may be involved since electron withdrawal is not believed to influence S_N2 reactions (4). Once formed, the disulfonic acid can react further to form other products including styrene-β-sulfonic acid structures.

In α-aryl ether structures, slight increases above pH 7 allow elimination reactions to compete favorably with sulfonation. The elimination of formaldehyde and, at even higher pH levels, water from the side chain leaves conjugated structures which are readily sulfonated. This results in

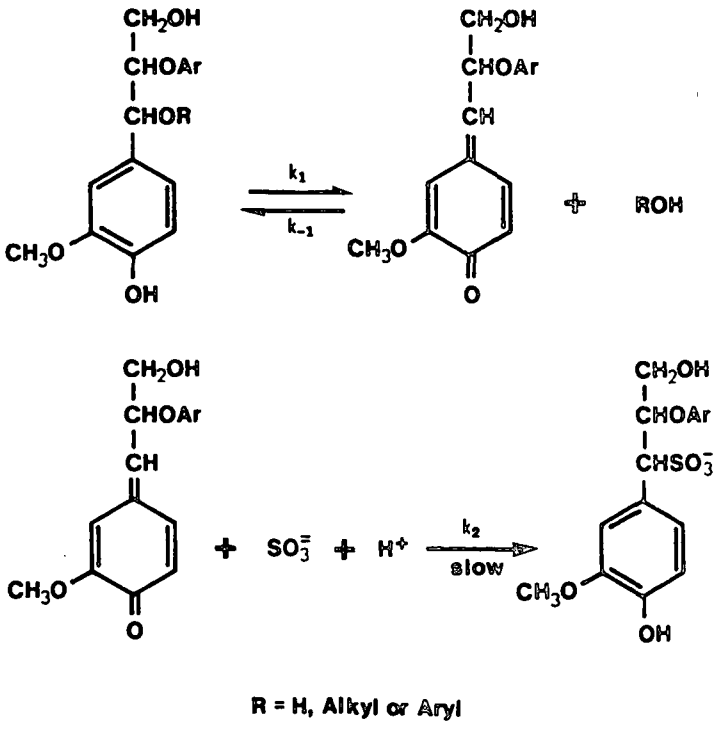

Figure 2. α-carbon sulfonation under alkaline conditions. Adapted from reference (5).

acceleration of α-ether cleavage and disulfonic acid formation. Elimination of water from the side chain will also result in sulfonation of γ carbons and subsequent trisulfonic acid formation. Under neutral to alkaline conditions, structures B through E in Figure 1 undergo sulfonation at the α and γ carbons through a quinone methide or other conjugated intermediate (1,2). Many of the pathways are similar to those observed in the α-aryl ether structures.

At neutral and alkaline pH levels, sulfonation also occurs in oxidized side chains. These reactions are not necessarily restricted to phenolic units (1). Sulfonation of a non-phenolic phenylpropane unit with an α-carbonyl and β-aryl ether is shown in Figure 3. The elimination reactions involved are very similar to those leading to β-carbon sulfonation in phenolic units. In the non-phenolic unit, the α-carbonyl is believed to facilitate sulfitolytic cleavage at the β-carbon in the same manner as the α-sulfonic acid group in the phenolic units (1).

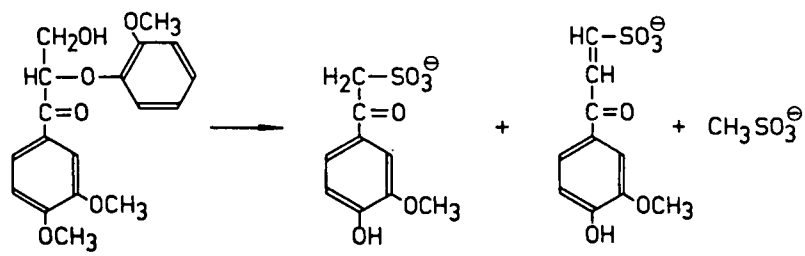

Figure 3. Sulfonation in a non-phenolic lignin with an α-carbonyl. From reference (1).

When the liquor pH is highly alkaline, the nature of the sulfonation differs from that under milder conditions. As with neutral sulfite pulping, the reactions of alkaline sulfite pulping involve nucleophilic displacement leading to sulfonation and fragmentation. Unlike neutral sulfite, alkaline sulfite conditions have two principle nucleophiles, hydroxyl and sulfite ions. These conditions allow attack of non-phenolic as well as phenolic lignin units (1). The exact nature of the sulfonation reactions is not as well understood as those which occur under neutral conditions. In addition to sulfonation, it is believed that ionization of lignin phenolates occurs (1,6). This reduces the number of hydrogen bonds and loosens the lignin structure.

Below a pH of around 5, a different mechanism for α-sulfonic acid formation prevails. As shown in Figure 4, α-carbon sulfonation occurs through a resonance-stabilized benzylium ion, which can form in phenolic and non-phenolic units (1,5). Lignin units containing carbonyls can also undergo sulfonation via a benzylium ion intermediate. Above pH 5, the quinone methide and other neutral pH mechanisms become more prevalent.

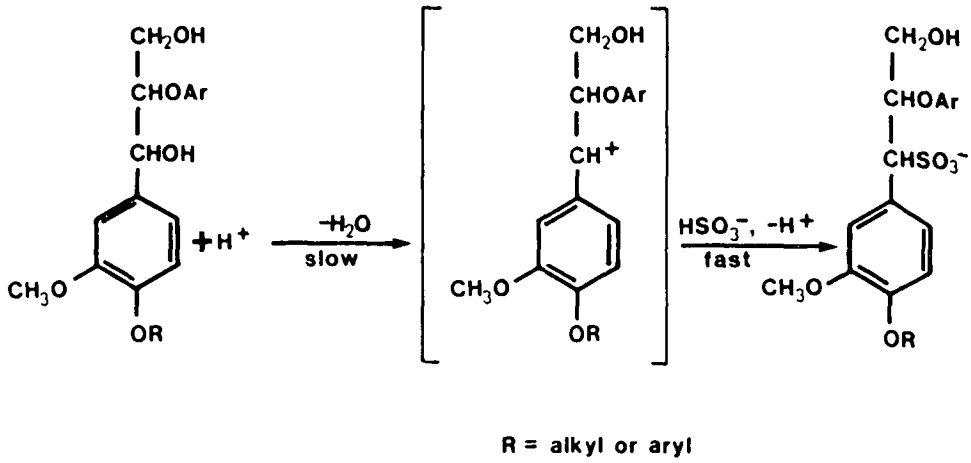

Figure 4. α-carbon sulfonation under acidic conditions. Adapted from reference (5).

SULFONATION KINETICS

At pH 7, the mechanism for α-sulfonic acid formation agrees with the following rate equation (7):

$$\text{Rate of Sulfonation} = \{k_1 k_2 \,/\, (k_{-1} + k_2[SO_3^{=}])\}\ (S_p - S)[SO_3^{=}]^2 \qquad (1)$$

S_p is the maximum obtainable sulfur content and S is the sulfur content at time, t. The rate constants, k_1, k_{-1}, and k_2, are defined in Figure 2. This reaction is first order in $[SO_3^{=}]$ as long as $k_2[SO_3^{=}] \gg k_{-1}$, which is the case at pH 7 (7). If the rate of sulfonation is expressed as:

$$\text{Rate of Sulfonation} = f(S^*) \times [SO_3^{=}]^b \qquad (2)$$

where S^* is the total sulfonate content, Beatson, et al. (5) found the dependence on $SO_3^{=}$ concentration to be to the 0.39 power for bisulfite liquor at pH 4. At pH 7, the dependence was first order, which is in agreement with the first rate equation (5).

EFFECTS OF SULFONATION ON PULP PROPERTIES

Below its glass transition temperature (T_g), lignin in the cell wall has a considerable influence on the properties of high-yield pulps. Anything that softens the lignin will soften the fiber walls and will influence wood and pulp properties. Lignin softening during sulfonation represents two phenomena:

1. Fragmentation of the lignin due to lignin-lignin bond cleavage.
2. Increased hydrophilicity and swelling of the lignin due to the formation of lignosulfonic acid groups.

The effects of sulfonation and the resulting softening on fiberization and pulp properties are shown in Table 1.

Table 1. Influence of sulfonation on fiberization and pulp properties.

FIBERIZATION	
Wood elastic shear modulus	↓
Specific refining energy (based on 5 km breaking length)	↓
Shive content	↓
Fiber damage	↓
Fines content	↓
PULP PROPERTIES	
Sheet density	↑
Tensile strength	↑
Tear strength	↑
Opacity	↑

It is important to understand the effects of sulfonation on wood properties because they determine the ease of fiberization, which in turn affects the condition of the liberated fibers. The degree of wood softening can be expressed in terms of changes in elastic shear modulus of the wood. The elastic shear modulus, as measured with a torsional pendulum, has been shown to decrease with increased sulfur content (6,10). Since the wood is softer, less energy is required to fiberize it (6,10). Both of these trends are shown in Table 1. In addition to simply softening the lignin, sulfonation can also lower the T_g of the lignin and reduce refining energy considerably at certain temperatures (6).

The condition of the liberated fibers in sulfite CMP is improved over that in RMP because the softer middle lamella lignin facilitates fiber separation and the softer fiber walls are better able to dissipate the refining load. As a result, the CMP fibers are generally more intact and less damaged. Easier fiber separation and reduced fiber damage have been demonstrated by increased long fiber fractions, lower shives contents, and reduced rejects with

increased sulfur content (8,9,10,11). Microscopic studies have shown that fibers liberated at higher sulfur contents have middle lamellae and outer secondary wall layers which are more intact (12,13).

In addition to producing fibers which are more intact and less damaged, sulfonation improves cell wall conformability, making the fibers more prone to collapse and conform in the web. Increased sulfonation, therefore, increases sheet density and fiber-fiber bonding. These, in turn, increase handsheet breaking length. Tear strength is also improved as long as high degrees of refining are avoided (14,15). An unfortunate consequence of the improved fiber-fiber bonding with sulfur content is the reduced specific scattering coefficient (14).

SULFONATION VARIABLES

As the previous discussion suggests, CMP properties can be controlled through the degree of sulfonation of the pulp. This can be done by manipulating the following independent sulfonation variables:

- Sodium sulfite concentration in the liquor
- Time at maximum temperature
- Temperature
- Liquor pH

In addition to affecting sulfur content, these variables may also influence CMP properties through their effects on cell wall sulfur distributions, yield, and reactions of other wood components. Most of the literature has focussed on sulfur content and yield as these are well understood and easy to measure.

From the kinetics of the sulfonation reaction, the effects of sodium sulfite concentration, time, and temperature on sulfur content are rather

obvious; increasing any one of these variables when all other variables are constant increases the sulfur content of the pulp. The curves in figure 5 show these trends. The tendency of these curves to level off can be attributed to a limit in the number of available sites for sulfonation on the lignin, or, at low sodium sulfite concentrations, limited amounts of sulfite. Heitner, Beatson, and Atack (7) have determined the maximum attainable sulfonate content to be around 2.0% (0.8% sulfur) at 140°C. This maximum is dependent on the presence of sufficient sulfite to sulfonate the available sites and on temperature. Temperatures of 80°C will give a maximum sulfonate content of around 1.5% (7). At extremely long cooking times, yield reduction may also reduce the maximum.

The influence of time, temperature, and sodium sulfite concentration on pulp properties have been explained on the basis of sulfur content and yield. Elevated sulfonate contents and lower yields obtained at increased times and temperatures increase fiber conformability and have been shown to increase sheet density and strength (8,15). Unlike time and temperature, sodium sulfite concentration has little influence on yield, which suggests that liquor sulfite concentration influences CMP properties primarily through its effect on chip sulfur content.

The influence of liquor pH on sulfonation is much more complex than that of the other variables. The rate of sulfonation is at a minimum in the weakly acidic pH range and increases as the pH increases towards the alkaline range and as it decreases towards strongly acidic levels (6). This is probably a result of the greater tendency for the benzylium ion and quinone methide intermediates to form in strongly acidic and alkaline pH levels. At weakly acidic pH's, these intermediates form rather slowly, therefore reducing the sulfonation rates (5).

a).

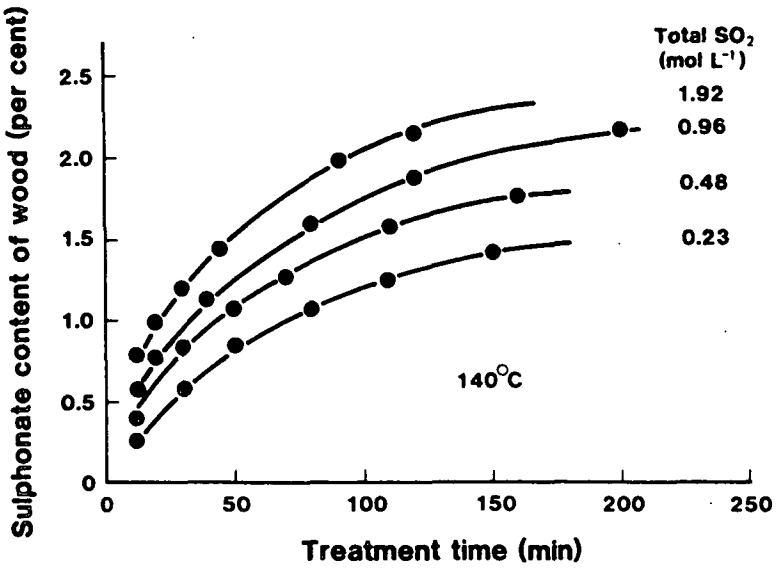

b).

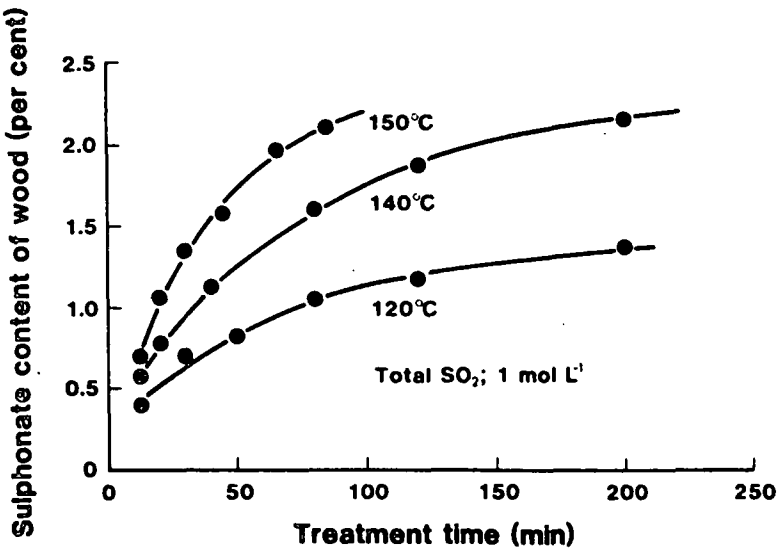

Figure 5. Influence of time, temperature, and sulfite concentration on sulfonate content (2.5 X sulfur content) at pH 4; a). effect of time and sulfite concentration; b). effect of time and temperature. From reference (5).

When extremes in pH are avoided, the influence of pH on pulp properties can be explained on the basis of sulfur content and yield. At extremes in pH, pulp properties are influenced by side-reactions which occur during the cook. Under strongly acidic conditions, condensation reactions compete with

sulfonation at the benzylium ion, increasing the degree of cross-linking within the lignin. As a result, the decline in glass transition temperature (T_g) is not nearly as pronounced as that found at higher pH levels (6). Under highly alkaline conditions, nucleophilic attack by hydroxide ions effectively competes with sulfonation reactions (1), thus degrading the lignin by a means other than sulfonation. As a result, pH levels above 13 give lignin degradation and substantial yield loss at low levels of sulfonation (12).

VAPOR-PHASE COOKS

An interesting approach to sulfonating wood chips is through the use of so-called vapor-phase cooks. These cooks involve three basic steps:

-impregnation of wood chips with liquor
-removal of impregnated chips from bulk liquor
-steaming of impregnated chips

Unlike liquid-phase cooks, which are performed at liquor-to-wood ratios of five or more, vapor-phase cooks use only that liquor which remains in the chips after impregnation and removal of the chips from the bulk liquor. Effectively, the liquor-to-wood ratio is only in the range of 0.6 to 1.2, depending on wood specific gravity.

A comparison of liquid-phase and vapor-phase cooks performed under almost identical conditions revealed both cooks to yield comparable sulfur contents and pulp properties (16). The only difference between the two were a higher initial pH for the vapor-phase cooks and a lower chemical charge in the vapor-phase cooks due to the lower liquor-to-wood ratio. The poorer buffer capacity of the vapor-phase system made this higher pH necessary in order to maintain

comparable pH levels. Use of chip impregnation for the vapor-phase cooks also improved the uniformity of sulfonation along the length of the chip.

SULFUR DISTRIBUTION

Most of the literature on sulfonation and high yield sulfite pulping views sulfonation as a wood chip or pulp property and has paid little attention to sulfur distribution across the fiber or cell wall. On the fiber level, the degree of sulfonation of the various cell wall layers influences pulp properties. In the case of the middle lamella, wood chips in which the middle lamella lignin is softened by extensive sulfonation will tend to fracture in the middle lamella during fiberization. This results in fibers with a lignin-rich surface (12,13). On the other hand, unsulfonated chips or chips with lower degrees of sulfonation tend to fracture in the outer secondary wall (12,13), leaving a carbohydrate-rich fiber surface with different bonding characteristics. As discussed previously, increased sulfonation of the secondary wall increases sheet density and strength through increased fiber wall flexibility and conformability. The distribution of bound sulfite across the secondary wall will also influence these properties. If the degree of sulfonation of the individual wall layers could be manipulated, pulp properties could be controlled to meet specific end use requirements.

Recent years have seen increased interest in the use of electron microscopy to evaluate the distribution of bound sulfur across the cell wall. Early work in this area attempted to use Auger electron spectroscopy, but was able to do little more than detect the presence of sulfur in the cell wall (17). A second study, which used scanning electron microscopy (SEM), with energy dispersive spectrometry (EDS), found middle lamella sulfur levels to be

higher than those in the secondary wall (18). However, the limited spatial resolution of the SEM prevented a more detailed description.

To obtain improved spatial resolution, Beatson, et al. (19) used transmission electron microscopy (TEM) with EDS to evaluate cell wall sulfur distribution in sulfonated black spruce. Spruce chips were saturated with water, soaked in sulfite liquor for 24 hours, and were then cooked at high liquor-to-wood ratios under a variety of conditions. Once the samples were prepared for the sulfur distribution work, the sulfur levels at closely spaced points across the cell wall were measured with TEM-EDS. The improved spatial resolution allowed isolation of the cell corner and the observation of the sulfur distribution across the secondary wall. This work found a ratio of cell corner to secondary wall sulfur counts of around 3.0 and a flat sulfur distribution across the secondary wall. See figure 6. These results were consistent for the tested combinations of liquor pH, temperature, time at temperature, and liquor sulfite concentration.

From these results, Beatson and his co-workers reached several conclusions concerning sulfonation and cell wall sulfur distribution. The observed ratio of cell corner to secondary wall sulfur counts was compared to a published lignin content ratio of 3.8 (20). From these values they concluded that the secondary wall lignin was 31% more sulfonated than the middle lamella lignin, which was in close agreement with other findings (13,21). Since sulfonation is believed to occur on phenolic units and the phenolic hydroxyl content of the secondary wall is believed to be twice that of the middle lamella (22,23), the secondary wall would be expected to be twice as reactive. Since the sulfur content of the secondary wall lignin was only 31% higher, they concluded that phenolic hydroxyl groups are rapidly formed in

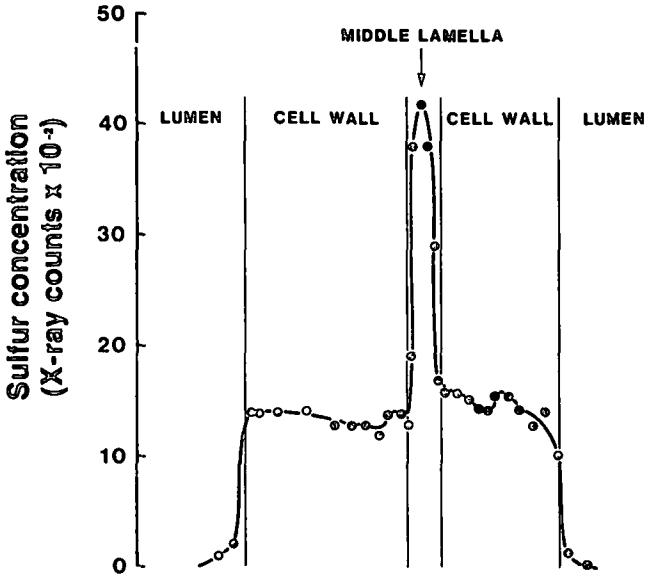

Temperature, °C	pH	Total SO_2 concentration, mol/L	Time, min	Lignin losses based on wood, %	Sulfur content of treated wood, %	Ratio of sulfur concentrations,* cell corner/cell wall
140	7	0.65	12	0.15	0.39	2.7 ± 0.2
140	7	0.65	30	1.02	0.56	2.8 ± 0.4
140	7	0.96	40	1.33	0.64	2.9 ± 0.2
80	7	0.91	1500	1.94	0.63	3.1 ± 0.4
140	4	1.00	15	1.70	0.29	2.9 ± 0.3
Average of the ratio of sulfur concentrations						2.9

*Mean ± 95% confidence limit.

Figure 6. Cell wall sulfur distribution curve and accompanying data for sulfonated spruce from Beatson, et al. (19).

the middle lamella during the early stages of the cook. From the consistency of the cell corner to secondary wall sulfur levels at different times and pH levels, they concluded that sulfonation occurred by the same mechanism in both wall layers at pH 4 and pH 7. Finally, they concluded the consistency of the cell corner to secondary wall sulfur count ratios at different temperatures suggested the absence of diffusion limitations.

STEM-EDS OPERATING PRINCIPLES

Earlier studies of elemental distribution across wood cell walls have used different forms of electron microscopy (SEM, TEM, STEM) in conjunction with x-ray microanalysis (EDS). For the purpose of measuring elemental

distributions, the electron microscope produces an electron beam which is defined into a narrow probe by a series of condenser lenses and apertures. A schematic of a scanning transmission electron microscope (STEM) with EDS is shown in figure 7. For the purposes of discussion, STEM will refer to either the process of scanning transmission electron microscopy, or the apparatus, scanning transmission electron microscope, depending on the context in which the term is used. The same will be done with the term SEM, which represents scanning electron microscopy (microscope), and the term TEM, which represents transmission electron microscopy (microscope).

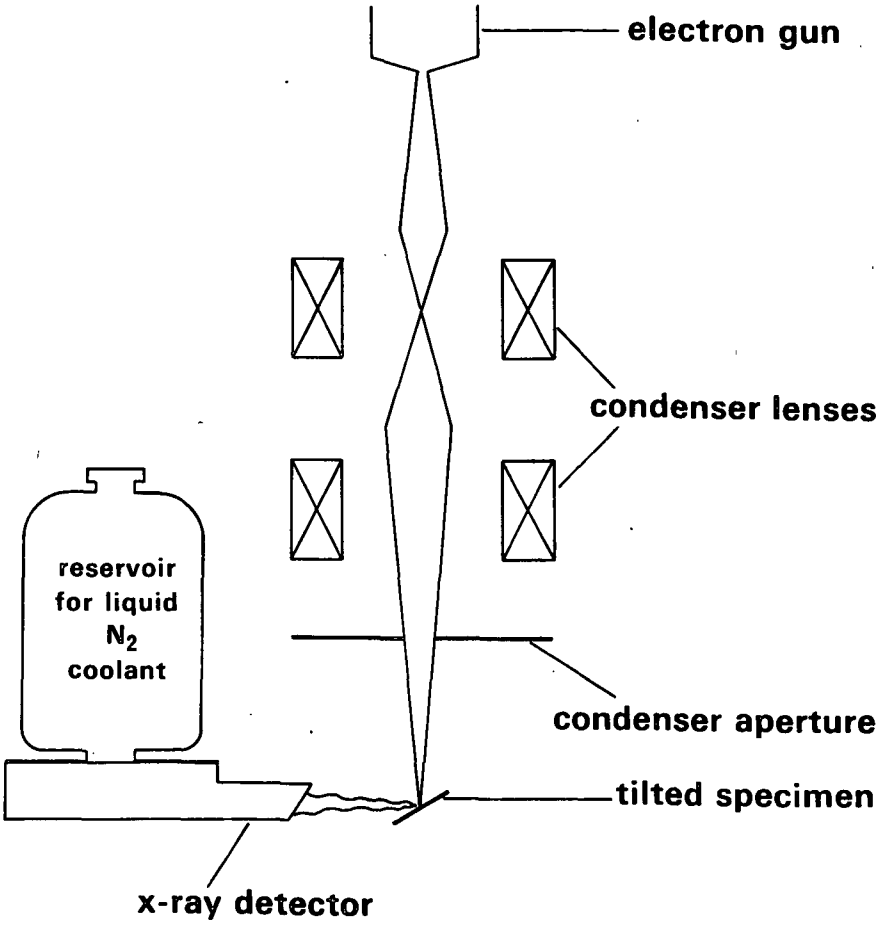

Figure 7. Schematic of a STEM with EDS.

Electron-Specimen Interactions

When the electron probe strikes the specimen, a number of interactions occur. These include inelastic scattering of the incident electrons, resultir in backscattered and secondary electrons, and elastic scattering of the incident electrons. Backscattered and secondary electrons are used for imagir in scanning electron microscopy (SEM). Those electrons which are transmitted through thin sections are used for imaging in transmission electron microscopy (TEM) and scanning transmission electron microscopy (STEM). In addition to these interactions, electrons impinging on a specimen will produce x-rays. Ir EDS work, these x-rays are collected by an x-ray detector and their signals ar then processed to obtain an x-ray spectrum such as that shown in Figure 8.

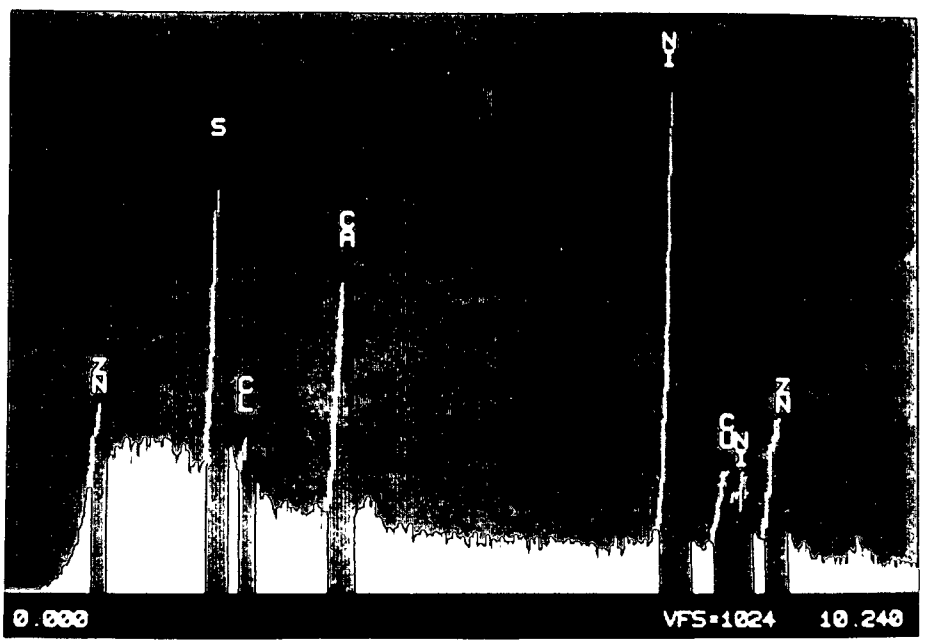

Figure 8. Typical x-ray spectrum from sulfonated wood with characteristic peaks (red) superimposed onto the continuum (light blue).

This spectrum, which plots x-ray intensity vs. x-ray energy (keV), has two principle features: the characteristic peaks (red), and the continuum (light blue). The characteristic peaks, which are superimposed onto the continuum, represent the different elements in the sample. An electron bombarding the sample will eject an electron from an inner shell orbital of an atom, thus elevating the atom to an excited state. The inner shell vacancy is generally filled by an electron from an outer shell. During the transition from the outer to inner shell, the electron loses a discrete amount of energy, which is emitted as an x-ray photon. The energy of this x-ray photon depends on the potential energy difference between the inner and outer electron orbitals involved in the transfer (24).

The energy transitions involved in x-ray production vary from element to element, thus allowing the identification of elements from the x-ray energies or peak positions in the spectrum. The area under the peak is a function of the concentration of that element in the sample. The energy level diagram in figure 9 indicates possible transitions in sulfur atoms. The prevalent transitions occurring in the electron microscope are those from the L-shell to the K-shell (K_α transitions). For sulfur atoms, these energy transitions are essentially the same, resulting in the fusion of the K_α sulfur peaks into a single K_α peak. The K_β peak is much smaller than the K_α peak and is similar enough in energy to be obscured by the larger peak.

The other kind of x-rays represented in the spectrum are the continuum, or bremsstrahlung, x-rays. These x-rays comprise a background intensity across the entire energy range of the x-ray spectrum. They are produced by the rapid deceleration of electrons in the field surrounding the nucleus and inner shell electrons (24). Since the characteristic peak is superimposed on the

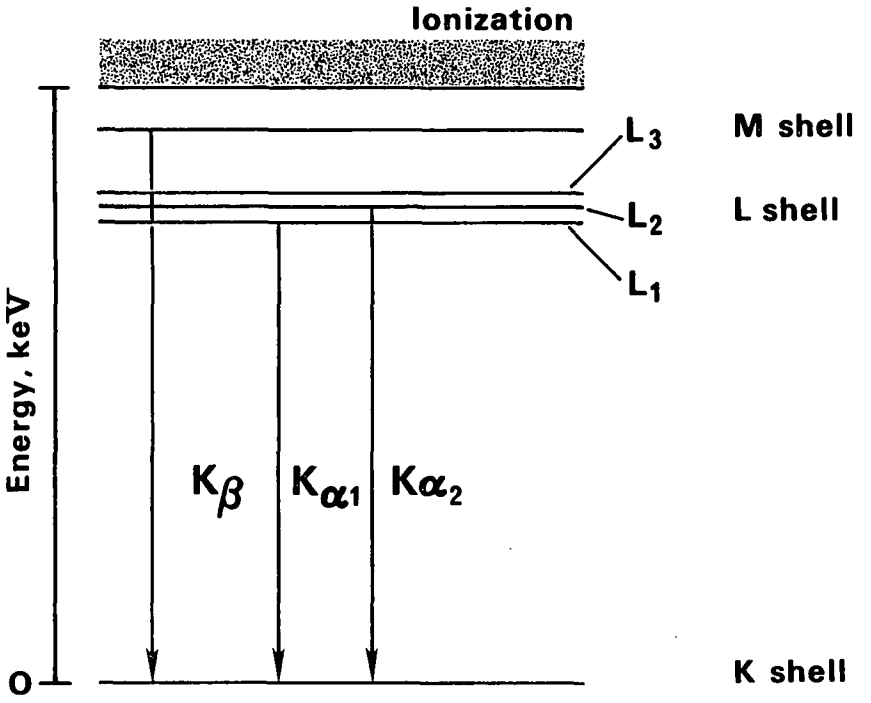

Figure 9. Schematic of an energy level diagram for sulfur.

continuum, it is necessary to subtract the contribution of the continuum, or in this context, background, from the characteristic peak in order to quantify the results.

Spatial Resolution in Electron Microscopy

In measuring cell wall sulfur distribution, the use of STEM has several advantages over use of SEM or TEM. The SEM work is generally performed with bulk samples which, as far as the electron beam is concerned, are infinitely thick, while the samples in the TEM or STEM are thin sections. As shown in figure 10, electron scattering in bulk samples yields a pear-shaped volume from which x-rays are generated. This results in a spatial resolution comparable to the diameter of the pear, which is 1 to 2 μm. In thin sections, the electrons have little opportunity to scatter before exiting the bottom surface of the

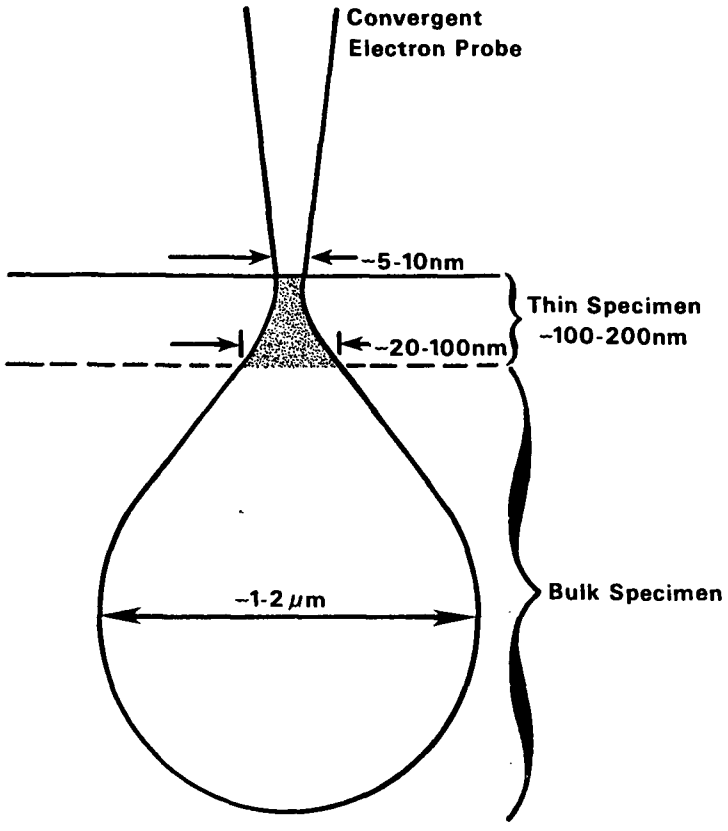

Figure 10. Volumes of electron beam/specimen interactions in bulk and thin samples (24).

sample. The volume from which x-rays are generated represents the narrow neck in the pear-shaped volume observed in the bulk samples. As a result, thin sections give improved spatial resolution.

The spatial resolution in thin sections represents the sum of the initial electron beam diameter and beam broadening or electron scatter within the sample. The effective beam broadening, b, is given by the relationship (23),

$$b = 6.25 \times 10^5 \, (Z/E_0)(\rho/A)^{0.5}(t)^{1.5} \quad \text{cm} \qquad (3)$$

where Z is the atomic number, E_0 is the electron energy in eV, ρ is the sample

density, A is the atomic weight, and t is the sample thickness in cm. This relationship is based on a formula derived by Rutherford for Coulomb deflection by a point charge (25).

The inverse relationship between beam broadening and E_o reveals another advantage of TEM or STEM. An SEM generally operates up to a 30-40 KV accelerating potential, while a TEM or STEM will often operate at 100 KV or higher. From equation 3, this higher accelerating potential should give less beam broadening and better spatial resolution. A higher beam current and thus higher count rate also accompanies the higher accelerating potential. This is particularly important in detecting elements at low concentrations.

The basic difference between TEM and STEM is the manner in which beam movement is controlled. In the conventional TEM, the beam is generally stationary. In order to measure elemental distribution across the cell wall, the sample must be moved between measurements at individual points across the cell wall. In STEM, the operator can control the movement of the electron beam while keeping the sample stationary. At the Institute of Paper Chemistry, the STEM-EDS has the capability of performing what are called STEM-EDS linescans. These are a series of equally-spaced point measurements oriented in a straight line across the cell wall or other object of interest. The number and spacing of points can be controlled by the operator. The STEM is also generally capable of producing a finer electron probe, giving improved spatial resolution.

STEM Control Parameters

With the STEM, the operator can manipulate x-ray count rate and spatial resolution through several controls. These controls and their effects on beam

intensity and diameter, x-ray counts, and spatial resolution are listed in Table 2. The accelerating potential (KV) controls the energy of the incident electrons and is also the primary control over beam current. Therefore, as the KV and beam current increase, count rates increase. Higher KV's also result in improved spatial resolutions due to a lower degree of scattering in the specimen (24).

The first condenser lens (C1), as well as the other condenser lenses, are electromagnetic lenses which control the convergence of the electron beam into a probe. A lower current in the lens results in a wider probe. Once the condenser lenses have established some control over the beam, it passes through the condenser aperture, which prevents part of the beam and stray electrons from passing to the sample. This helps give a narrower and more defined beam.

Table 2. STEM control parameters and their effects on beam intensity and diameter, x-ray counts, and spatial resolution (26,27).

		Effects of increasing control parameter			
Control Parameter	Range	Beam Intensity	Beam Diameter	X-ray Counts	Spatial Resolution
accelerating potential (KV)	0-100	↑	-	↑	↑
beam current (μA)	0-110	↑	-	↑	-
C1 lens current[1]	2.8-4.6	-	↓	↓	↑
condenser aperture (μm)	20-400	-	↑	↑	↓
specimen tilt (degrees)	0-40	-	-	↑	↓

[1] Units for lens current are not known.

X-rays which are produced by electron beam/specimen interactions will not reach the detector unless the specimen is tilted towards the detector, as shown in figure 11. As the specimen tilt is increased, more x-rays reach the detector. This is due to the geometry of x-ray emission and the increase of the section's effective thickness by a factor of $t/\cos\theta$, where t is the section thickness and θ is the tilt angle. As demonstrated by equation 3, this increased effective thickness also yields a poorer spatial resolution.

Mass Loss

When performing EDS work with thin sections, the influence of beam-induced mass loss on the results must be considered. Several studies have investigated this phenomenon in biological samples irradiated in TEM (28,29,30). Of particular interest is the work done by Mary, et al. (30) on

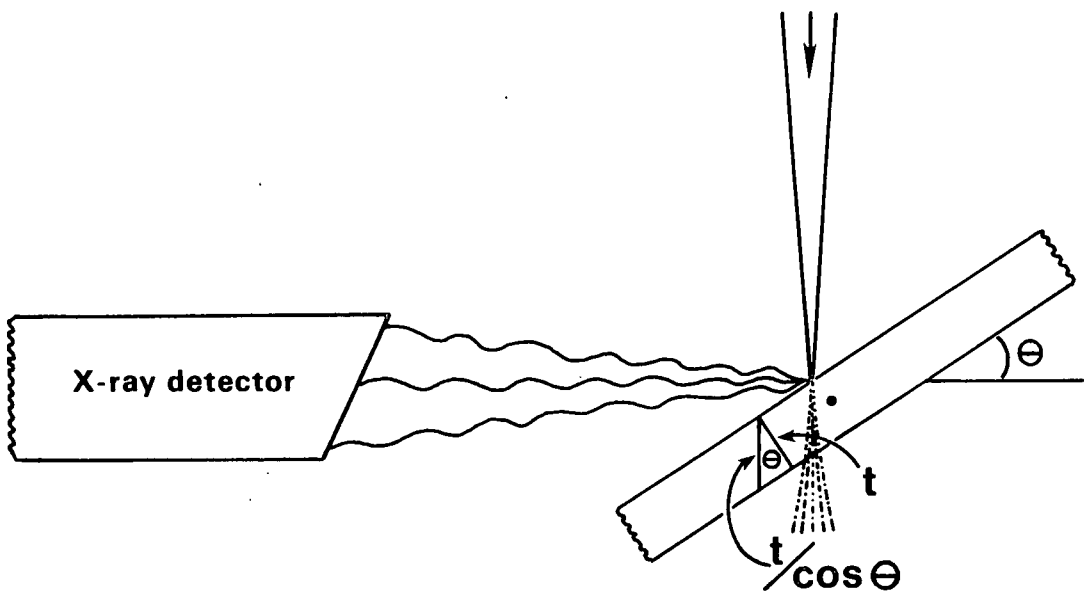

Figure 11. Schematic showing the relative positions of the specimen and x-ray detector. Note the effect of specimen tilt on effective sample thickness ($t/\cos\theta$).

mass loss in non-embedded wood samples. In samples irradiated at room temperature, 58% of the original wood mass was lost when given electron doses of 5 X 10^{-8} C/μm^2 or higher. These doses are comparable to those used in X-ray microanalysis. The different wood components were subject to mass loss to varying degrees with lignin (30% mass loss) being the most resistant and cellulose (68% mass loss) being the least resistant. Cooling the samples with liquid nitrogen or helium and embedding the samples should reduce mass loss, but the extent is not known.

ULTRAVIOLET MICROSCOPY

Unlike other cell wall components, lignin absorbs strongly in the ultraviolet range of the spectrum (31). A typical UV spectrum for lignin is shown in Figure 12. This spectrum is characterized by a maximum at around 205 nm, from which absorbance decreases to a minimum at around 260 nm. A second

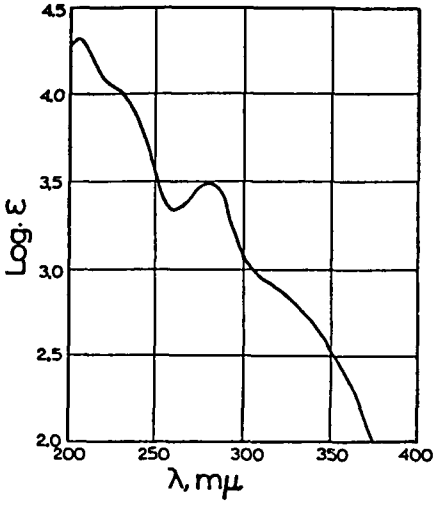

Figure 12. UV spectrum from sulfonated lignin (31). ϵ is the extinction coefficient. ϵ is proportional to absorbance at constant sample thickness and lignin concentration. See equation (5).

peak is found at 280 nm, from which absorbance declines as wavelengths approach the visible range. Since no other cell wall components absorb appreciable amounts of UV light, absorbance of incident UV light can serve as a measure of lignin concentration. Differences in UV absorbance across the cell wall could, therefore, represent the lignin distribution.

The use of ultraviolet microscopy in measuring cell wall lignin distribution has been reviewed by several authors (32,33,34). In the UV microscope, the sample is illuminated by a monochromatic UV light; a wavelength of 280 nm is frequently used. Due to absorbance of the incident light, its intensity, I_O, is reduced to an intensity, I_X, after passing through the sample. Assuming the embedding resin does not absorb at the wavelength of the incident light, the intensity of light transmitted through the resin in the lumen, I_L, can serve as a measure of I_O. For any cell wall layer, X, the UV absorbance, A, can be defined as (32):

$$A = \log (I_L/I_X) \tag{4}$$

The UV absorbance at any point in the cell wall is related to lignin concentration by the Beer-Lambert Law (32),

$$A = (\epsilon)(d)(C) \tag{5}$$

where ϵ is the extinction coefficient (l g^{-1} cm^{-1}), d is the thickness of the sample (cm), and C is the lignin concentration (g/cm^{-3}). The relationship was found by Scott, et al. (32) to be valid for thin wood sections.

If ϵ and d are known, the absorbance data can be used to give a quantitative determination of lignin concentration in the cell wall or any cell wall layer. Although section thickness can be determined by interference

methods, the extinction coefficient of lignin in situ has not been accurately determined (34). Such uncertainty in the value of ϵ makes the acquisition of accurate cell wall lignin concentrations by UV microscopy difficult.

This uncertainty can be avoided with the use of a second quantitative technique (33). In this technique, the absorbance of the S2 layer is used as a baseline to which the absorbance in other cell wall regions are proportioned. If the total lignin concentration, L_{Total}, were determined by other techniques, such as Klason lignin, the S2 lignin concentration (L_{S2})can be represented by the following equation:

$$1/L_{S2} = [V_{S2} + \Sigma(A_X/A_{S2})(V_X)] \diagup L_{Total} \qquad (6)$$

V_{S2} and V_X are the volume fractions for the S2 layer and other cell wall regions, respectively, and A_{S2} and A_X are the corresponding absorbances. Although this technique does not require values for extinction coefficent or sample thickness, they are assumed constant among the various cell wall layers. Another sensitivity is the potential effect of non-uniform lignin concentration among different fibers on the accuracy of the results. This could be a problem in samples rich in compression wood, due to the higher lignin content of the compression wood (35).

If only semi-quantitative results are needed, the Beer-Lambert Law can be applied under the assumption of constant or known section thickness and constant or known extinction coefficient. The assumptions concerning known thickness and extinction coefficient have already been discussed and the assumption concerning constant thickness can be tested with interference methods. The assumption of constant extinction coefficient between wall layers has been confirmed by Hardell and co-workers (22). Their experiments with

secondary wall and middle lamella fractions from fractionated wood found lignin concentrations obtained by UV methods to be comparable to those obtained by methoxyl content determination after nitrobenzene oxidation. Since use of the assumption of constant extinction coefficient yielded results comparable to those obtained by another method, the assumption was determined to be correct.

Several methods are available for measuring UV absorbance in the UV microscope. The more traditional method involves recording an image of the UV-irradiated sample on film, and then measuring the density of colloidal silver in the negative with a densitometer. Higher transmittance (lower absorbance) of the incident monochromatic light by an area in the sample gives higher densities of colloidal silver on the corresponding area in the film. These areas are darker on the negative. In contrast, areas of low transmittance (higher absorbance) give lower densities of colloidal silver, and thus, lighter images on the negative. The densitometer has a narrow light beam which is scanned across the image of the cell wall on the negative. The density profile across the negative, represented by light transmitted through the negative, is then recorded by the densitometer.

At short times of exposure, the density (D) of silver on the negative is related to absorbance by the equation (32):

$$A_X = (D_L - D_X)/\gamma \qquad (7)$$

where A_X = the absorbance in wall region, X,
D_L = density of colloidal silver in the lumen on the negative,
D_X = density of colloidal silver in wall layer, X, on the negative,
γ = constant related to film light sensitivity.

Using the Beer-Lambert Law and the above equation,

$$C_{CC} = (D_L - D_{CC}) \diagup [(\epsilon)(d)(\gamma)]$$
$$C_{S2} = (D_L - D_{S2}) \diagup [(\epsilon)(d)(\gamma)] \qquad (8)$$
$$C_{CC}/C_{S2} = A_{CC}/A_{S2} = (D_L - D_{CC}) \diagup (D_L - D_{S2})$$

where CC represents the cell corner and S2 represents the secondary wall.

A more direct means of measuring lignin distribution through UV absorbance is with a photometer attached to the microscope. In such a system, a narrow beam of light is placed in the areas of interest or scanned across the cell wall. The amount of transmitted light is recorded by the photometer. Since absorbance is a function of the amount of transmitted light, differences in UV absorbance, and hence, lignin concentration can be recorded. In the case of scans, the transmitted light data will yield lignin distribution profiles.

THESIS OBJECTIVES

The idea of selectively sulfonating one portion of the cell wall over another offers some intriguing prospects for the development of sulfite CMP properties. Current practice entails sulfonating wood chips to a desired level with little regard for the distribution of bound sulfite across the cell wall.

Consideration of the effects of sulfonation at the cell-wall level reveals the importance of cell wall sulfur distribution. The extent to which the middle lamella is sulfonated influences the manner in which fibers separate. This will affect fiber surface properties and the extent to which the fibers are damaged. Sulfonation of the fiber secondary wall will influence the conformability of the fiber and the manner in which the fibers dissipate refining energy. These will affect the density and strength of the paper product as well as the extent to which the fibers are damaged. Control over the extent to which the fiber wall and middle lamella are sulfonated could provide numerous combinations of fiber mechanical and surface properties which could be applied to specific end uses.

With this long-term goal in mind, the intent of this thesis has been to evaluate the influence of sulfonation variables on cell wall sulfur distribution in southern pine latewood. The sulfur distributions were measured using STEM-EDS linescans. In addition to evaluating sulfonation variables and their influence on cell wall sulfur distribution, this thesis also investigated the origin of the observed distributions and any variation in sulfur distribution. In particular, the investigation studied the role of lignin distribution, lignin reactivity, and diffusion limitations.

The evaluation of cell wall sulfur distribution in this work differs from

that of Beatson, et al. (19) and others in several ways. The primary difference between the present work and others reflects the motivation behind the studies. The principle concern of previous studies has been the topochemistry of sulfonation, in general, and the manner in which it may vary between several treatments. The present work is concerned with these matters, but has gone one step further by aggressively seeking treatments which would yield differences in cell wall sulfur distribution.

Several measures were taken to achieve this goal. The first measure was the evaluation of a wider variety of treatments, including vapor-phase cooks. The poorly buffered environment within the chips in the vapor-phase cooks had the potential of yielding some interesting distributions, resulting from diffusion limitations or variation in the chemical environment across the cell wall. A second measure was avoiding long exposures of the chips to the liquor prior to cooking. The longer impregnation times used by Beatson, et al. (19) are more likely to result in some lignin degradation and increased swelling in the chips. This may lift diffusion barriers which could otherwise influence cell wall sulfur distribution. The present work used impregnation times of 30 minutes or less.

In addition to studying a wide variety of high-yield sulfite cooks, the present work is unique in its rigorous statistical analysis of the sulfur distribution data obtained from the cooks. The cooks were performed in a series of factorial experiments which investigated such variables as sodium sulfite concentration, temperature, time at temperature, and liquor pH. Analysis of variance performed on each of the experiments tested for significant effects of each of these variables over the effects of random sources of variation within and between chips.

The sulfur distributions obtained in the present work also provided a more detailed picture of cell wall sulfur distribution than previous works. Work performed with bulk samples in an SEM provided little detail of the secondary wall sulfur distribution due to poor spatial resolution. Beatson's work (19), which was done with TEM-EDS, provided reasonably good spatial resolution, but only measured around 10 points across the secondary wall. The present work performed the sulfur distribution evaluation with STEM-EDS linescans, which gave, on the average, more than 20 measurement points across each secondary wall. Through the use of a smaller beam diameter, the spatial resolution in the the present work was improved over those in previous works. The greater number of measuring points and the improved resolution at each point provided a more detailed picture of the secondary wall sulfur distribution, which is especially important when comparing S3 and inner S2 sulfur levels.

A final difference between this and previous work is the wood source. While previous studies used spruce, this study used southern pine latewood. Latewood was chosen for this study because the thicker cell walls provide the the greatest opportunity to observe differences in sulfur distribution. Southern pine provides a fairly abrupt transition between earlywood and latewood, allowing easier separation of latewood chips with a fairly uniform cell wall thickness. This species difference could also influence lignin distribution and variations in lignin reactivity, which, in turn, could influence cell wall sulfur distribution.

EXPERIMENTAL

WOOD SOURCE

The wood source for this study was a 25 year-old southern pine log. The log was cut into 2.5 cm thick disks, which were subsequently cut into small wedges. A hand guillotine was used to cut latewood chips from these wedges. These chips were 2.5 cm long, 1 to 2 mm thick in the radial direction and .5 to 1 cm wide in the tangential direction. Since the outer growth rings of the wood source were very narrow, it was very difficult to separate earlywood and latewood from these rings. Therefore, the latewood chips were obtained from growth rings 7 to 13, which would classify these chips as juvenile wood. After these chips were extracted in benzene-ethanol, ethanol, and hot water, they were air dried.

SULFITE COOKS

The prepared chips were sulfonated in a number of high-yield sulfite cooks which were divided into three factorial experiments, which are summarized in Table 3. These experiments evaluated the following sulfonation variables:

- Sodium sulfite concentration in liquor
- Time at temperature
- Temperature
- Liquor pH
- Type of cook (liquor-to-wood ratio)

The last variable, type of cook, refers to vapor-phase cooks at a 0.65:1 liquor-to-wood ratio and liquid-phase cooks at a 10:1 liquor-to wood ratio. Of the three factorial experiments, two studied vapor-phase (VP) cooks, and the third studied liquid-phase (LP) cooks.

Table 3. Experimental designs

Experiment	Type of cook	Factorial	Variables
VP1	vapor-phase	3X2	sulfite ion concentration; time
VP2	vapor-phase	2X2	time-temperature combinations; sulfite ion concentration
LP1	liquid-phase	3X2	liquor pH; time

All cooks in each of the three experiments were performed in three steps. These were:

-vacuum impregnation
-cooking
-excess liquor removal

Each of these steps and more details on the experimental designs are discussed below.

Vacuum Impregnation

Two separate vacuum impregnation procedures were used. For the VP1 and LP1 cooks, vacuum impregnation was performed in a vacuum desiccator. The chips were placed in beakers containing liquor, which were subsequently placed in the desiccator. Vacuum was applied to the desiccator for ten minutes, relieved, and then reapplied and relieved for two more 10 minute intervals for a total time of 30 minutes. The chips were then immediately cooked.

The VP2 chips were impregnated in a different apparatus which could impregnate the chips faster and more efficiently. In the vacuum desiccator, the chips were immersed in liquor before vacuum was applied. When vacuum was

applied, the surface tension of the water within the chips may have prevented some of the air from escaping. In this new impregnation apparatus, shown in figure 13, the chips in the upper chamber were evacuated before the liquid was introduced. Once the chips were fully evacuated, stopcock 1 was opened and liquor filled the top chamber and entered the chips with less resistance. Relief of the vacuum created a positive pressure differential which forced liquor into the chips. This apparatus gave water uptakes of around 99% of those obtained after soaking the chips for 24 hours. This compares to a value of 90-95% for the vacuum desiccator. This high efficiency can also be achieved after only one 5 minute cycle. The high efficiency of this apparatus provided more thorough and uniform chip impregnation while shortening the impregnation time.

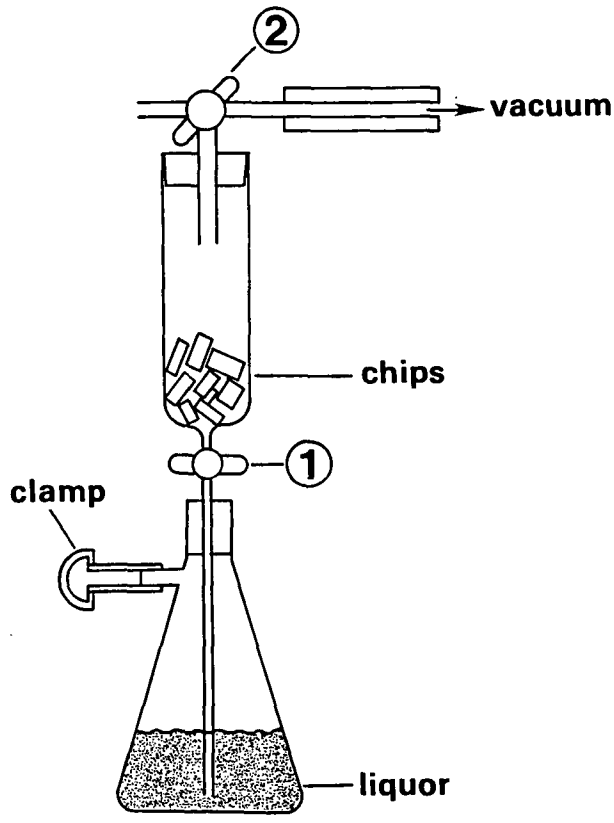

Figure 13. Impregnation apparatus used for VP2 cooks.

Cook Details

Table 4 summarizes the conditions under which all of the cooks were performed. The times listed are only times at temperature; the heat-up and exhaust times and other details for each experiment are discussed below.

The VP1 cooks constituted a 3X2 factorial experiment evaluating liquor sodium sulfite concentration and time at temperature. The liquor consisted of sodium sulfite solutions with enough sodium hydroxide added to obtain an initial pH of 11.5. After impregnation in the vacuum desiccator the chips were placed in Buchner funnels lined with glass beads. These funnels were covered loosely with foil and placed in beakers. The beakers were then placed in an autoclave where, after an 8 minute heat-up to 134°C, the chips were cooked for the desired times. After a 2 minute exhaust, the chips were removed from the autoclave, rinsed, and then soaked in distilled water to remove excess liquor.

The removal of excess liquor from the cooked chips entailed repeated 12 hour soakings of the chips in 200 ml of distilled water. These soakings were continued until a potassium iodate titration detected no more sulfite in the soaking water. The titration procedure used is based on Tappi Standard T-604. The procedure was modified by adding larger aliquots of the sample in order to detect lower sulfite levels.

The VP2 cooks constituted a 2X2 factorial experiment which evaluated sulfite ion concentration and two time-temperature combinations. The liquors were produced in the same manner as those used for the VP1 cooks. Since the autoclave could not attain the higher temperatures needed for this experiment, the cooks were performed in an oxygen bleaching vessel, where the chips sat in baskets. This vessel required 2 minutes to reach 140°C and 6 minutes to reach

Table 4. Summary of sulfite cooks.

Experiment	Sulfite ion conc., mole/l	Time, min	Temp., °C	Initial pH	L:W	Initial chip moisture content, %OD wood
VP1	0.48	20	134	11.5	0.65:1	6.3
	0.48	40	134	11.5	0.65:1	6.3
	1.03	20	134	11.5	0.65:1	6.3
	1.03	40	134	11.5	0.65:1	6.3
	1.59	20	134	11.5	0.65:1	6.3
	1.59	40	134	11.5	0.65:1	6.3
VP2	0.48	5	160	11.5	0.65:1	29.0
	0.48	20	140	11.5	0.65:1	29.0
	1.03	5	160	11.5	0.65:1	29.0
	1.03	20	140	11.6	0.65:1	29.0
LP1	1.03	0	140	3.3	10:1	6.3
	1.03	0	140	10.0	10:1	6.3
	1.03	0	140	12.5	10:1	6.3
	1.03	60	140	3.3	10:1	6.3
	1.03	60	140	10.0	10:1	6.3
	1.03	60	140	12.5	10:1	6.3

160°C. The exhaust times were 5 minutes and 6 minutes, respectively. After exhaust, the chips went through the same procedure as the VP1 chips.

The LP1 cooks were performed in a 3X2 factorial experiment which evaluated the effects of liquor pH and time at temperature. The pH 10.0 liquor was a simple sodium sulfite solution. The pH 12.5 liquor was produced by adding enough sodium hydroxide to a sulfite solution to obtain the 12.5 pH. The acidic liquor (pH 3.3) was a sodium bisulfite liquor into which SO_2 had been bubbled in order to obtain the lower pH. After impregnation, these chips were cooked at a 10:1 liquor-to-wood ratio in 70 ml titanium bombs, which were heated in an oil bath. The heat-up rate was 1.4°C per minute and the cool-down time was around 2 minutes. As with the vapor-phase cooks, excess liquor was then removed from the chips through repeated soakings.

SULFITE COOK DATA

The principle data obtained from the cooks were chip sulfur content, final liquor pH, and yield. The sulfur content data were obtained by Schoniger flask combustion - ion chromatography, the procedure for which was derived from several sources (36,37). For each treatment, duplicate combustions were performed in the Schoniger flasks on 40 mg of wood meal obtained from no fewer than 5 chips. During the combustions, all sulfite in the samples was oxidized to sulfate, which was then collected in a $NaHCO_3/Na_2CO_3$ buffer solution within the flask. This solution was diluted and then injected into the ion chromatograph, from which a sulfate peak was obtained. The sulfur content of the sample was then determined from the height of the sulfate peak and the oven-dried weight of the original sample.

The final liquor pH's from the liquid-phase cooks were obtained from the spent liquor of the cooks. Since the vapor-phase cooks produced no spent cooking liquor, final pH was measured in the water from the first washing (soaking) of the treated chips. Yield data were expressed on an oven-dried treated wood basis.

SULFUR DISTRIBUTION

Sample Preparation

Sample preparation for STEM-EDS linescans involves embedding the wood chips in epoxy resin, sectioning the embedded samples, and mounting the sections on support grids. Air-dried treated chips were impregnated with Spurr epoxy resin (38) through an acetone, 50/50 acetone/Spurr, 100% Spurr series. Under vacuum, the chips were submerged in 100% Spurr resin for several days.

The resin was changed every one or two days. Once the chips had been submerged in the Spurr for several days, the resin was hardened at 70°C overnight.

The embedded samples were trimmed with a razor blade and smoothed with a glass-knife in a Sorvall Porter-Blum MT2-B ultra-microtome. The samples were trimmed such that the sections would be 1/4 mm wide and 3 mm long. Transverse sections 1/4 μm thick were obtained from the samples using a diamond knife on the MT2-B ultra-microtome. Sectioning was performed in the radial direction with respect to the wood sample, and all sections came from the center of the chip with respect to the chip's longitudinal axis. The sections were collected on 200 mesh ultrahigh-transmission nickel grids. The bars of the grids were coated with formvar in order to improve section adhesion to the grid.

The above procedures for sectioning are fairly standard for biological materials. However, since wood is extremely hard when compared to other biological materials, several precautions had to be followed when sectioning the wood chips. Special care had to be taken while trimming and smoothing the samples because any substantial pressure on the sample or sectioning of thick sections would introduce minute cracks in the sample, making it difficult to obtain good quality sections. The width of the section was also critical. Most materials can be sectioned at a width of 1 mm, but the wood offers so much resistance to sectioning that narrower sections (around 1/4 mm) were necessary. In addition to precautions with the sample, care must also be taken in keeping the diamond knife clean. With the samples as fragile as they are, small amounts of dirt on the cutting edge give poor section quality.

STEM-EDS Linescans

The STEM-EDS linescans were performed with a Jeol-100CX scanning transmission electron microscope with a Tracor Northern TN-2000 energy

dispersive spectrometer (EDS). The 100CX was equipped with a liquid nitrogen-cooled anticontamination trap to help reduce specimen damage under the electron beam. Before each session with the STEM, the beam intensity was standardized by adjusting the beam current to obtain a given number of counts from a copper grid standard.

STEM operating conditions

Preliminary tests were performed in order to establish STEM-EDS operating conditions. The STEM-EDS operating conditions chosen are as follows:

Accelerating potential:	100 KV
Beam current:	100 μA
Condenser aperture:	200 μm
C1 lens current reading:	2.800 (units unknown)
Specimen tilt:	33^{o}
Magnification:	5000-8000X

These conditions were the best compromise between high count rate, reasonable collection time, minimal specimen damage, and good spatial resolution. The conditions chosen gave adequate counts at 30 to 60 seconds per pixel, depending on the sample sulfur content, and gave spatial resolutions below the maximum acceptable value of 100 nm. The spatial resolutions obtained in the 100CX and the influence of some operating variables on spatial resolution are discussed in the following section.

STEM beam diameter and spatial resolution

The primary advantage of using thin sections for the sulfur distribution work was the marked improvement in spatial resolution over that in bulk samples. Two factors influence spatial resolution: beam diameter, and beam spreading in the sample. The beam diameter, which, at a constant KV, is

controlled by the C_1 lens current and the condenser aperture, consists of a central probe and a halo of "spherically aberrated" electrons (24). The C1 lens current controls the size of the central probe, with higher currents yielding finer probes. In theory, the condenser aperture does not influence probe size, but at the probe sizes and apertures being used, it can influence the presence and size of the halo of "spherically aberrated" electrons (24). Since this halo can be responsible for a large proportion of the x-ray counts, the diameter of this halo will represent the total beam diameter.

Beam spreading in the section is described in equation 3. In order to account for the effect of tilting the specimen on beam spreading, the thickness, t, can be replaced by the effective thickness, $t/\cos \theta$, which is illustrated in Figure 11.

Although manufacturers data on probe diameter (27) and an equation to describe beam broadening (25) were available, no information on the halo and, hence, beam diameter was available. To meet this need, estimates of the beam diameter were obtained by direct measurement. Generally, linescans were performed in what is called Standard mode on the 100CX scanning unit. For the purposes of measuring the electron beam diameter, it was necessary to use a different mode, $\mu\mu$ diffraction mode, in order to image the electron beam at a 100,000 X magnification. Pictures of the probe image were taken at an exposure of one-eighth that recommended by the 100CX exposure meter. The diameters of the central probe and halo were measured directly off the negatives. The results obtained at various settings are shown in Table 5.

On the negatives, the beam appeared as a dark central spot surrounded by a dark gray halo, which was surrounded by a light gray halo. The central probe is represented by the dark central spot, the measured diameters from which

Table 5. Spatial resolution in the 100CX for 250 nm thick wood cross-sections. Accelerating potential = 100 KV.

Condenser aperture, μm	C1 lens current	Jeol probe dia., nm	Meas. probe dia., nm	Beam (halo) dia., nm	Spatial res., nm 0°	33°
100	4.010	5.0	5	20	32.7	36.9
100	3.367	10.5	9	24	36.6	40.7
100	3.100	16.0	16	28	40.4	44.6
200	4.010	5.0	6	21	33.7	37.8
200	3.367	10.5	10	26	38.5	42.7
200	3.100	16.0	17	41	53.1	57.1
400	4.010	5.0	6	25	37.5	41.7
400	3.367	10.5	10	46	57.8	62.0
400	3.100	16.0	18	63	74.2	78.4

agree rather well with the manufacturer's (Jeol) data. The dark gray halo is assumed to be that from the beam, while the light gray halo is believed to be the result of horizontal photon scattering through the film during exposure. In many cases, the boundary between the dark and light halos was not very clear, so the estimate of the beam halo diameter, and hence, the beam diameter itself, was subject to error. In those cases where the halo diameter was unclear, the estimates were made such that the data in Table 5 are, most likely, overestimates.

The spatial resolutions in Table 5 were obtained by adding the measured beam diameters to the beam broadening value (b) obtained from equation 3. At a 0° tilt, the value of b was 13.9 nm. This value was based on a 100 KV beam, and a 250 nm thick specimen with an average density of 1.36 g/cm^3, an average atomic number of 4.1, and an average atomic weight of 7.7. The density used was based on a cell wall void volume fraction of 0.282, a cell wall substance specific gravity of 1.46 (78), and a resin specific gravity of 1.1. The atomic number and atomic weight were based on carbon: hydrogen: oxygen ratios of cell

wall components in a cell wall of 50% cellulose, 25% hemicellulose, and 25% lignin. Replacing the thickness, t, with $t/\cos\theta$ at a 33° tilt yielded a value of 18.2 for b and the corresponding values for spatial resolution.

The data in Table 5 demonstrate an influence of both C_1 lens current and condenser aperture on halo diameter. Only C1 lens current influenced the diameter of the central probe, while both parameters influenced beam (halo) diameter. All conditions gave a spatial resolution of less than 100 nm. This testing evaluated lens currents in the 3.100 - 4.010 range as possible settings for the linescan work. A final choice of 2.800, which was not in the range tested, was ultimately chosen in order to improve count rates. The other settings used for the linescan work were a 200 μm aperture and a 33° tilt angle. Based on the data for these settings, the spatial resolution for the 2.800 lens current would probably be around 80 nm. A 400 μm condenser aperture, which would yield higher count rates at an acceptable spatial resolution, was not used due to a problem with sample damage under the electron beam.

Linescan collection

The collection of linescan data was controlled in the Tracor Northern TN-2000 by the SECTION sub-routine (39) of a program called IPP (Image Processing Program). The SECTION sub-routine, with the help of the SETX sub-routine, has the following capabilities:

-Control of electron beam movement during a linescan.
-Simultaneous recording of linescan data for up to eight elements.
-Subtraction of background counts.
-Establishment of boundaries between cell wall layers in the linescan histograms.
-Calculation of average counts from selected sections of cell wall.
-Writing and reading of linescan data to and from disk.
-Linescan data print-outs

Although the TN-2000 is quite versatile in its linescan collection capabilities, it has limited editing and data analysis capabilities. In order to analyze the linescan data it had to be transferred to another computer. The Data Transfer Program (DTP) was derived from part of the SECTION sub-program in order to transfer the linescan data, one file at a time, from the TN-2000 to an IBM-PC. DTP also has some linescan editing capabilities. The code for DTP is shown in Appendix 1. On the IBM-PC the downloading was handled by Qmodem, which read each linescan data file and created a corresponding ASCII file. These files could then be edited on Lotus-123 and then undergo analysis on the PC or be uploaded to the Burroughs B6900 for analysis.

A typical x-ray spectrum obtained from a sulfonated wood chip is shown in figure 14. Among the peaks which project above the continuum (background) is

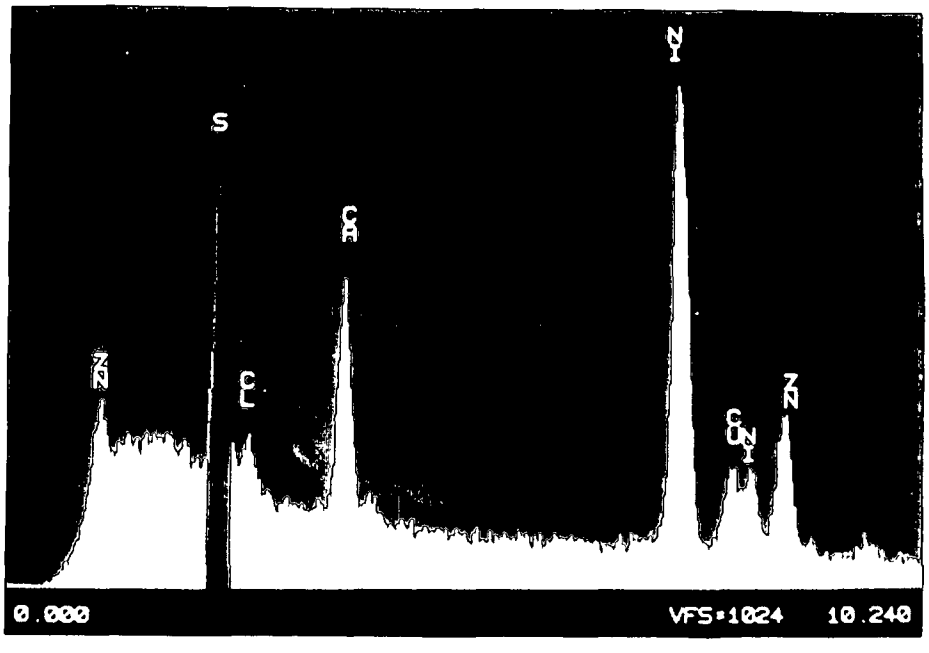

Figure 14. Typical spectrum from sulfonated wood showing the sulfur peak and region for background subtraction.

the K_α sulfur peak, which is shaded red. This peak represents the x-ray energy range of 2.180 to 2.440 keV. In order to obtain truly representative sulfur count data, the continuum portion of the peak had to be removed. IPP accomplished this by subtracting background counts from the total sulfur counts. The resulting sulfur counts were termed net sulfur counts. The background counts of any peak are best represented by an adjacent region of the continuum with the same width as the peak. For the sulfur peaks in this work, the region to the left of the sulfur peak (shaded yellow in Figure 14) served as the background region.

In anticipation of a large natural variation in sulfur distribution in various regions of the wood chip, the experimental design for linescan data collection was designed to quantify the hierarchy of variances in the data. For the main experimental variables studied, this would allow rigorous statistical testing of the significance of their effects. Separate experimental designs were established for each of the three sets of cooks. The experimental design for the VP1 cooks is shown in figure 15. As demonstrated in figure 15a, two chips were evaluated per treatment, and within each chip, double walls at three different locations were scanned. These were chosen to be at specific points across the thickness of the chip (along the radial axis of the wood source.): one at the chip center, one near an outside face, and one at an intermediate point. See figure 15b. Compression wood was avoided. Duplicate scans were made across each double wall (tangential wall), giving a total of 12 scans per treatment. In all but a few chips, a cell corner scan was performed in an adjacent cell corner for each of the double-wall scans.

After the analysis of the VP1 cooks, some changes were made in the linescan collection procedure for the VP2 and LP1 chips. The reasoning behind making these changes is discussed in the results. The number of chips per

a).

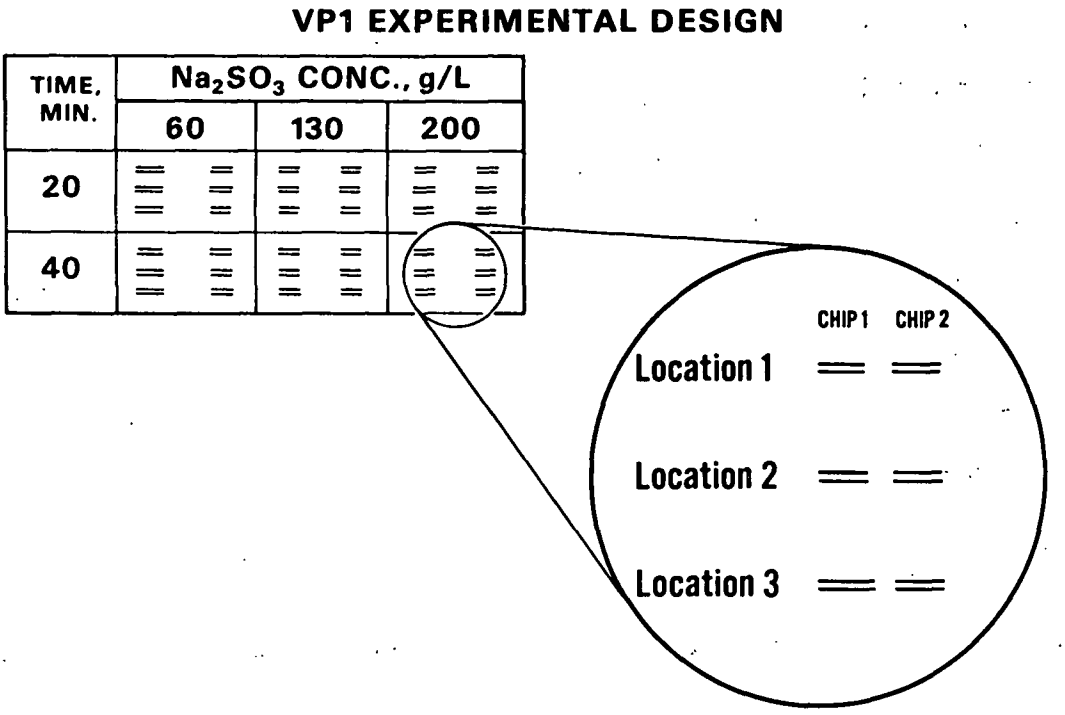

b).

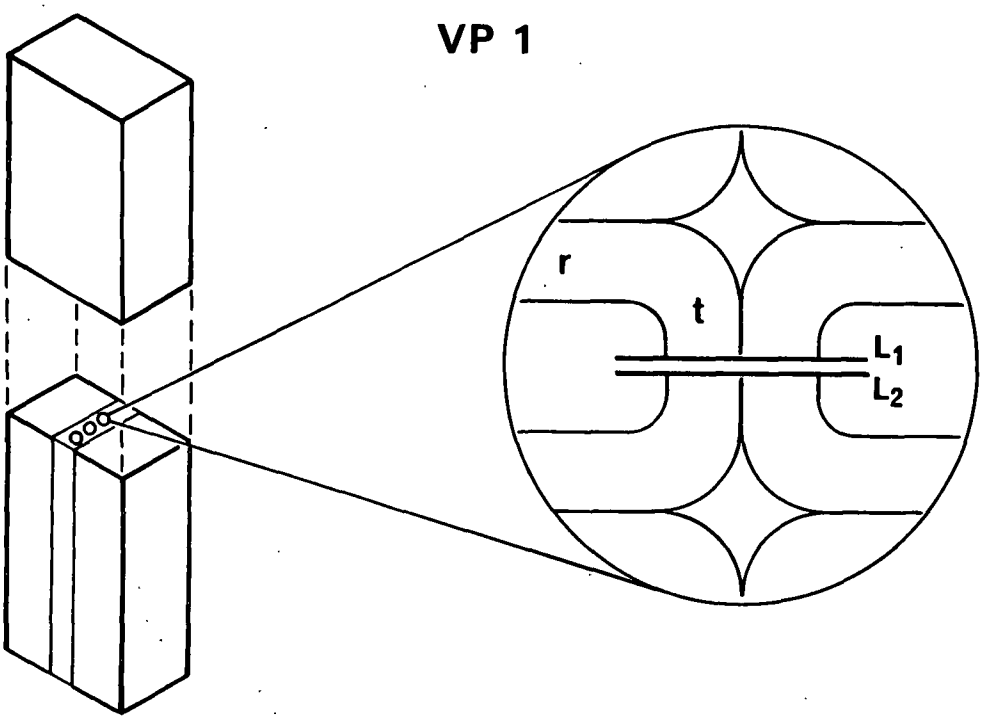

Figure 15. Experimental design for VP1 linescan analysis; a). Treatments evaluated, showing the division of the scans between treatments, chips, and locations (walls) within the chip; b). Locations of the scans within the chip and across the tangential wall.

VP 2 EXPERIMENTAL DESIGN

a).

TEMP., °C	TIME, Min.	Na_2SO_3 CONC., g/L	
		60	130
140	20		
160	5		

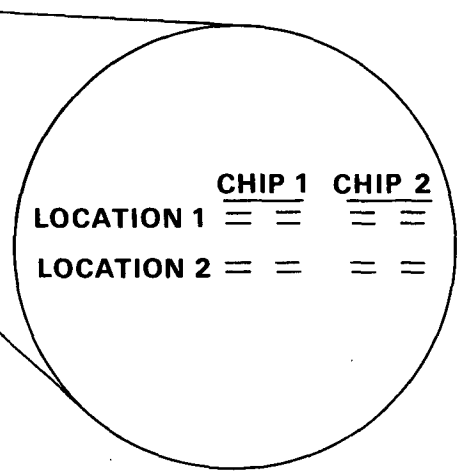

LP 1 EXPERIMENTAL DESIGN

b).

TIME, Min.	LIQUOR pH		
	4.3	8.4	10.5
0			
60			

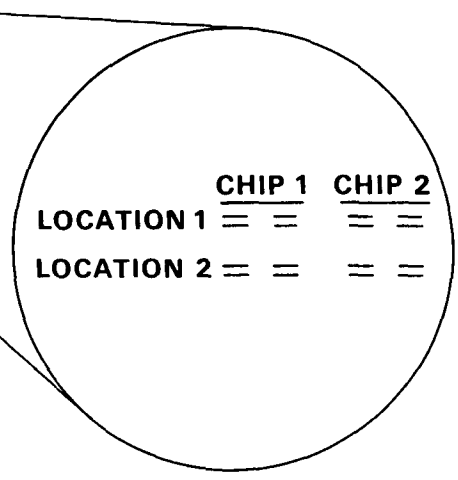

Figure 16. Experimental design for VP2 and LP1 cooks, showing the division of the scans between the treatments, chips, and locations within the chip; a). VP2 cooks; b). LP1 cooks.

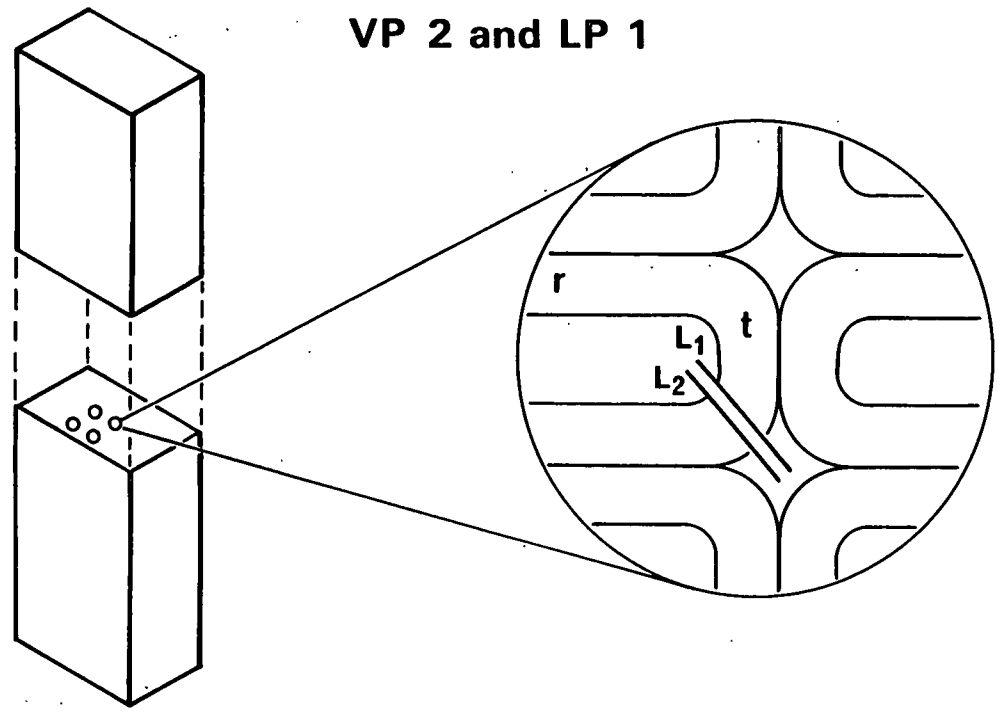

Figure 17. Locations of scans within the chip and walls of the VP2 and LP1 cooks.

treatment was kept at 2, but the number of cell walls evaluated within each chip was increased from three to four. See Figure 16 and 17. Instead of three locations, these four walls were divided between two locations within the chip; two walls were near the center, and two were near an outside face. As with the VP1 cooks, duplicate scans were performed across each cell wall, but as shown in figure 17, these scans extended across a single wall from the lumen into the cell corner and not across the double wall. Since the scans extended into the cell corner, separate cell corner scans were not necessary.

MASS LOSS

Mass loss and loss of sulfur from the thin wood sections were measured in order to understand the possible effects of mass loss on the sulfur distribution data. Two types of tests for mass loss were performed. The first test

used STEM-EDS linescans to measure mass loss over longer time intervals. Linescans were performed across a cell wall at different times per pixel. Five scans were performed per time. If mass loss were occurring, it was assumed the x-ray count rates (a measure of average sample density) would be lower for longer times.

Mass loss at shorter time intervals was measured with STEM-EDS timescans, which measured changes in counts from a spot or area as a function of time. Time increments ranging from $1X10^{-4}$ seconds to over 6 seconds were available, but the longer time increments were generally necessary in order to obtain a sufficient number of counts. Measurements were generally made by approaching the area to be tested blindly and starting the timescan the moment this area was first exposed to the beam. Unlike the linescan data, timescans could only collect data for one element at a time.

The total mass loss can be represented by changes in the x-ray continuum counts since mass per unit volume and continuum counts are proportional (28). To represent the continuum, this work has concentrated on the regions from 4.2 to 7.2 keV and 0 to 7.2 keV in the x-ray spectrum. The wider of these two regions contains the sulfur peak and a few other small peaks, which do not necessarily undergo a decline in counts proportionately with the continuum during mass loss. This may introduce some systematic error into the mass loss results, but the higher number of counts from this region are helpful in reducing random error.

The loss of sulfur was measured by monitoring changes in the K_α sulfur peak (2.18 to 2.44 keV). Since the timescans can only collect one set of data at a time, background counts could not be simultaneously collected and subtracted from the total sulfur data to obtain net sulfur data. To obtain

net sulfur mass loss data, total mass and total sulfur timescans were collected from two adjacent areas, and a spectrum was then collected from one of these areas to give total sulfur (TS), background (BG), and net sulfur (NS) data for an area which had undergone mass loss. Since the background region (1.92 to 2.18 keV) is part of the continuum, the percent loss of background should be comparable to percent mass loss. The net sulfur loss can be obtained from these data using the following relation,

$$[\text{counts}/(100\text{-ML})]\text{TS} = [\text{counts}/(100\text{-ML})]\text{BG} + [\text{counts}/(100\text{-ML})]\text{NS} \qquad (9)$$

where ML is the percent mass loss of the element in question. The counts in each term are the counts from the spectrum.

The mass loss experiments tested several different conditions. Since samples were exposed to a broad TEM beam and a fine STEM beam during linescan collection, total mass loss was measured in both modes. The TEM beam intensity (dose per unit time) was estimated from the reading (in pA/cm^2) of the TEM screen brightness indicator. The STEM beam had no intensity indicator, but judging from the behavior of the sample under the beam, the STEM beam was probably more intense. In TEM mode, the influence of beam intensity on total mass loss was evaluated. Insufficient count rates prevented any rigorous test of sulfur loss in TEM mode, but total mass loss and sulfur loss data were collected in STEM mode.

LIGNIN DISTRIBUTION

Thin sections were prepared and mounted on grids for lignin distribution studies to be performed with ultra-violet (UV) microscopy. This work was designed to yield several types of information:

1. Measurements of the secondary wall lignin distribution would help determine whether the observed secondary wall sulfur gradients can be attributed to lignin distribution.
2. Comparison of S2 (particularly outer S2) lignin levels with cell corner lignin levels would help account for observed differences in relative sulfur levels between these two areas of the cell wall.

The samples used for this study are described in Table 6. The sample 1 sections, which were from non-treated wood, basically served as a control. The nonembedded samples, which have not been treated nor embedded, were compared to the embedded sample 1 sections to determine the effect of embedding on the UV data.

Samples 3 and 4 were both from the factorial experiments and were from cooks which demonstrated different sulfur distributions. Sample 3 represented a cook which yielded a rather pronounced secondary wall sulfur gradient. Since the yield loss was very low, sample 3 results were expected to be comparable to

Table 6. Samples for UV microscopy.

Sample	Sulfur Content(%)	Chip	Plane of Section	Thickness(μm)
1	0	1	cross-section	1/4; 1/2
1	0	2	cross-section	1/4; 1/2
3	0.48	1	cross-section	1/4; 1/2
3	0.48	2	cross-section	1/4; 1/2
3-EM	0.48	1	cross-section	1/4; 1/2
4	0.78	1	cross-section	1/4; 1/2
4	0.78	2	cross-section	1/4; 1/2
Nonembedded	0	1	cross-section	1/2; 1.5

Sample 1: Nontreated extracted latewood embedded in Spurr resin
Sample 3: Vapor-phase cook; 1.03 molar Na_2SO_3; 20 mins. at 140°C; embedded in Spurr resin.
Sample 4: Liquid-phase cook; 1.03 molar Na_2SO_3; 60 mins. at 140°C; final pH = 10; embedded in Spurr resin.
Nonembedded: Nontreated extracted latewood; not embedded.

those from sample 1. Some of the sample 3 sections were irradiated under the electron beam of the STEM. These samples, designated 3-EM, were used for determining the effects of electron beam irradiation on lignin distribution. Sample 4 represented a cook which gave a relatively low yield (90%), a flatter secondary wall sulfur gradient, and a low CC/B ratio. The lignin distribution data were expected to yield some interesting results with regard to the above sulfur distribution data.

The ultra-violet microscopy was performed on two separate pieces of equipment: the UV microscope at the U.S. Forest Products Lab in Madison, and a Zeiss UMSP-80 UV microscope at Zeiss, Inc. The work at the Forest Products Lab involved taking photos of samples irradiated under a 300 nm UV light source and then collecting densitometer tracings across the cell wall images on the negatives. This is the same basic procedure used by Scott and coworkers (32). The UV microscope at the Forest Products Lab was an old Zeiss microscope equipped with a monochromater and a 35 mm camera. Mounted sections from chip 2 of sample 1 and sample 3-EM were placed between a quartz slide and cover slip in an immersion-glycerin solution and examined under a 100X objective at a 300 nm wavelength. While UV absorbance work on lignin is generally done at 280 nm, the choice of a 300 nm wavelength for this work was based on a previous finding that Spurr resin absorbs significantly below 290 nm (31). Subsequent work in this study confirmed this finding, but also found some absorbance above 290 nm. Three areas of approximately 75 X 75 μm were photographed from each sample on Kodak technical pan 2415 film. The exact magnification of the photos is not known, but it was probably around 500X.

After the film was developed, two negatives, representing two areas in the chip, were chosen for each sample. Densitometer traces were obtained from two

walls in each of the negatives. This work was performed on a Joyce Loebl double-beam microdensitometer which scanned a narrow beam of light across the cell walls on the negatives and recorded density variations, representing variations in lignin concentration, on a piece of graph paper. The settings used on the microdensitometer could theoretically yield spatial resolutions in the cell wall of 0.15 μm.

The Zeiss UMSP-80 is a state-of-the-art UV microscope which offers several advantages over the other equipment available. These include the ability to collect linescan and spectral data, and a low signal-to-noise ratio. Data were collected from all of the samples in Table 6. These data included scans across cell walls at 280 nm and spectral data from the lumen, secondary wall, and cell corner. A special effort was made to obtain good data from the S3 layer. The data from the non-embedded samples consisted of spectra from the cell wall. All data were processed and smoothed by the Lambda-scan program, which was developed by Zeiss for this purpose.

RESULTS

SULFITE COOK DATA

Table 7 describes the final pH, yield, and sulfur content results obtained from the vapor-phase and liquid-phase cooks. The liquor pH data reveal one key difference between the liquid-phase and vapor-phase cooks. The change in pH during the liquid-phase cooks was much less pronounced than during the vapor-phase cooks. This is due to the greater buffer capacity in the liquid-phase cooks provided by the bulk liquor. The bulk liquor serves as a reservoir of cooking chemicals and as a sink for acidic by-products, such as lignosulfonic acids. The chips in a vapor-phase cook, on the other hand, are in a much more poorly buffered system. This makes a high initial pH necessary in order to maintain neutral or alkaline pH levels. The final pH data for the vapor-phase cooks also suggest that high sodium sulfite concentrations are important in maintaining a more stable pH.

The yield data are all in the ultra-high yield pulping range, with all of the vapor-phase and some of the liquid-phase cooks resulting in virtually no yield loss. This implies that lignin dissolution should have little to no effect on the sulfur distributions in most samples. Although the changes in yield are minute in many cases, the yield data reveal a general decline in yield as the value of any of the four listed treatment variables increases.

The sulfur content data demonstrate some interesting trends with respect to treatment variables. The VP1 cooks gave increased sulfur contents with increased sodium sulfite concentration, but extending the cooks from 20 to 40 minutes had little effect on these data. This lack of a time effect does not agree with the STEM-EDS sulfur count data, which will be discussed in an upcoming section. The VP2 cooks showed the same concentration effects, while

Table 7. Final pH, yield, and sulfur content results from high-yield sulfite cooks.

Experiment	Time, min	Temp., °C	Na_2SO_3 conc., mole/l	Initial pH	Final pH	Yield %ODT wood	Sulfur Content %ODT wood
VP1	20	134	0.48	11.5	6.80	98.9	0.41
VP1	20	134	1.03	11.5	7.50	98.7	0.53
VP1	20	134	1.59	11.5	7.95	98.5	0.70
VP1	40	134	0.48	11.5	6.71	99.0	0.40
VP1	40	134	1.03	11.5	7.26	98.8	0.59
VP1	40	134	1.59	11.5	8.21	98.5	0.71
VP2	5	160	0.48	11.5	6.12	99.3	0.30
VP2	5	160	1.03	11.5	7.01	99.0	0.46
VP2	20	140	0.48	11.5	6.75	99.6	0.32
VP2	20	140	1.03	11.5	6.98	99.5	0.48
LP1	0	140	1.03	3.3	4.26	98.8	0.44
LP1	0	140	1.03	10.0	8.39	97.3	0.61
LP1	0	140	1.03	12.5	10.52	99.8	0.58
LP1	60	140	1.03	3.3	4.87	98.3	0.64
LP1	60	140	1.03	10.0	8.46	94.8	0.81
LP1	60	140	1.03	12.5	10.00	90.1	0.78

the two time-temperature combinations yielded practically the same sulfur content. This will provide a good basis for comparing the two types of treatments.

Unlike the VP1 cooks, the LP1 cooks yielded an increase in sulfur content with time. It is likely that the lower liquor-to-wood ratio of the vapor-phase cooks (0.65:1 vs. 10:1) and the proportionately smaller sodium sulfite charge prevented further sulfonation beyond that obtained at the shorter times. Although the bound sulfur (sulfur content data) accounts for less than half of the applied sulfur in the vapor-phase cooks, the remaining sodium sulfite may have been unavailable due to such processes as adsorption onto surfaces within the fiber wall. In the liquid-phase cooks, the high liquor-to-wood ratio provides a bulk liquor phase with an excess of sodium sulfite.

As previously discussed, the bulk liquor in the liquid-phase cooks also serves as a sink for acidic by-products, such as lignosulfonic acids. If the accumulation of these acids and other by-products were limiting sulfonation in the VP1 cooks, possibly through a decline in pH, their diffusion from the chips into the bulk liquor during liquid-phase cooks would reduce such a limitation and allow sulfonation to continue at a faster rate.

The observed effects of pH on sulfur content conforms to our current understanding of the effects of pH on sulfonation rate (5,6,19,40,41). The lower sulfur contents obtained at the acidic pH (bisulfite cook) agree with the results obtained in other studies (6,19,41). All of these agree with the rate data presented in the background section (5). The two alkaline pH's yielded slight differences in sulfur content, but they probably are not significant. This would agree with the findings of Wenneras (40), who found pH to have no effect on sulfur content in the pH range of 7 to 9.5. Engstrand, et al. (40), on the other hand, found a significant decrease in sulfur content as pH increased from 8.0 to 9.5, which suggests that the trend observed in the alkaline LP1 data may be real.

The repeatability of the Schoniger flask - ion chromatography sulfur contents was good. For most of the samples tested, the duplicates yielded sulfur contents which agreed to within .03%. Most of the results represented averages from five or more chips. In order to test for chip-to-chip variability, the sulfur contents of individual chips were determined for several treatments. Single determinations on five chips from the VP2 cook yielding .32% sulfur content gave a 95% confidence interval of .32 $\pm$ .032%. Another vapor-phase cook, not in Table 5, gave a 95% confidence interval of .612 $\pm$ .020%.

SULFUR DISTRIBUTION DATA

The general shape of the cell wall sulfur distributions was basically the same for all treatments. These distributions had two key components. As shown in Figure 18, one component was a pronounced sulfur gradient across the secondary wall with higher sulfur levels toward the lumen and lower levels toward the middle lamella. The extent of this gradient varied from very sharp to almost flat.

The second component was the markedly higher sulfur counts in the middle lamella, presumably due to the higher lignin concentration there. Comparison of the compound middle lamella data from the double-wall scan (Figure 18a) with the cell corner data from the cell corner scan (Figure 18b) reveals a marked difference between the two types of middle lamella data. This can be attributed to poor resolution of the narrow compound middle lamella. The compound middle lamella consists of a thin layer of true middle lamella sandwiched between the primary walls of the adjacent cell walls. These primary walls have a lower lignin concentration than the true middle lamella, and hence, would be expected to have lower sulfur levels. Because of limitations in spatial resolution, STEM-EDS data from the compound middle includes data from the primary wall and, probably some data from the S1 layers, which have even less lignin. This would give lower sulfur levels from the thin compound middle lamella than from the thick cell corner, which is predominantly true middle lamella. The resin-filled lumen produced no net sulfur counts, an observation which validates the background subtraction technique employed.

In order to evaluate the effects of sulfonation variables on cell wall sulfur distribution, it was necessary to quantitatively describe the distribution or its components. A number of parameters were reviewed, but none

a).

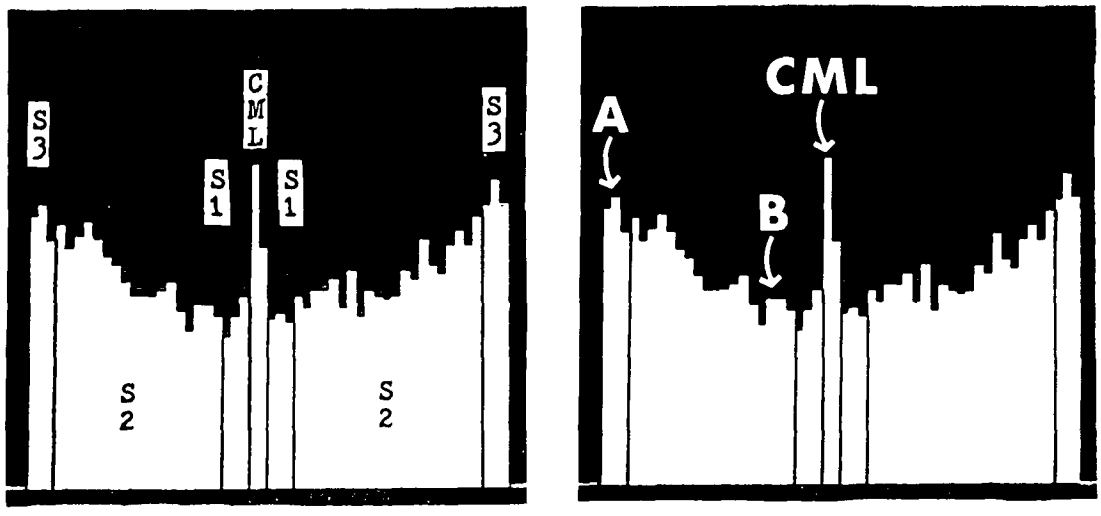

b).

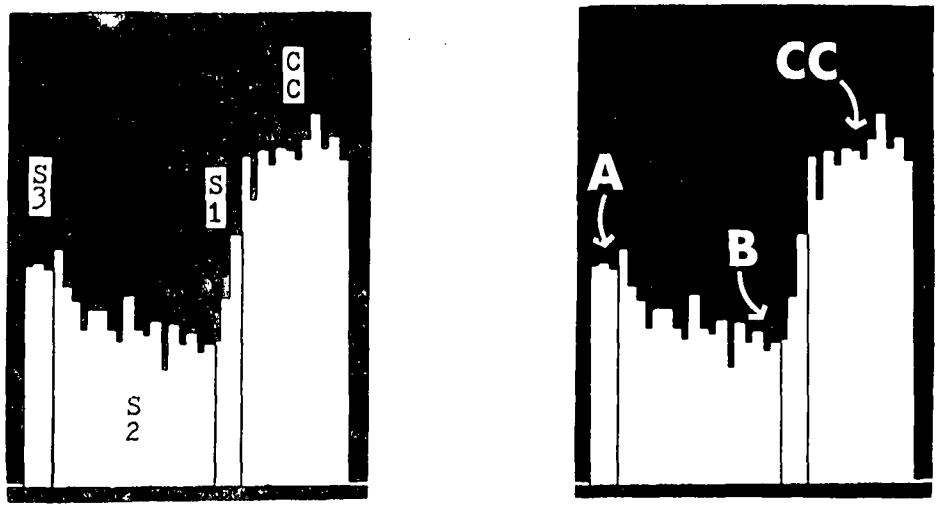

Figure 18. Typical linescan histograms displaying the secondary wall gradient and higher sulfur levels in the middle lamella; a). double-wall scan; b). cell corner scan.

provided a totally satisfactory description of the secondary wall sulfur gradient. The most meaningful and easily interpreted technique for describing the components of the cell wall sulfur distribution involves defining key points across the cell wall and calculating the ratios between the counts at these points. These points, shown in Figure 18, are the maximum (A) in the secondary wall near the lumen, the minimum (B) in the secondary wall near the middle lamella, and the average cell corner counts (CC). Since the compound middle lamella (CML) is poorly resolved in the double-wall scans, data from the adjacent cell corners were used instead.

The distribution across the secondary wall can be partially described as the ratio of point A to point B, and has been termed the A/B ratio. Given the degree of scatter in the linescan histograms, such as those in Figure 18, defining points A and B from the data in this form would be rather difficult. To simplify this task, the secondary wall (S2 plus S3 only) data were smoothed using the BMDP2R program for stepwise polynomial regression on the Burroughs B6900. Most of the regression curves represented polynomials of order 3 or less, such as those in Figure 19, while some represented higher order polynomials.

The cell corner sulfur levels were described by taking the ratio of the average cell corner counts (CC) to the value B in the adjacent secondary wall. This ratio has been called the CC/B ratio. The ratio of CC to the average secondary wall sulfur counts may also be an appropriate parameter to describe cell corner sulfur counts. However, if the gradient across the secondary wall is the result of some reactivity trend or diffusion limitations, comparison of cell corner counts to those in the adjacent portion of the secondary wall may be more appropriate.

a).

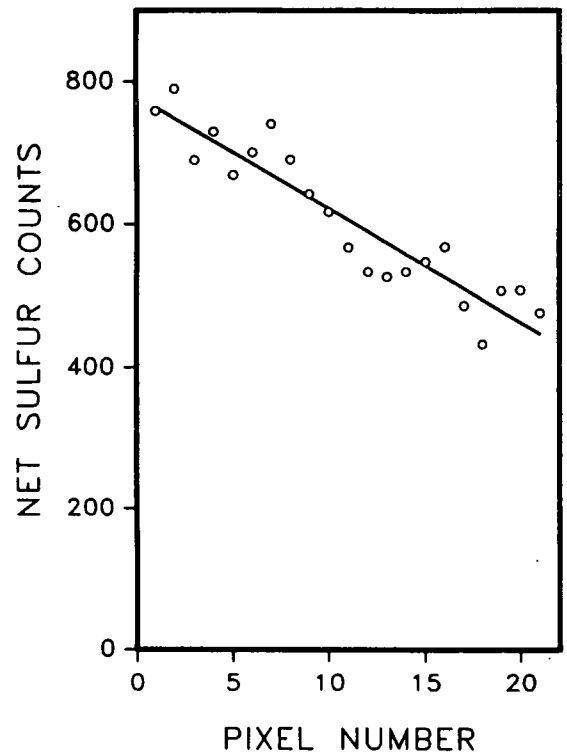

b).

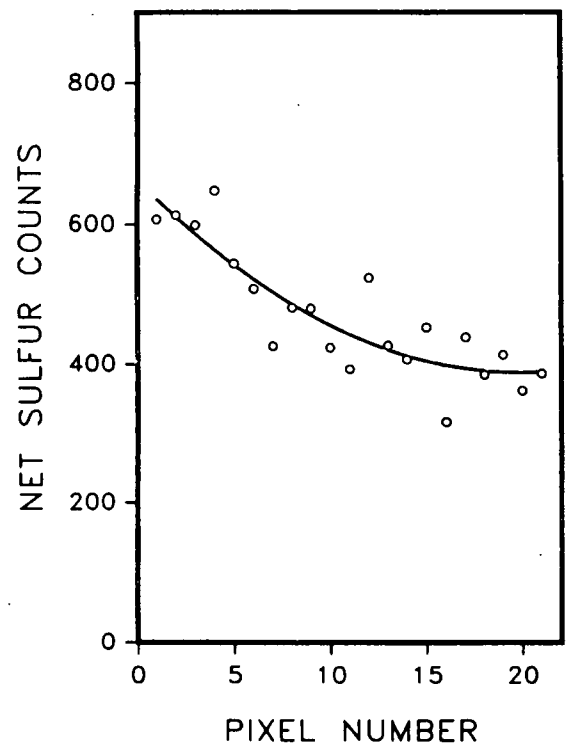

Figure 19. Linescan data for single secondary walls smoothed by stepwise polynomial regression (program BMDP/2R);
a). from the wall on the left in Figure 18a;
b). from the wall in Figure 18b.

VP1 Results

This and the upcoming sections discuss the linescan results for each of the three experiments. The linescan results are summarized in the manner shown in Table 8 for the VP1 data. Included in the table are the treatment means for net sulfur counts at selected points in the cell wall (A, B, CC), sulfur count ratio data (A/B, CC/B), and the average net sulfur counts per pixel (S) for the secondary wall (S2+S3).

Table 8. VP1 treatment means for various parameters used to describe the degree of sulfonation or relative degree of sulfonation of different cell wall layers. Sulfur content data from Table 7 included. 95% C.I. = 95% confidence interval.

Time, min.	Na_2SO_3 conc., mole/l	Parameter						Sulfur Content
		A	B	CC	A/B	CC/B	S	
20	0.48	288	188	530	1.65	2.97	225	0.41
20	1.03	393	262	773	1.49	2.89	304	0.53
20	1.59	585	402	1154	1.45	2.92	455	0.70
40	0.48	270	185	537	1.59	3.18	212	0.40
40	1.03	433	277	799	1.68	2.84	343	0.59
40	1.59	913	640	1733	1.42	3.08	722	0.71
	MEAN ±95% C.I.				1.55 ±.15	2.97 ±.22		

Within each of the experimental designs, the influence of treatment variables on the A/B and CC/B ratios was evaluated using an analysis of variance (AOV). The design of the AOV was a mixed model which accounted for all sources of variability in the data. These sources are illustrated in Figures 15 to 17. AOV tables for the VP1 cooks are shown in Table 9. Using

Table 9a as an example, all treatment terms (Time, Na_2SO_3 concentration) and their interaction (Time X Na_2SO_3) are fixed variables. Terms which account for random wall-to-wall variability (Wall), chip-to-chip variability (Chip), and variability between duplicate scans (Scan) are random variables nested within the treatment terms. The term, Location, accounts for systematic variations between walls near the edge of the chip and walls near the center of the chip. The AOV results from the three experiments will be discussed with their corresponding linescan results in each of the upcoming sections.

The A/B ratio and CC/B ratio data in Table 8 suggest no significant effects of time or sodium sulfite concentration on these parameters. The AOV results in Table 9a confirm the absence of these effects in the A/B ratio data. The AOV results for the CC/B ratio data in Table 9b also demonstrate no significant sodium sulfite concentration effect, but missing data prevented a rigorous analysis of the time effect. The AOV tables for both the A/B and CC/B ratio data demonstrated significant random wall-to-wall variability (Wall term), but the low F-ratio for the Location term demonstrated no systematic variability across the chip in the radial direction. There was also no significant chip-to-chip variability (Chip term) beyond that which can be attributed to variation between walls within the same chip.

All of the sulfur count data in Table 8 demonstrated an increase in net sulfur counts with sodium sulfite concentration, and an increase in net sulfur counts with time at only high liquor concentrations. These trends are confirmed by the analysis of variance table for S, the average net secondary wall counts, in Table 9c. This table demonstrates significant effects due to time, sodium sulfite concentration, and their interaction term (Time X Na_2SO_3). As with the A/B and CC/B ratio data, only random wall-to-wall variability (Wall) was significant among the other terms.

Table 9. AOV table for VP1 cooks; a). net A/B ratio; b). net CC/B ratio; c). net secondary wall sulfur counts (average net sulfur counts per pixel)

a). Net A/B ratio

Source	Error term	Sum of squares	DF	Mean square	F	Tail prob.
Time	Chip	0.03920	1	0.03920	0.06	0.809
Na_2SO_3 concen.	Chip	0.04516	2	0.02258	0.04	0.964
Time X Na_2SO_3	Chip	0.66032	2	0.33016	0.54	0.610
Chip	Wall	3.69049	6	0.61508	1.88	0.143
Location	Wall	0.40990	2	0.20495	0.63	0.557
Wall	Scan	7.20003	22	0.32727	10.10	0.000
Scan		1.16603	36	0.03239		

b). Net CC/B ratio

Source	Error term	Sum of squares	DF	Mean square	F	Tail prob.
Na_2SO_3 concen.	Chip	0.30766	2	0.15383	0.43	0.669
Chip	Wall	2.14789	6	0.35798	0.47	0.843
Location	Wall	0.49476	2	0.24738	0.32	0.734
Wall	Scan	12.20325	18	0.76270	2.96	0.006
Scan		6.95780	27	0.25770		

c). Net secondary wall sulfur counts (S)

Source	Error term	Sum of squares	DF	Mean square	F	Tail prob.
Time	Chip	150655	1	150655	8.03	0.030
Na_2SO_3 concen.	Chip	1845894	2	922947	49.22	0.000
Time X Na_2SO_3	Chip	227137	2	113568	6.06	0.036
Chip	Wall	112504	6	18751	0.37	0.585
Location	Wall	10415	2	5208	0.10	0.999
Wall	Scan	1119797	22	50900	420.66	0.000
Scan		4358	36	121		

The results for the mean net secondary wall sulfur counts are in close agreement with the corresponding sulfur content results, except for the presence of a time effect at higher sodium sulfite concentrations, which was not observed in the sulfur content data. A plot of sulfur count data against Schoniger flask sulfur content data is shown in Figure 20. The co$ined VP2 and LP1 data demonstrate a linear trend. The first five VP1 cooks (squares) demonstrate a linear trend which deviates markedly from that of the other two experiments. The sixth VP1 cook, which yielded mean secondary wall sulfur counts of 722, deviates considerably from the other VP1 data and is actually more in agreement with the VP2 and LP1 data.

These results suggest that the five VP1 cooks are actually deviating from the norm. Unusual levels of mass loss or deviations in section thickness would be likely sources for this deviation, but this is probably not the case. Such differences would appear as comparable differences in linescan background counts, which were not observed. A more likely source for this deviation may be incomplete chip impregnation. Recall that the VP1 cooks were impregnated using a procedure which gave only 90-95% impregnation. Assuming impregnation in the longitudinal direction is limiting (8,16), improper chip impregnation should yield lower sulfur contents in the center of the chip, where linescan data were collected. Although the sulfur content in the center of the chip is markedly affected, the effect on overall chip sulfur content is probably minimal.

In the case of the sixth VP1 cook, which deviates from the other five, it is likely that the longer time combined with the higher sodium sulfite concentration allowed excess sodium sulfite to diffuse into the center of the chip, resulting in more complete sulfonation there. This process may not occur at

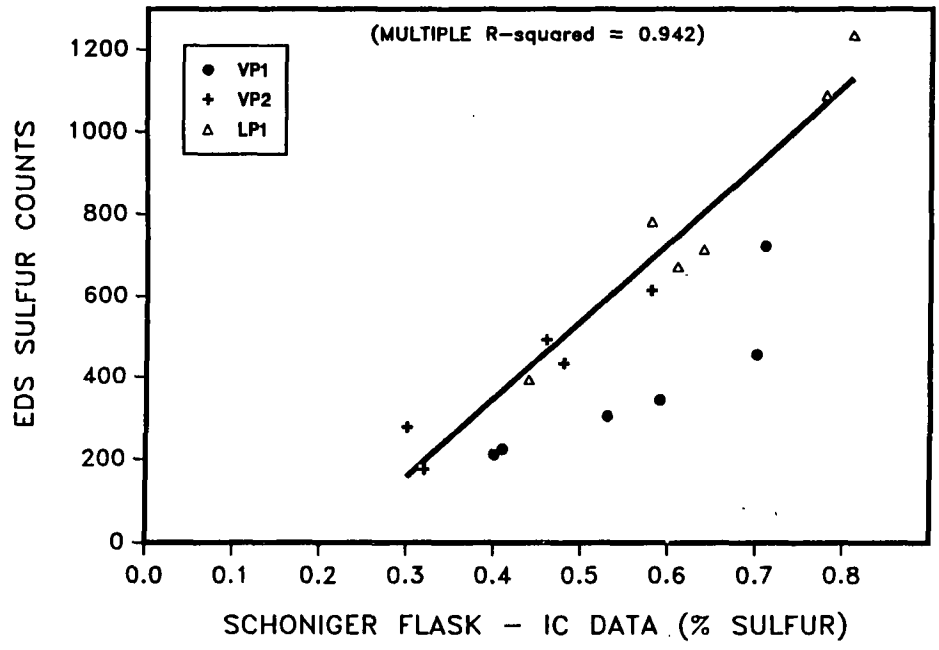

Figure 20. Plot comparing mean secondary wall net sulfur count data with Schoniger flask/ion chromatography sulfur contents.

lower liquor concentrations because of depletion of sulfite ions and, possibly, a more rapid reduction in liquor pH. These phenomena may restrict sulfite diffusion and consumption in the center of the chip during the later stages of the cook, thus maintaining the lower sulfur levels there. This would account for the interaction term in Table 9c.

VP2 Results

The analysis of the VP1 cooks revealed a great deal of variability which could be attributed primarily to random variability between cell walls. Systematic variability across the chip (Location) and random chip-to-chip variability (Wall) were not significant. Given these findings, some changes were made in the linescan collection procedure for the VP2 and LP1 cooks. Since random wall-to-wall variability, and not chip-to chip variablilty, was

the major source of random error, the number of chips evaluated was kept at two and the number of walls per chip was increased from three to four. Since systematic wall-to-wall variability did not seem to be too important, these four walls were divided among only two locations within the chip instead of three. These locations were near the edge (tangential face) of the chip and near the center of the chip with respect to the radial axis.

The linescans for the VP2 and LP1 cooks were performed from the lumen to cell corner instead of across the tangential double wall. This was done for two reasons. First, the double wall scans provided little added information over that from the single wall scans, and required more time to acquire. Second, the compound middle lamella data from the double-wall scans were found to be of little use. Single-wall scans into the cell corner provided all of the required data in one scan.

The treatment means for the VP2 cooks are shown in Table 10. The independent variable, effective Na_2SO_3 concentration, accounts for cooking liquor dilution in the chip by moisture which was in the chip prior to liquor impregnation. At the time of liquor impregnation, the chips used for the VP2 cooks had a moisture content of 29% (based on OD wood) due to conditioning at 100% RH. The chips used for the VP1 and LP1 cooks were bone dry, so the effective concentration would be that of the cooking liquor. These effective concentrations are used in the regression analysis and computer modeling.

As with the VP1 cooks, the A/B ratio results for the VP2 results are very consistent. These results imply that cooking to the same sulfur content at different temperatures does not influence the secondary wall sulfur distribution in vapor-phase cooks. This conclusion is confirmed by the AOV results in Table 11a, which reveal no other sources of variation.

Table 10. VP2 treatment means for various parameters used to describe the degree of sulfonation or relative degree of sulfonation of different cell wall layers. Sulfur content data from Table 7 included. 95% C.I. = 95% confidence interval.

Time, min.	Temp., °C	Na_2SO_3 conc., mole/l Liquor	Na_2SO_3 conc., mole/l Effective*	Parameter A	B	CC	A/B	CC/B	S	Sulfur Content
5	160	0.48	0.26	418	252	808	1.66	3.21	278	0.30
5	160	1.03	0.55	698	448	1396	1.63	3.15	492	0.46
20	140	0.48	0.26	253	156	477	1.66	3.12	176	0.32
20	140	1.03	0.55	621	388	975	1.62	2.54	434	0.48
		MEAN ± 95% C.I.					1.64 ±.06	3.01 ±.17		

* The effective Na_2SO_3 conc. accounts for liquor dilution by chip moisture within the chip.

The CC/B ratio data in Table 10 suggest a difference between treatments, but the AOV results in Table 11b cannot attribute this difference to the treatment variables. The interaction term (Time X Na_2SO_3) is also not significant. Although no significant random chip-to-chip variability was present, both random (Wall) and systematic (Location) wall-to-wall variability were found. The CC/B ratio was found to be higher towards the edge of the chip than it was towards the center.

The average sulfur count data for the secondary wall (S) in Table 10 demonstrated higher sulfur counts at higher sodium sulfite concentrations, and, in the case of the cooks using 1.03 molar sodium sulfite, demonstrated comparable sulfur counts at both time-temperature combinations. These results agree with the corresponding sulfur content data. The one discrepancy between the two sets of data is the relationship between the two cooks performed with

Table 11. AOV table for VP2 cooks; a). net A/B ratio; b). net CC/B ratio; c). net secondary wall sulfur counts (average net sulfur counts per pixel).

a). net A/B ratio

SOURCE	ERROR TERM	SUM OF SQUARES	DF	MEAN SQUARE	F	TAIL PROB.
Time-temp.	Chip	0.000594	1	.000594	0.01	0.925
Na_2SO_3 conc.	Chip	0.025881	1	.025881	0.43	0.547
Time X Na_2SO_3	Chip	0.000193	1	.000193	0.00	0.958
Chip	Wall	0.239517	4	.059879	0.99	0.445
Location	Wall	0.167383	1	.167383	2.77	0.116
Wall	Scan	1.387641	23	.060332	1.34	0.229
Scan		1.446042	32	.045189		

b). net CC/B ratio

SOURCE	ERROR TERM	SUM OF SQUARES	DF	MEAN SQUARE	F	TAIL PROB.
Time-temp.	Chip	1.927238	1	1.92724	2.77	0.171
Na_2SO_3 conc.	Chip	1.604022	1	1.60402	2.31	0.204
Time X Na_2SO_3	Chip	1.075369	1	1.07537	1.55	0.282
Chip	Wall	2.783253	4	0.69581	2.02	0.134
Location	Wall	1.768235	1	1.76824	5.11	0.030
Wall	Scan	7.925922	23	0.34461	6.25	0.000
Scan		1.764033	32	0.05513		

c). net secondary wall sulfur counts (S)

SOURCE	ERROR TERM	SUM OF SQUARES	DF	MEAN SQUARE	F	TAIL PROB.
Time-temp.	Chip	101841	1	101841	9.68	0.036
Na_2SO_3 conc.	Chip	892316	1	892316	84.85	0.001
Time X Na_2SO_3	Chip	7332	1	7332	0.70	0.451
Chip	Wall	42063	4	10516	0.56	0.832
Location	Wall	41057	1	41057	2.20	0.500
Wall	Scan	428965	23	18651	274.28	0.000
Scan		2183	32	68		

0.48 molar sodium sulfite. The two sulfur contents are comparable, while the sulfur counts (S) for the 140 ^{o}C cook are much lower than those obtained from the 160^{o}C cook.

The AOV results in Table 11c confirm the presence of the concentration effect observed in both sets of data and a significant effect due to the time-temperature combinations. The presence of this second effect can be attributed to the two 0.48 molar sodium sulfite cooks. Table 11c also reveals significant wall-to-wall variability with no other sources of variation.

LP1 Results

The LP1 data differ from the vapor-phase cook data with regard to changes in A/B ratio with treatment variables. The data in Table 12 show a marked decline in the A/B ratio as the pH shifts from acidic to alkaline, but no effect due to time. The AOV results in Table 13a confirm this observation. The A/B ratio data demonstrated random wall-to-wall and chip-to-chip variation, but no significant effect due to location within the chip.

The CC/B ratio data appear to be influenced by time and liquor pH. Although the AOV results in Table 13b demonstrate a significant time trend, the apparent trend due to pH is not significant, probably due to high chip-to-chip variability. The contributions of the Wall and Location terms are as before.

The LP1 sulfur count data, in Table 12, are in close agreement with the sulfur content data. Both types of data show a pronounced increase with increased time and when the pH is shifted from the acidic to alkaline range. The AOV results for the mean secondary wall sulfur count data in Table 13c confirm the existence of these trends, as both the time and pH effects are significant. Although there is no significant systematic variation across the

Table 12. LP1 treatment means for various parameters used to describe the degree of sulfonation or relative degree of sulfonation of different cell wall layers. Sulfur content data from Table 7 included.

Time, min.	Liquor pH	Parameter						Sulfur Content
		A	B	CC	A/B	CC/B	S	
0	4.3	608	345	1064	1.76	3.07	394	0.44
0	8.4	864	625	1796	1.36	2.88	672	0.61
0	10.5	1062	707	1826	1.50	2.57	781	0.58
60	4.3	1067	637	1724	1.69	2.77	714	0.64
60	8.4	1696	1140	2316	1.48	2.05	1234	0.81
60	10.5	1277	1021	2001	1.26	1.99	1087	0.78
	MEAN				1.51	2.55		

thickness of the chip, significant random wall-to wall variability and chip-to-chip variability are present.

The observed changes in A/B and CC/B ratio with pH and time could be attributed to the influence of these two treatment variables on diffusion through the cell wall and reactivity differences across the cell wall. If diffusion were a limiting factor in these cooks, pH could influence the A/B ratio through its effects on cell wall diffusivity. Alkaline pH levels are more likely to induce swelling in the cell wall, which will open the wall structure and increase cell wall diffusivity. The higher diffusivities should then yield flatter distributions. Yield loss during the 60 minute alkaline cooks could have also increased diffusivity, resulting in flatter distributions. In addition to these effects, condensation reactions during acidic or bisulfite pulping will result in the formation of cross-links between lignin

Table 13. AOV table for LP1 cooks; a). net A/B ratio; b). net CC/B ratio; c). net secondary wall sulfur counts (average net sulfur counts per pixel).

a). net A/B ratio

SOURCE	ERROR TERM	SUM OF SQUARES	DF	MEAN SQUARE	F	TAIL PROB.
Time	Chip	0.097219	1	.09722	0.67	0.445
pH	Chip	2.334710	2	1.16736	8.03	0.020
Time X pH	Chip	0.510797	2	0.25540	1.76	0.251
Chip	Wall	0.872090	6	0.14535	3.21	0.014
Location	Wall	0.090221	1	0.09022	2.00	0.187
Wall	Scan	1.582616	35	0.04522	4.61	0.000
Scan		0.470653	48	0.00981		

b). net CC/B ratio

SOURCE	ERROR TERM	SUM OF SQUARES	DF	MEAN SQUARE	F	TAIL PROB.
Time	Chip	7.773678	1	7.77368	6.94	0.039
pH	Chip	7.107676	2	3.55384	3.17	0.115
Time X pH	Chip	1.105924	2	0.55296	0.49	0.633
Chip	Wall	6.721078	6	1.12018	3.85	0.005
Location	Wall	0.143840	1	0.14384	0.49	0.492
Wall	Scan	10.182418	35	0.29093	24.75	0.000
Scan		0.564185	48	0.11754		

c). net secondary wall sulfur counts (S)

SOURCE	ERROR TERM	SUM OF SQUARES	DF	MEAN SQUARE	F	TAIL PROB.
Time	Chip	3773887	1	3773887	30.30	0.000
pH	Chip	3240628	2	1620314	13.01	0.007
Time X pH	Chip	330565	2	165282	1.33	0.333
Chip	Wall	747216	6	124536	4.31	0.039
Location	Wall	6	1	6	0.00	0.999
Wall	Scan	1011578	35	28902	69.31	0.000
Scan		20012	48	417		

units, inhibiting swelling even further. This could enhance diffusion limitations under bisulfite pulping conditions. In the case of the CC/B ratio, the decrease in this parameter with time could be a result of selective sulfonation of the outer S2 or selective delignification of the middle lamella in the later stages of the cooks.

Analysis of the sulfur distribution data from the three factorial experiments has yielded several important results.

1. Under vapor-phase cooking conditions, the parameters used to describe the secondary wall sulfur distribution (A/B ratio) and cell corner counts (CC/B ratio) were not influenced by time, temperature, or sodium sulfite concentration. The CC/B ratios obtained agree with the results of Beatson, et al. (17).
2. Under liquid-phase cooking conditions, alkaline pH levels yielded flatter secondary wall sulfur distributions, as measured by the A/B ratio, than acidic pH levels.
3. Under liquid-phase cooking conditions, longer cooking times gave lower relative cell corner counts (CC/B ratio).

Of principle importance is the presence of the secondary wall sulfur gradients. The existence of these gradients is confirmed by the 95% confidence intervals for the mean A/B ratio data in Tables 8 and 10. These intervals were all well above a value of 1.0, which represents a flat distribution. This demonstrates that the secondary wall gradients exist beyond any reasonable doubt.

Other linescan data

Along with the samples from the above experiments, two other sets of samples underwent linescan analysis. The first set of samples was latewood chips which had undergone no sulfite treatment. The average sulfur content of these chips was determined by Schoniger flask combustion - ion chromatography to be 0.003%. Given the sensitivity of this test, this result could be interpreted as a 0% sulfur content determination. This is confirmed by STEM-

EDS spectral data which yielded average net sulfur counts of zero, and by linescan data collected at 120 seconds per pixel which detected virtually no sulfur in the cell wall.

The second set of samples was a set of chips which underwent vacuum impregnation with the VP1 chips in 1.59 molar sodium sulfite. After the 30 minute impregnation, the chips underwent repeated soakings in distilled water in the same manner as the cooked chips. Schoniger flask combustions with ion chromatography yielded a sulfur content of 0.19% for these samples.

Linescans were performed on two of these chips using the experimental design used for the VP2 and LP1 chips. Because of the low sulfur contents, the linescans were collected at 90 seconds per pixel. The average A/B ratio for these samples was 1.70, while the average CC/B ratio was 3.64. The presence of the pronounced secondary wall sulfur gradient may be attributed to slow penetration of the dry cell wall by the liquor during impregnation (42,43,44) combined with rapid sulfonation at sulfur contents below 0.1% (38). The higher CC/B ratio may be the result of different relative reactivities between the secondary wall and middle lamella lignin at low levels of sulfonation.

The CC/B ratio of 3.64 is higher than those obtained from the other samples, which were cooked. This apparent drop in CC/B ratio between impregnation and the end of the cook contradicts the results obtained from cell wall tissue fractions by Whiting and Goring (21). At the early stages of 140°C sulfite cooks (no impregnation or heat-up time), the sulfur contents of their secondary wall and middle lamella fractions represented CC/B ratios of 2 or less. As the cooks progressed, the data suggested an increase in CC/B ratio to a value comparable to those obtained in the present study. The difference

in these two sets of results may be a consequence of the difference in temperature at which at which the early stages of sulfonation occurred. Sulfonation at room temperature may not exhibit the differences in relative reactivity observed at higher temperatures, which suggests possible differences in the sulfonation mechanism at these two temperatures. Species differences and the nature of the samples (tissue fractions vs. chips) may also be factors.

Analysis of combined data

In order to detect general trends which may not have been detected in the individual experiments, linear regression analyses were performed on the A/B ratio data from all of the cooks against a variety of cook variables. Figures 21 and 22 show the linear regression results obtained when the A/B ratio is plotted against liquor pH and chip sulfur content, respectively. Although the correlation coefficients are rather low, these graphs suggest that the secondary wall sulfur distribution becomes flatter as final pH and chip sulfur content are increased.

Performance of a stepwise regression against a wide number of independent variables yielded the results in figures 23 and 24. As with the simple linear regressions, the multiple correlation coefficients are not overly high, but Figure 23 suggests a decline in A/B ratio with increased pH and sulfur content. The apparent influence of pH on the secondary wall sulfur distribution can again be attributed to the greater tendency for the wood to swell at higher pH levels, resulting in faster sulfite ion diffusion across the cell wall. The influence of sodium sulfite concentration can also be explained in terms of limited diffusion and will be discussed with the diffusion model results.

One problem with this particular analysis is the description of sulfur distribution in terms of sulfur content, which is not an independent variable.

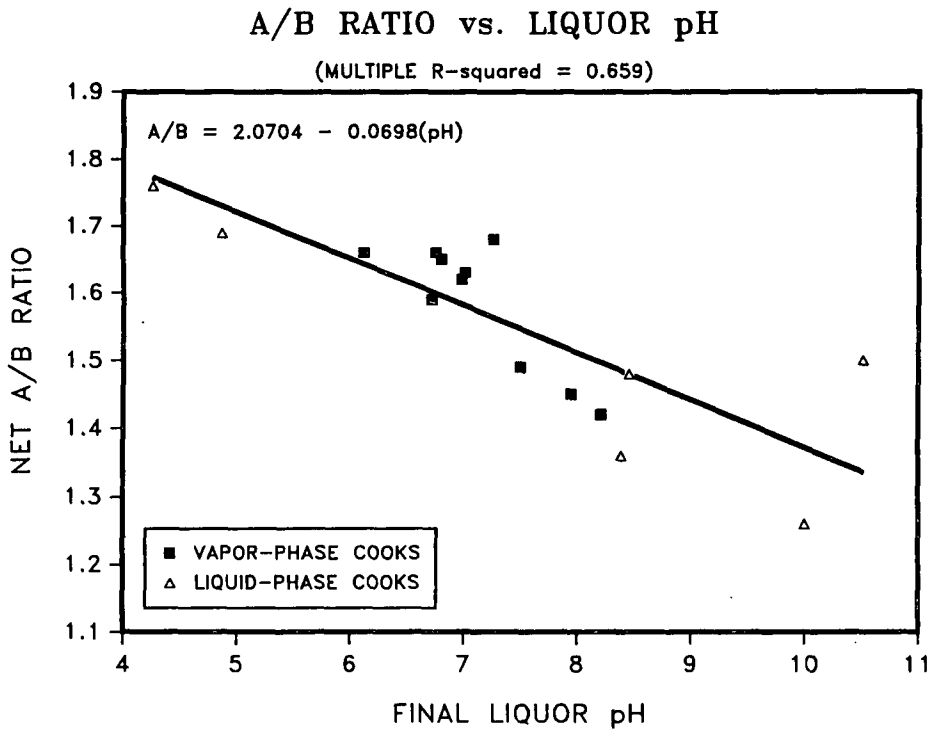

Figure 21. Simple linear regression of A/B ratio vs. liquor pH.

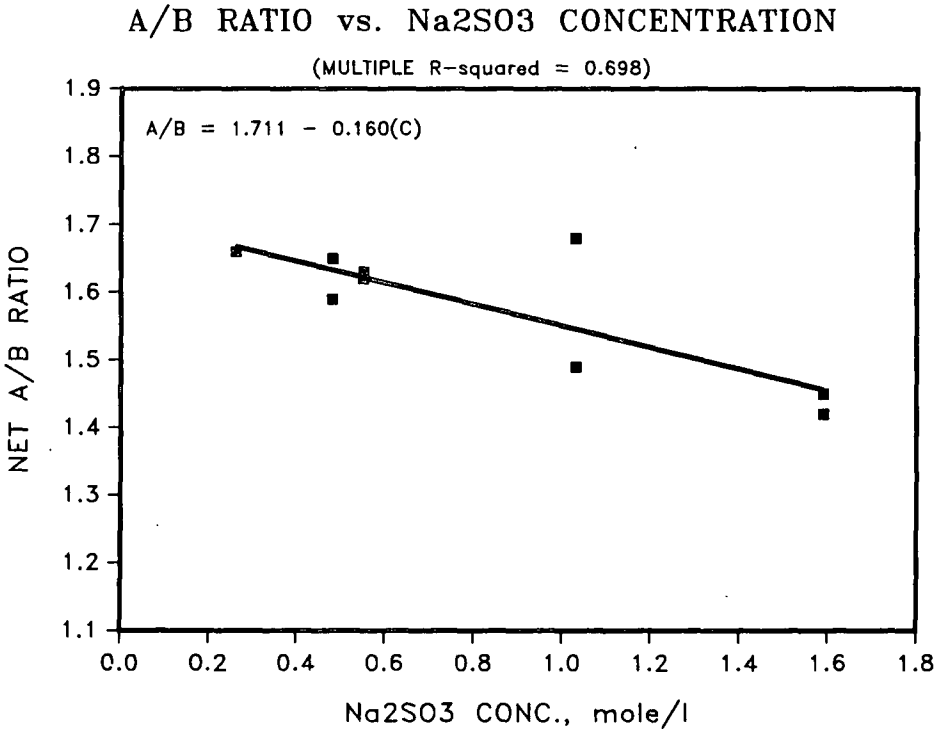

Figure 22. Simple linear regression of A/B ratio vs. liquor Na_2SO_3 concentration. VP cooks only.

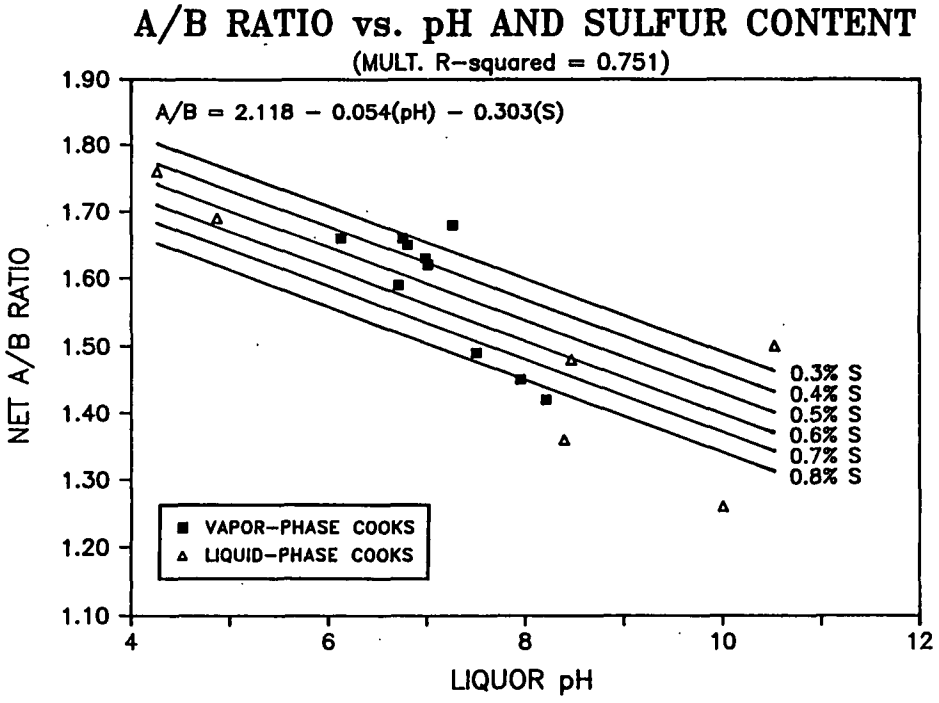

Figure 23. Multiple linear regression of A/B ratio vs. liquor pH (abscissa) and chip sulfur content (parallel lines).

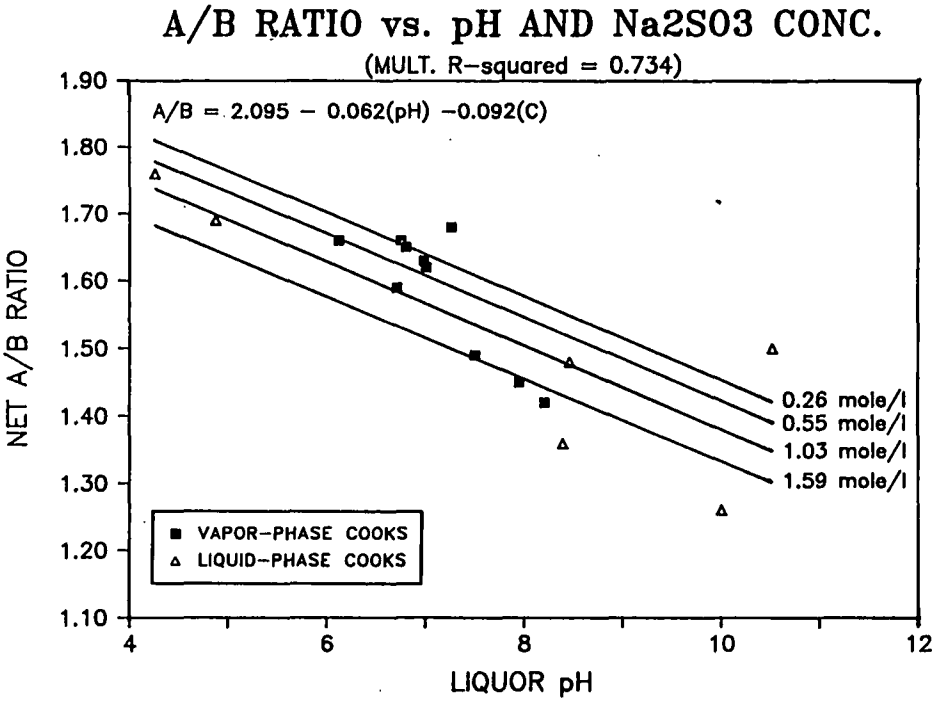

Figure 24. Multiple linear regression of A/B ratio vs. liquor pH (abscissa) and liquor sodium sulfite (Na_2SO_3) concentration (parallel lines).

If the sulfur content were replaced with liquor sodium sulfite concentration, the same general relationship is obtained, as shown in figure 24. The similarity between the two figures can be attributed, in part, to a close relationship between sulfur content and sodium sulfite concentration. See figure 25. Sulfur content depends rather strongly on sodium sulfite concentration in the vapor-phase cooks, but since the liquid-phase cooks were all done at 1.03 mole/l, no such conclusion can be made for these cooks.

MASS LOSS

The test for mass loss at long exposures tested exposures of 20 to 60 seconds. The results from this test, which are shown in Table 14, revealed no

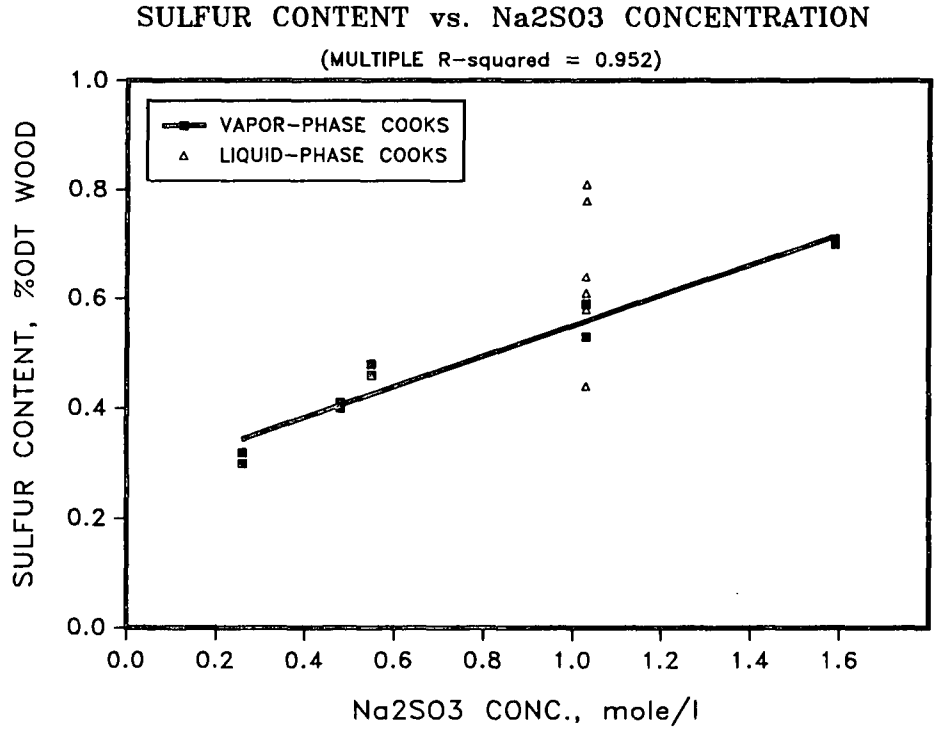

Figure 25. Simple linear regression of A/B ratio vs. liquor sodium sulfite (Na_2SO_3) concentration. Regression lines are for vapor-phase cooks only.

Table 14. Comparison of net sulfur counts at various linescan accumulation times. The consistency of the count rates was initially interpreted as an absence of mass loss.

Accumulation time, secs/pixel	Average counts/pixel	Average counts/sec
20	123.4	6.2
30	185.5	6.2
45	288.9	6.4
60	377.3	6.3

change in count rate with exposure time. This suggested that the mass per unit volume did not change between 20 and 60 seconds exposure. Under the assumption that mass loss was gradual, it was tentatively concluded that mass loss was not occurring in the STEM.

The findings of Mary, Revol, and Goring (30), which were published several months after the above test was done, cast much doubt on the conclusion that mass loss was not occurring. Their data demonstrated mass loss to occur very rapidly (within a few seconds) in wood samples under conditions used for x-ray microanalysis. In the above test, mass loss may have occurred within a few seconds, resulting in constant count rates beyond that time. The higher counts during this short time interval probably did not make a significant contribution to the total counts obtained after 20 or 60 seconds, so there was no apparent difference between these two times. Since the test at longer times was unable to detect rapid mass loss, the mass loss determinations using timescans at shorter times were performed.

On the average, mass loss in TEM was approximately 40%. Two mass loss curves from timescans are shown in Figure 26. The curve in Figure 26a has a

a).

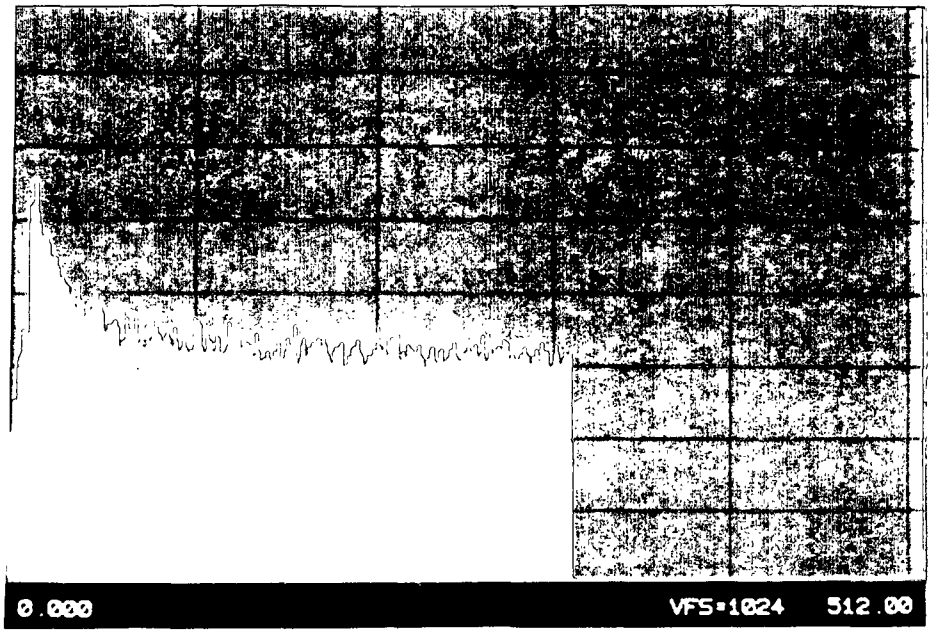

b).

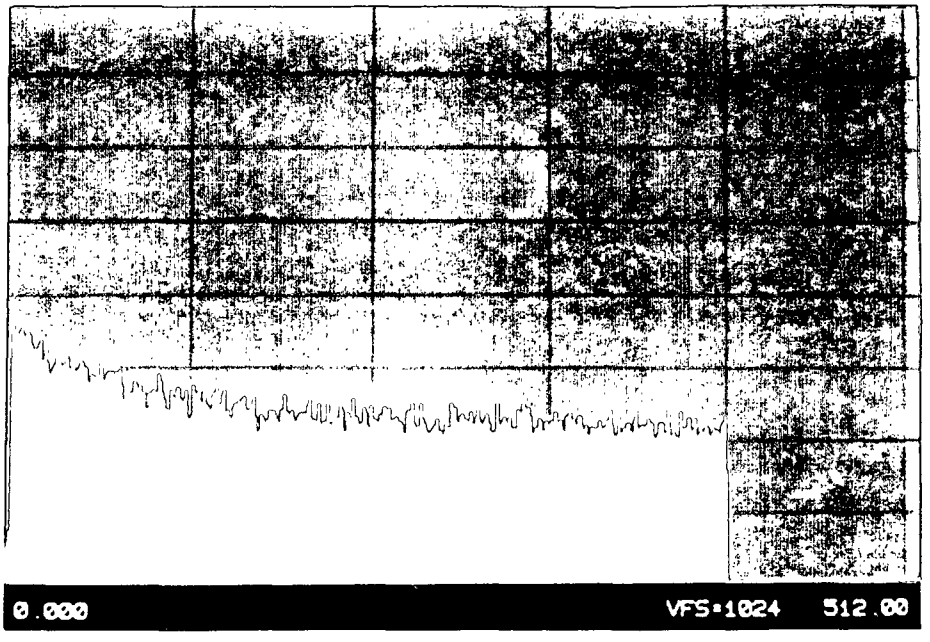

Figure 26. Mass loss curves for 250 nm thick sulfonated wood cross-sections embedded in Spurr epoxy resin;
a). higher beam intensity giving 42.6% mass loss;
b). lower beam intensity giving 38.6% mass loss.

much faster rate of mass loss due to a higher beam intensity (electron flux), but the overall mass loss is comparable to that obtained at a lower beam intensity (Figure 26b). This agrees with other studies which found increased beam intensity to increase the rate of mass loss, but always yielded the same final mass loss (30,45). If mass loss were plotted against electron dose, which encompasses beam intensity and time, different beam intensities give very similar mass loss curves (30).

During the course of linescan collection, the samples were exposed to several types of electron beams of varying intensity. Initially, the sample was examined under a TEM electron beam of moderate intensity in order to search for a suitable wall to scan. Once the wall was found, the linescan was set up in a STEM scanning mode, while the linescan itself was performed in what could be called STEM dot mode. Dot mode refers to the situation where a very fine and intense electron probe is stationary on the sample for a significant period of time (10 - 60 seconds). It was suspected that exposing the sample to such a probe, as opposed to the broader TEM beam, would induce added mass loss in the irradiated area. To test this possibility, samples were exposed in TEM mode for a sufficient amount of time to allow the mass loss curve to level off. The 100CX was then switched to STEM scanning mode for a few minutes and to STEM dot mode. The results showed that after the initial mass loss in TEM mode, no further mass loss occurred in STEM mode.

This observation could be the result of conformance with the observed trends concerning the relationship between electron dose and mass loss, or to a stabilization of the sample under the less intense TEM beam or STEM scanning beam. Data generated in this work support the existence of a stabilization effect in at least some cases. Linescans were performed in areas which had been exposed to a STEM scanning beam for at least 5 minutes and adjacent areas

which had never been exposed to the electron beam. In a number of cases, the linescan across the area which had been previously exposed to the STEM scanning beam gave higher counts than that across the adjacent previously unexposed area. This suggests that the previously exposed area, or the resin in this area, was in some way cured by the electron beam in a manner which increased sample stability. In the case of a very intense beam irradiating a previously unexposed area, extensive mass loss can occur before the curing effect can occur.

Because of low count rates, it was difficult to collect good sulfur loss data in TEM mode. Mass loss and total sulfur loss data obtained in scanning STEM mode are shown for the secondary wall and cell corner in Tables 15 and 16. The overall mass loss results for the secondary wall generally agree with those obtained in TEM mode. The loss of net sulfur counts was much lower than the overall mass loss. This is probably due to the greater resistance of the sulfonated lignin to mass loss (30).

Table 15. Secondary wall mass loss data obtained from STEM scanning mode.

Sample	Wall	Timescan loss data, % Total-mass	Net-sulfur
1	1	-41.5	-8.5
1	2	-53.2	-26.5
1	3	-47.3	-16.6
1	4	-44.4	-6.0
1	Mean	-47.8	-14.4
2	1	-34.6	-20.8
2	2	-41.6	-7.7
2	3	-47.3	-5.3
2	4	-41.5	-12.1
2	Mean	-41.3	-11.5
Overall	Mean	-44.6	-13.0

Table 16. Cell corner mass loss data obtained from sample 1 in Table 15 using STEM scanning mode. These data were not obtained from the same walls as the secondary wall data.

Wall	Total mass loss, %
A	-21.1
B	-38.3
C	-26.7
D	-11.6
E	-24.0
Mean	-24.3

Sample 2 in Table 15 also provided total mass loss data for the cell corner. These data are shown in Table 16. No sulfur loss data were available because the high magnifications required to obtain cell corner data caused rapid mass loss. This required short time increments which prevented accumulation of sufficient sulfur counts. As shown in Table 16, the cell corner mass loss results are much lower than those from the secondary wall, probably as a result of the higher lignin levels in the cell corner. Assuming the absence of matrix effects, the sulfur loss levels are probably comparable to those in the secondary wall.

As shown in Table 17, the relative amounts of total mass loss between the secondary wall and cell corner in these experiments are comparable to those derived from the results of Mary, et al.(30). These previous results supplied mass loss results for individual cell wall components. To convert these results to those in Table 17, a secondary wall with a 25:25:50% lignin : hemicellulose : cellulose ratio and a cell corner of 100% lignin were assumed. As shown in Table 17, their results demonstrated greater mass loss levels than those obtained in this work. The difference is probably due to the presence of resin in the samples used in this work. This helped stabilize the sections against further mass loss.

Table 17. Comparison of mass loss results with those of Mary, et al.(30). The wall layer mass loss data for Mary, et al. was estimated from mass loss data for individual wall components and rough estimates of their relative proportions within the wall layers.

Wall layer	Mass loss, % This work	Mary, et al.
Secondary	-41.3	-55.3
Cell corner	-22.3	-30.0
Ratio (CC/2° wall)	0.54	0.54

The mass loss results presented here indicate that mass loss and sulfur loss can have a pronounced effect on the detected sulfur levels within the section. However, their influence on cell wall sulfur distribution is not as clear. In order to measure differences in sulfur loss across the cell wall, scanning STEM timescan data must be collected at high magnifications from selected areas in the cell wall. As with the cell corner data, higher magnifications in scanning STEM mode result in higher mass loss rates. The shorter time intervals required to detect the loss in counts yield sulfur counts which are too low to give useful results. Therefore, the measurement of sulfur loss across the cell wall was not possible.

POSSIBLE SOURCES OF THE OBSERVED SULFUR DISTRIBUTIONS

All sulfonation treatments tested resulted in cell wall sulfur distributions possessing two key characteristics: a bound sulfur gradient across the secondary wall, and a high bound sulfur concentration in the middle lamella. The secondary wall gradients were characterized by a decline in bound sulfur concentration from the S3 layer to a point in the S2 layer at or near the S1 layer. The sulfur concentration then increased by a factor of two to

three from the outer S2 layer to the middle lamella. Possible sources of the observed secondary wall sulfur gradient have been investigated through the literature, experiments, and mathematical modeling. The sources investigated were lignin distribution and reactivity, and limitations on sulfite ion diffusion into the cell wall from the lumen.

LIGNIN DISTRIBUTION

Previous Studies

Numerous studies have evaluated lignin distribution in a variety of species, including southern pine. These studies have used a variety of techniques, such as lignin skeletonizing (35,46), UV microscopy (32,47), and x-ray analysis of brominated wood (33,34,48,49). All techniques found a fairly uniform S2 lignin distribution in all species evaluated, but a number of studies found higher lignin levels in the S3 layer. In black spruce branchwood, Scott and Goring (47) found enhanced S3 lignin concentrations in many, but not all, of the cells examined. Although many peaks appearing at the lumen/S3 interface were artifacts, spectral data confirmed that many of the observed absorbance peaks at the S3 layer were the result of higher lignin concentrations and not an artifact.

Of primary concern are the lignin distribution studies performed on loblolly (southern) pine. Studies based on lignin skeletonzing and X-ray analysis of brominated wood have indicated a uniform lignin distribution across the S2 layer and higher levels in the S3 layer (35,46,48,49). A schematic of such a distribution is shown in Figure 27. In an effort to quantify this difference, Saka and co-worker (48,49) found the ratio of S3 to S2 lignin levels to be about 1.4. These findings were not confirmed by those of Plouff (33), who with x-ray analysis of brominated latewood, found a uniform

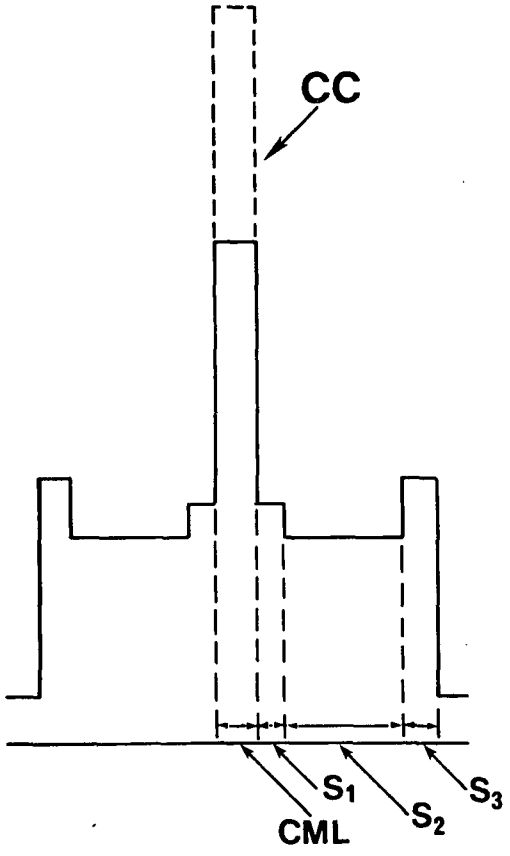

Figure 27. Schematic of the cell wall lignin distribution in loblolly pine (48,49).

lignin concentration across the entire secondary wall. It is likely that the contradiction in results could be the result of the inconsistent presence of the lignin-enriched S3 layer, such as that observed by Scott and Goring (47) in spruce branchwood. As it now stands, both the accuracy of the skeletonizing and bromination techniques are questionable due to the lack of a thorough knowledge of the chemistry involved in the two techniques (34,35).

A higher lignin level in the S3 could account for much of the difference in sulfur counts between the S3 and the minimum near the S1. However, the S3 includes only the first few pixels in the linescan and, as exemplified by the data in Figure 18, a gradual decline that extended well beyond the S3 layer was

usually observed. If the sulfur distributions were entirely the result of the lignin distributions recorded in the literature, there would be a sulfur peak in the S3, an abrupt drop in counts at the S3-S2 interface, and a flat distribution across the S2. In order to obtain a better understanding of cell wall lignin distribution in the southern pine latewood used for this study, lignin distribution was evaluated with UV microscopy.

UV Microscopy of Southern Pine latewood

The lignin distribution data obtained by UV microscopy took several forms. Data obtained at the U.S. Forest Products Laboratory consisted of photographs of the cell walls taken in a UV microscope and densitometer traces across the cell walls obtained from the negatives of these photographs. Lignin distribution profiles were also obtained with the help of Carl Zeiss, Inc. using UV microspectrophotometry. This equipment also provided UV spectra from various regions of the cell wall. Despite limitations, these data provided a somewhat clearer picture of cell wall lignin distribution.

The UV photographs obtained from two of the samples provided a good gualitative view of cell wall lignin distribution. A photo from a treated wood chip is shown in Figure 28. The photo reveals a darker middle lamella due to the higher lignin levels there. The S3 layer is also darker in some places, suggesting a lignin-enhanced S3 layer.

The dashed line across the double wall indicates the path of a densitometer trace, the profile from which is shown in Figure 29. This profile represents the lignin distribution across the cell wall, which, in this case, consists of a middle lamella peak, a flat distribution or gradient across the S2 layer, and a peak in the S3 layer. Most of the distributions

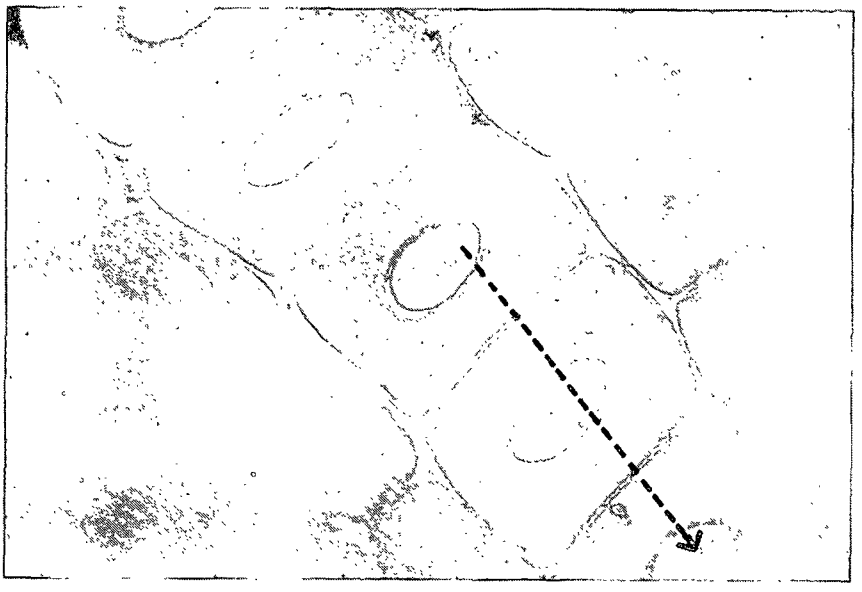

Figure 28. UV photograph of cell walls from sample 3JX-EM, showing the path of the densitometer trace. Photograph taken using a 300 nm light source.

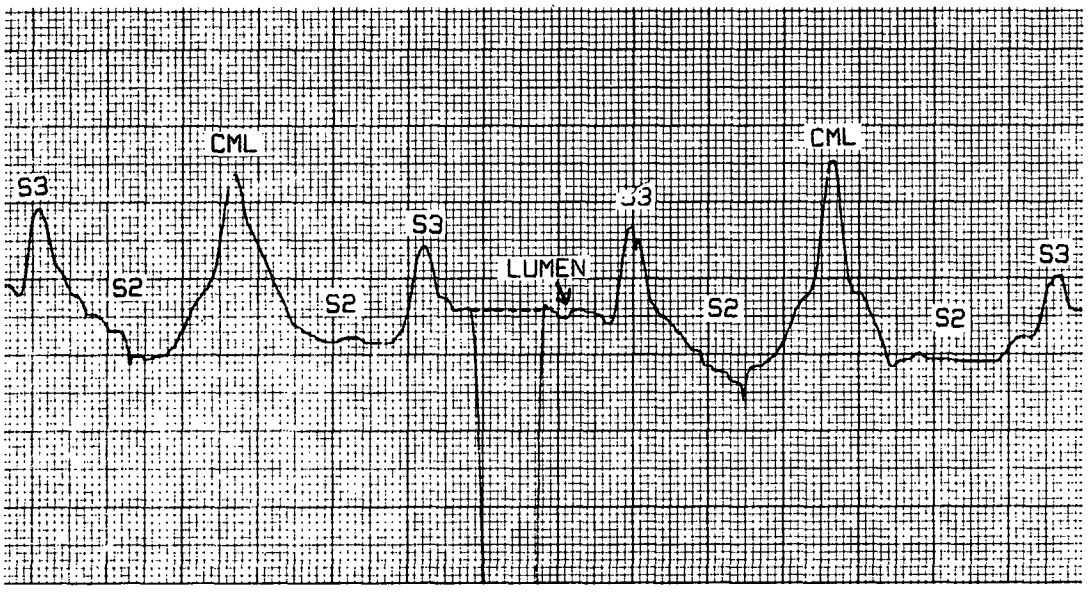

Figure 29. Densitometer trace from the above cell wall.

obtained had flat S2 layer distributions or slight gradients across the S2 layer. Many had peaks in the S3 layer. The other profiles are shown with their corresponding UV photographs in Appendix 2.

These lignin distributions had many simularities to the observed sulfur distributions, but these data should be interpreted with some caution. A lack of familiarity with the densitometer prevented the establishment of a scale by which to measure density variations. This problem was complicated by the necessity of using different exposures to obtain the negatives; the negatives for the non-treated samples were obtained at a higher exposure than those for the treated samples. Because density and contrast in the UV negatives rely heavily on exposure, particularly exposure time (47), comparisons between the two samples should be done with caution.

Interpretation of the S2 distribution data also requires some caution. It is generally assumed in this kind of work that the section thickness is uniform across the cell wall. However, thickness variations across the S2 layer, such as those arising from sectioning artifacts, could create what appear to be lignin gradients across the S2 layer. This is probably the case with the two gradients observed in Figure 29. Examination of the corresponding walls in Figure 28 can detect the lighter regions (lower absorbance) in the outer secondary wall which result in the observed gradients. Although it may not be apparent in Figure 28, closer examination of the original photograph for Figure 28 reveals a strong orientation of these areas in the direction perpendicular to the direction in which these samples were sectioned. These lighter areas were sometimes observed extending into adjacent cells. These observations strongly suggest that the observed S2 gradients in Figure 29 are sectioning artifacts. Although the presence of artifacts is not obvious in the other walls displaying an S2 lignin gradient, this finding does cast some doubt

30a).

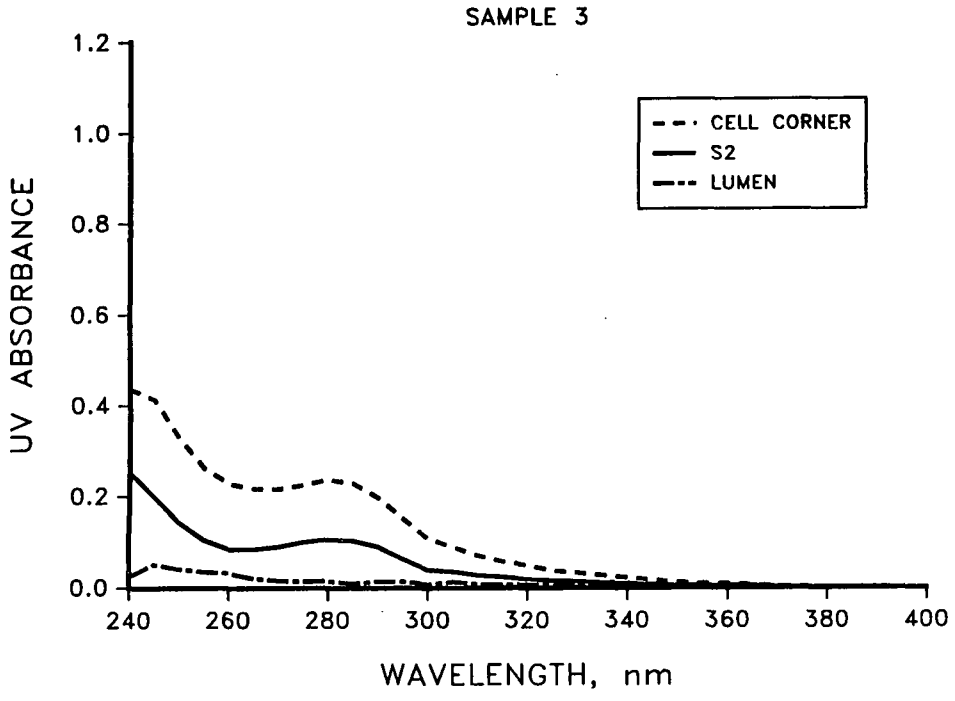

30b).

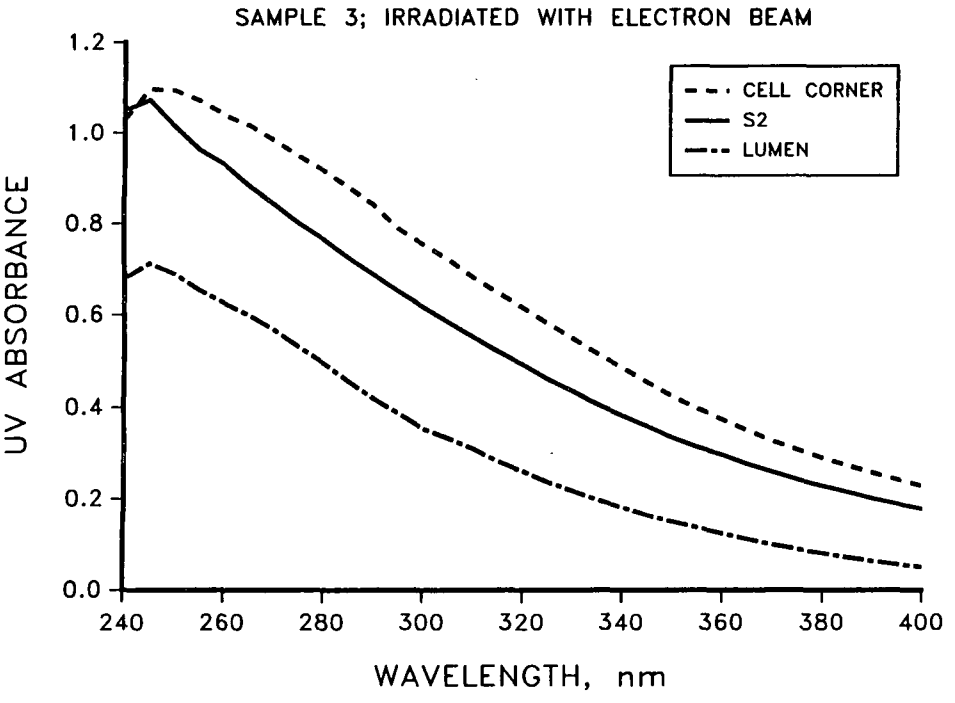

Figure 30. UV spectra obtained by microspectrophotometry.
a). Sample 3, showing little absorbance by the resin;
b). Sample 3-EM, showing considerable UV absorbance by the resin after electron beam exposure;
c). Sample 1, showing significant absorbance by the resin.

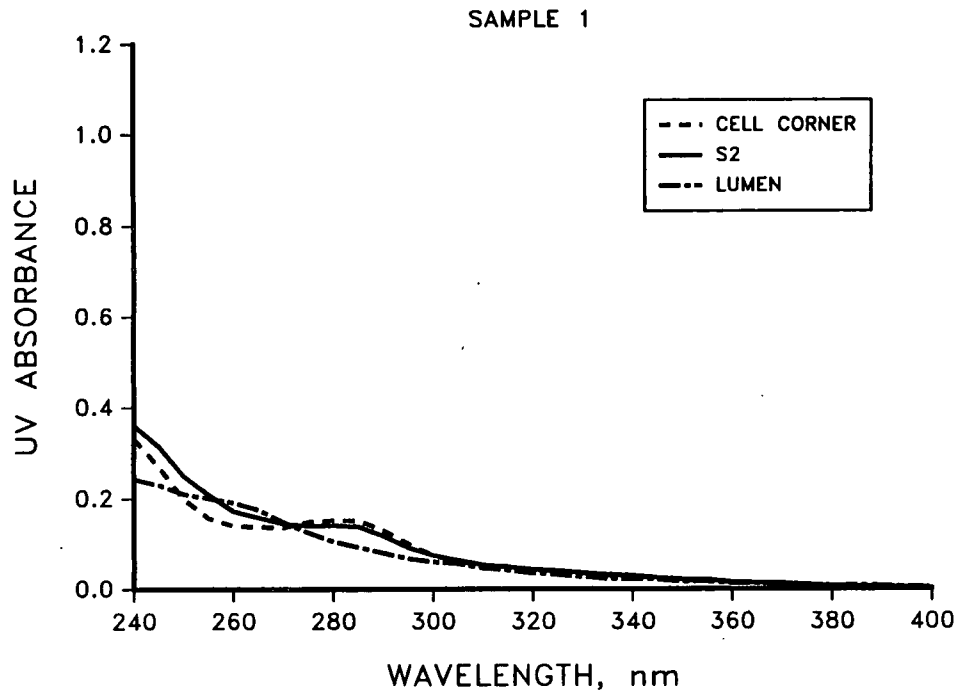

30c).

on their existence. In any case, the flat S2 lignin distribution predominated and most of the observed gradients were not overly pronounced.

The spectra and distributions obtained from the UV microspectrophotometry supplemented the data obtained from the densitometry work. The spectra, examples of which are shown in Figure 30, reveal the relative absorbances of the secondary wall (S2 layer), cell corner, and the resin in the lumen throughout the UV spectrum. The spectrum in Figure 30a represents most of the data obtained. In this spectrum, the more lignified cell corner absorbs more UV radiation than the S2 layer. The resin had little absorbance above 272 nm. After subtracting resin absorbance, the absorbance ratios obtained were generally between 2.0 and 2.7 in the 280-300 nm range. This compares to a value of 2.9 obtained by UV microscopy of southern pine (33), and a value of 3.8 by bromination/SEM-EDS of loblolly pine (49).

Figures 30b and 30c demonstrate some inconsistencies in the spectral data, which also appear in some of the distribution data. Both sets of spectra reveal significant absorbance by the resin. Comparison of Figures 30a and 30b suggests an influence of electron beam irradiation on UV absorbance by the resin. These two sets of spectra were obtained from sections of the same chip (sample 3; chip 1). All samples are described in Table 6. Those used to acquire the data in Figure 30a were not irradiated with an electron beam (sample 3), while those used to acquire Figure 30b were irradiated (sample 3-EM). The resin in the sections which were irradiated had a much higher UV absorbance. Chip 2 from sample 3 also gave sections which had extremely high UV absorbances after irradiation under the STEM electron beam. This can be seen in the UV photographs and densitometer traces in Appendix 2.

In some cases, the resin in samples which were not irradiated with an electron beam demonstrated substantial UV absorbance. An example of this is shown in shown in Figure 30c, where the resin absorbance at 260 nm is actually higher than that of the S2 layer or cell corner. The occurrence of high resin absorbance in some of the samples could reflect inconsistencies in the resin supply or in resin preparation in the lab. Since there is an unknown amount of resin in the cell walls, the contribution of the resin absorbance to the wall absorbance is not known. This complicates any efforts to obtain quantitative or semi-quantitative results from samples showing high UV absorbance by the resin.

An example of lignin distribution data obtained at 280 nm by UV microspectrophotometry is shown in Figure 31. This lignin distribution data has most of the same features as those from the microdensitometry. The three basic characteristics are the middle lamella peak, the generally flat S2 distribution, and a frequent S3 peak. There is some scatter in the data,

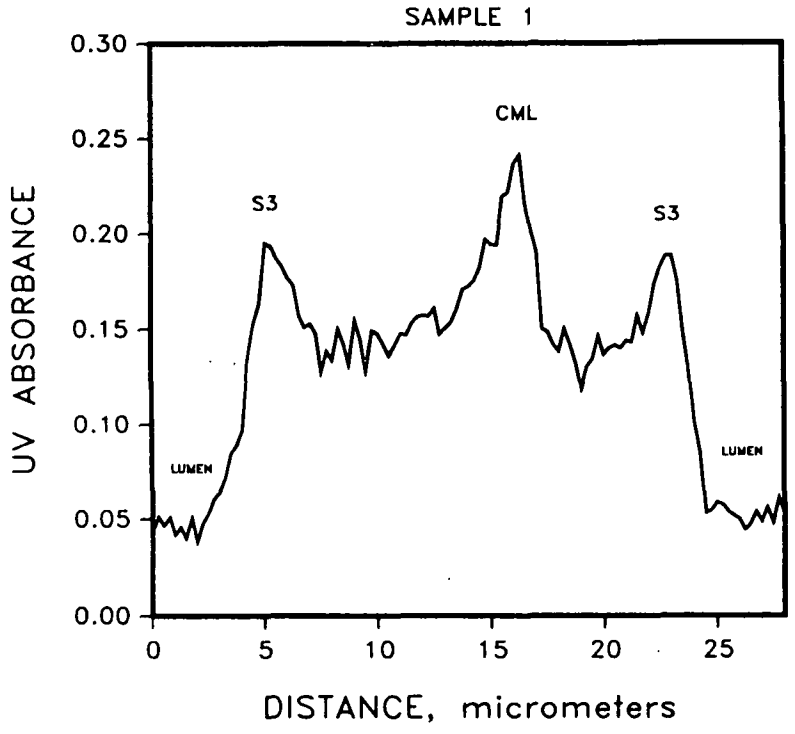

Figure 31. Lignin distribution obtained by UV microspectrophotometry. Sample 1, chip 1.

probably due to some imperfections in the section and, possibly, some noise in the data. Wider beams give smoother profiles, but this obscures important details in the distribution. Other scans are shown in Appendix 3. As with the microdensitometer data, some of these data exhibit high levels of UV absorbance by the resin.

The data from both experiments reveal some interesting results concerning lignin distribution in southern pine latewood. As has been observed in other studies (33,35,46,47,48), these experiments have demonstrated an S2 lignin distribution which is usually flat. A significant number of cell walls exhibited an S2 gradient, but at least some of these could be attributed to artifacts, while many of the other gradients were not overly pronounced.

The observation of a peak in the S3 layer also agreed with many of the previous works (35,46,47,48). The findings of Scott and Goring (47), however, suggest caution when studying lignification of the S3 layer with UV microscopy. They found that separation of the resin and cell wall at the lumen/S3 interface results in diffraction of the incident light in such a way as to form what appears to be a pronounced absorbance peak at the interface. Careful examination of the UV photographs demonstrated that a number of the S3 layers, and not the interface between the resin and S3, were indeed darker than the adjacent S2 layer. This observation confirms that lignin-enriched S3 layers were indeed present.

The presence of this S3 lignin peak suggests that lignin distribution may have some effect on the secondary wall sulfur distribution in southern pine latewood, but the absence of a consistent or pronounced S2 lignin gradient indicates other factors are involved. The inconsistent presence of these S3 lignin peaks may help account for the substantial wall-to-wall variability in the sulfur distribution data.

LIGNIN REACTIVITY

Due to difficulties in assessing lignin reactivity differences across the cell wall, this possible source of the observed sulfur distributions has received less attention than lignin distribution. Much of what is known in this area concerns reactivity differences between the secondary wall and middle lamella. Differential reactivity across the secondary wall has been the subject of much speculation, but little evidence is available to support its presence or absence.

Several studies with spruce have provided evidence for secondary wall phenolic hydroxyl contents which are twice those in the middle lamella (22,23).

Under neutral and alkaline pH levels, the sulfonation of α-carbons requires a phenolic hydroxyl in order to form the quinone methide intermediate (1,2). As a result, a sulfite cook would initially be characterized by a higher lignin reactivity in the secondary wall due to the higher phenolic hydroxyl content. As the cook progresses in the ultra-high yield range, this difference narrows, possibly the result of more rapid phenolic hydroxyl formation in the middle lamella during the course of the cook (50). This change in relative reactivity was observed by Whiting and Goring (21), who found the sulfur content of the secondary wall lignin to be at least twice that of the middle lamella lignin in the first few minutes of a high-yield sulfite cook. After 60 minutes at 140^{o}C, the sulfur content ratio of the secondary to middle lamella lignin had decreased to a value of around 1.3. These results suggest that the CC/B ratios obtained from the STEM-EDS work were not only influenced by lignin distribution, but by changes in relative reactivity of the lignin in the two cell wall regions.

Possibly related to these differences in phenolic hydroxyl contents are observed differences in the extent of cross-linking in the secondary wall and middle lamella. Berry and Bolker (51), using gel degradation theory, determined the degree of cross-linking in the middle lamella lignin to be twice that in the secondary wall lignin. The agreement between this finding and the observed differences in phenolic hydroxyl content suggest that these added cross links in the middle lamella are mostly ether bonds which tie up the phenolic hydroxyl groups.

In addition to phenolic ether bonds, evidence suggests that a higher degree of cross-linking in the middle lamella can be attributed to a higher degree of condensation in the middle lamella lignin. This was shown by Westermark (52) in acidolysis experiments on whole wood and middle lamella

fractions. Studies on cell wall formation have also revealed a more condensed lignin structure in the middle lamella (53,54). These studies have found that the middle lamella lignin (including cell corner) forms earlier and under different environmental conditions than the secondary wall lignin. Some of the environmental factors which have been related to lignin structure include type of lignin unit (guaiacyl, p-hydroxyl phenyl), amount and type of carbohydrate present, and the concentration of peroxidase enzyme (53,54).

It is likely that some of these environmental factors may also extend their influence into the outer secondary wall, giving the lignin in this region a more condensed structure. Some of the additional linkages involved in these condensed structures tie up phenolic hydroxyl groups, effectively reducing the phenolic hydroxyl content in the affected region of the cell wall. Therefore, possible lignin structural differences across the secondary wall could influence the secondary wall sulfur distribution.

In contrast to the above hypothesis, a number of studies which have found uniform reacted sulfur, or bromine, distributions across the secondary wall (19,48) have supplied indirect evidence for uniform S2 layer lignin reactivity. Some of these studies found higher levels of these elements in the S3 layer. These were attributed to higher lignin levels in the S3, but differences in reactivity between the S3 and S2 may also be a factor.

One exception to the findings of S2 layer uniformity was the finding of non-uniform secondary wall sulfur distributions in sulfonated aspen (55). Lower sulfur levels were found toward the lumen and higher levels toward the middle lamella. On the assumption of a uniform lignin distribution, this observation was probably the result of differences in the distribution of guaiacyl units, which are readily sulfonated, and syringyl units, which are

not readily sulfonated (55). Since syringyl units are virtually absent in softwoods, these findings cannot explain the observed sulfur gradients in southern pine, but they do demonstrate the potential effects of reactivity differences across the secondary wall.

At this time, there are no known lignin reactivity differences across the secondary walls in southern pine. Given the known or suspected structural differences between the secondary wall and middle lamella lignins, it is likely that a broad transition between the two types of lignin could extend into or completely across the secondary wall from the middle lamella. However, most techniques for measuring such trends would involve subdividing the secondary wall, procedures for which have not been developed.

LIMITED DIFFUSION ACROSS THE CELL WALL

Along with lignin distribution and reactivity, limited diffusion of sodium sulfite from the lumen into the cell wall could also influence cell wall sulfur distribution. In order to investigate this possibility, sulfite diffusion across and reaction within the cell wall were modeled mathematically. A key piece of information required for such modelling is the diffusivity within the cell wall. Since there are no published data for sodium sulfite diffusivity across the cell wall, this work had to rely on theory and data concerning cell wall physical properties and diffusion in porous solids. This information, when applied to the model, verifies the feasibility of a limited diffusion mechanism, but does not supply enough insight into cell wall diffusion to yield accurate quantitative results. Therefore, many of the results presented are more qualitative in nature.

While this work focused on the influence of limited diffusion on the development of a secondary wall bound sulfur gradient, the model also provides other information. With information on lignin distribution across the cell wall, it can predict the combined effects of limited diffusion and lignin distribution on cell wall sulfur distribution. In the case of the middle lamella and CC/B ratio, the model can also evaluate the effects of differences in lignin reactivity between the wall layers. It can also predict many of the observed trends in cell wall sulfur distribution and chip sulfur content, but a lack of a thorough knowledge of cell wall diffusion prevents an accurate quantitative prediction.

In reviewing the model, the following discussion will describe model development, factors affecting diffusivity in the cell wall, and the diffusion modeling results. The actual diffusing species is sodium sulfite, which is in the form of dissociated but electrostatically tied sodium and sulfite ions (56). Since the presence of the sodium ions influences the diffusivity of the sulfite ions, all calculations were based on sodium sulfite diffusion. However, since the diffusion of sulfite is of primary concern in this work, this discussion will focus on diffusion of the sulfite ions.

Model Development

The model is based on the system in figure 32. This system consists of a section of cell wall spanning from the S3 the center-point of the middle lamella and a portion of the adjacent lumen spanning from the center of the lumen to the S3 layer. Vapor-phase cooking conditions are assumed, so that the only liquor involved in the cook is that which has impregnated the walls and occupies the lumen. With the exception of boundary conditions at $X = L$, the depletion of sulfite ion in the lumen and wall and the accumulation of bound

sulfite in the wall are considered independent of the surrounding walls and lumen.

The model describes the development of profiles for sulfite ion concentration (S) and bound sulfur concentration (S^*) across the secondary wall as the cook progresses and sulfite ions diffuse across the wall from the lumen. It is based on nonsteady state diffusion (Fick's Second Law) with reaction and is described by the equations:

$$\delta S/\delta t = D_{eff}\ (\delta^2 S/\delta x^2) + R \qquad (10)$$

$$R = (\delta S/\delta t)_{rxn} = -(\delta S^*/\delta t) = -k(S)(S_p - S^*) \qquad (11)$$

where R is the reaction term, k is the second order rate constant, S_p is the maximum possible bound sulfite concentration, and D_{eff} is the effective diffusivity of sulfite ion in the cell wall. This last parameter can depend on

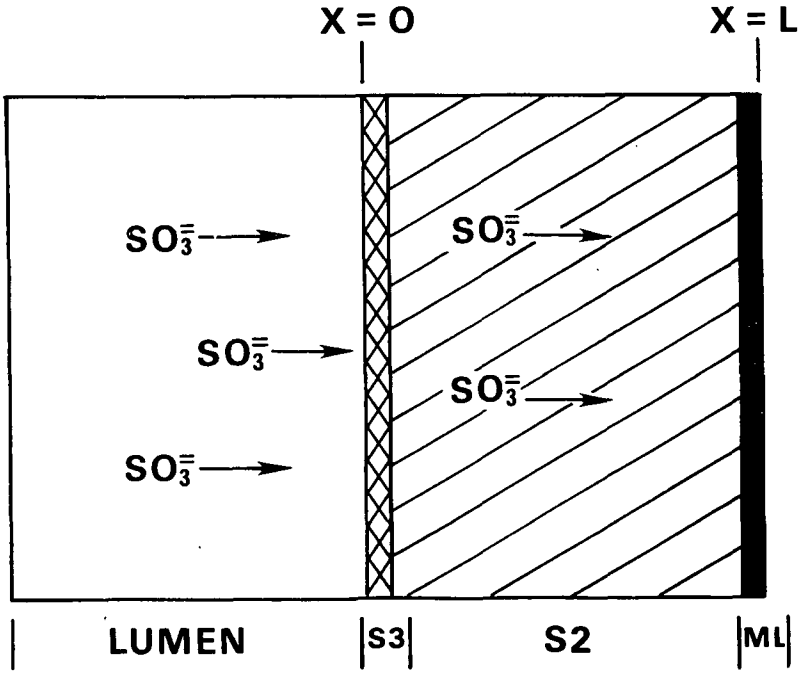

Figure 32. System used for diffusion modelling. Sodium ions, which are diffusing with the sulfite ions, are not shown.

a variety of factors which include the diffusivity of the sulfite ion in water, the effects of sulfite ion hydration, porosity and tortuosity of the cell wall, viscous drag, adsorption, and electrostatic effects.

In order to solve these equations, a number of initial and boundary conditions have been established. Initially, the lumen contains a sodium sulfite solution of known concentration (S_o). The wall is assumed to be thoroughly impregnated with the liquor at the outset, and none of it has reacted. In other words,

$$\begin{aligned} &\text{At } t = 0, \quad && S_L = S_{wall} = S_o \\ & && S^* = 0 \end{aligned} \tag{12}$$

where S_L is the sulfite ion concentration in the lumen at any time, t, during the course of the cook. The upcoming discussion reveals that diffusivity across the lumen is much higher than that across the cell wall. As a consequence, any sulfite ion gradients across the lumen are probably negligible when compared to those across the cell wall, so the sulfite ion distribution across the lumen is assumed to be uniform.

During the cook, the system is subject to the following boundary conditions:

$$\begin{aligned} &\text{At } x = 0, \quad && S = S_L \\ & && dS^*/dt = k(S_L)\ (S_p - S^*) \\ &\text{At } x = L, \quad && dS/dx = 0 \\ & && dS^*/dx = 0 \end{aligned} \tag{13}$$

The boundary condition for S^* at $x = 0$ is simply the solution of the reaction term (equation 11) for $S = S_L$. The boundary conditions for $x = L$ are based on the assumption of symmetry between the profiles of adjacent walls.

All aspects of the diffusion modelling are controlled by a diffusion modelling (DM) program. Within the DM program, equations 10 and 11 are solved using the IMSL subroutine, DPDES, which transforms any set of partial differential equations to a series of ordinary differential equations using the method of lines (57). DPDES then solves these ordinary differential equations using other IMSL subroutines. The DM program calls DPDES at designated time intervals at which it solves the equations for S and S^* simultaneously at designated points across the wall.

At each time interval, the main program calculates a new value for S_L using the mass balance,

$$(V_l + P(V_w))\ (S_o) = V_l(S_L) + P(V_w)\ (S + S^*) \qquad (14)$$

where V_l and V_w are the volumes of the lumen and wall, respectively, and P is the porosity of the cell wall. The term, $P(V_w)\ (S + S^*)$, is the sum of the integrals for sulfite ion concentration and bound sulfite concentration across the wall. They are obtained by way of a Taylor series. This procedure for obtaining S_L calculates S and S^* at time, t+1, using the S_L value obtained at time, t. This could introduce some error in the results, but this error could be minimized by using short time intervals, such that the change in S_L between time intervals is negligible.

The DM program has been designed to evaluate a wide variety of diffusivities, times, temperatures, and sodium sulfite concentrations, which are input by the user. In order to evaluate diffusion in cell walls with different lignin distributions, two versions of the DM program have been developed. Both are shown in Appendix 4. The first version, DMU1, assumes a uniform lignin distribution across the secondary wall. The middle lamella is given a lignin concentration or S_p which is four times that of the S2 and S3

layers, but has a rate constant (k), which is lower than that of the S2 and S3 layers by a factor of 1.5 (58). The second version, DMS1, evaluates a secondary wall with a lignin-enriched S3 layer. The S3:S2 lignin concentration ratio or S_p ratio is given a value of 1.4 (49). The middle lamella is treated in the same manner as in the DMU1 program.

Effective Diffusivity

Among the variables and constants utilized by the diffusion model, the effective diffusivity, D_{eff}, within the cell wall is probably the least understood. In order to gain a better understanding of diffusion across the cell wall, the literature concerning cell wall structure and diffusion in membranes and porous solids has been reviewed. Consideration of all of the factors affecting cell wall diffusivity should give a good approximation of its value. Insertion of this value in the diffusion model should allow us to conclude whether limited diffusion could indeed be a factor in the observed sulfur distributions.

For the purpose of modelling diffusion across the cell wall, the wall is being viewed as a porous solid. The sulfite ions are being viewed as spheres diffusing through the pores, as shown in figure 33. The speed with which the sulfite ions pass across the cell wall through the pores depends on a number of factors, which can be divided into three categories:

1. Bulk diffusivity
2. Mechanical blocking
3. Hindered diffusion within the pores

These categories are subdivided into individual phenomena in Table 18. The effective diffusivity, D_{eff}, is obtained from the bulk diffusivity, D_B, through

a series of correction factors (CF_n) which are based on these phenomena. This relation is described in equation form as follows:

$$D_{eff} = \left(\prod_{i=1}^{n} CF_i\right) D_B \qquad (15)$$

Limited knowledge of these phenomena makes only an approximation of D_{eff} possible.

Bulk diffusivity

The bulk diffusivity for sodium sulfite was determined at infinite dilution from equivalent ionic conductivities (59) using the Nernst-Haskell equation (60),

$$D = (RT/F^2)\ (1/n_+ + 1/n_-)/(1/l_+ + 1/l_-) \qquad (16)$$

where R is the gas constant, T is in degrees Kelvin, F is the Faraday constant, n_+ and n_- are the cationic and anionic valences, and l_+ and l_- are the cationic and anionic conductivities. At 25°C, $D_B = 1.23 \times 10^{-5}$ cm^2/sec for sodium sulfite (Na_2SO_3).

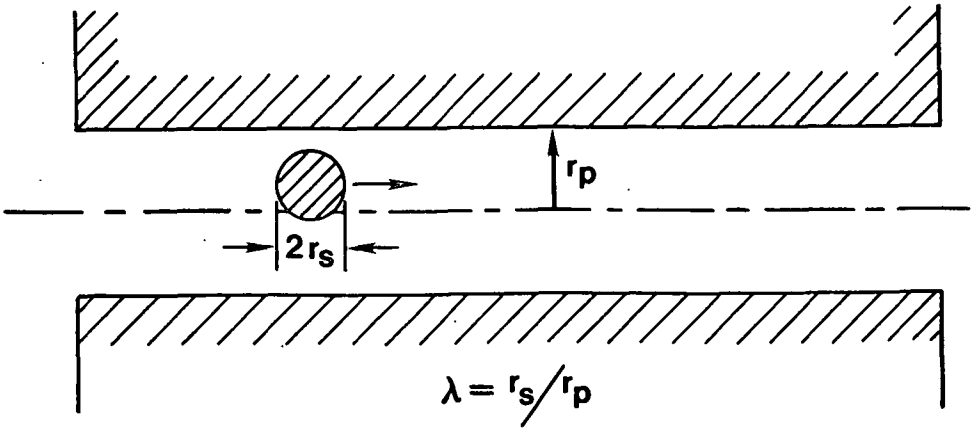

Figure 33. Spherical solute diffusing through a cell wall pore.

Table 18. Sources of diffusivity correction factors.

I. BULK DIFFUSION COEFFICIENT
   A. Temperature effects
   B. Concentration effects

II. MECHANICAL BLOCKING
   A. Porosity (ϵ)
   B. Tortuosity (τ)
   C. Pore-size distribution

III. HINDERED DIFFUSION IN PORES
   A. Water monolayer on pore wall
   B. Steric effects
   C. Hydrodynamic effects
   D. Electrostatic effects
   E. Enhanced solvent viscosity
   F. Solute adsorption

The above equation reveals a dependence of D_B on temperature. The effect of temperature can be better illustrated by the Stokes-Einstein equation (56), which is as follows:

$$D_B = k_B T / (6\pi\mu r_s) \qquad (17)$$

This equation demonstrates that the relationship not only reflects a direct proportionality between D_B and temperature, T, but also an indirect effect through the influence of temperature on solvent viscosity, μ. The other components of the equation are Boltzmann's constant (k_B), and the radius of the

diffusing species (r_s). From the above equation, D_B at temperature, T, can be determined from the following relationship:

$$D_{BT} = D_{298} \ (T_T/T_{298}) \ (\mu_{298}/\mu_T) \tag{18}$$

The viscosity of the solvent, water, can be determined at any temperature by the following equation (61):

$$100/\mu_T = 2.260\{(T-285.5)+[(T-285.5)2+9854]0.5\}-142.2 \tag{19}$$

where μ_T is in cp and T is in degrees Kelvin.

The diffusivity data discussed above were obtained at infinite dilution, while these sulfonation studies were performed using sodium sulfite concentrations ranging from 0.30 to 1.59 moles/liter. The effect of these higher concentrations on diffusivity is described by the following equation (62):

$$D = D_B \ [1 + c(\delta \ln(y)/\delta c)] \tag{20}$$

where c is the molarity of the solution and y is the molar activity coefficient for the solute. In this case, no activity coefficients were available for sodium sulfite (Na_2SO_3); therefore, activity coefficients for sodium sulfate (Na_2SO_4) were used and should supply a reasonable approximation of the activity coefficients for sodium sulfite. In the case of a 1.03 molar sodium sulfite solution, D_B would be reduced from 1.23×10^{-5} cm^2/sec at infinite dilution to 0.70×10^{-5} cm^2/sec.

Mechanical blocking

This series of corrections accounts for cell wall porosity and cell wall pore structure. These effects have often been described by the equation, $D_{eff} = D^B \ (\epsilon/\tau)$, where ϵ is the cell wall porosity and τ is the tortuosity of

the cell wall pores (63). The porosity, ϵ, was determined from fiber saturation point data to be 0.282 ml void volume/ml cell wall.

A value for cell wall tortuosity, τ, is much more difficult to determine, as it requires assumptions concerning cell wall structure. For the purposes of determining D_{eff}, the cell wall will have an ultrastructure such as that described in figure 34. Here we have groups of three or four radially attached cellulose protofibrils surrounded by a lignin-hemicellulose matrix (63). The groups of cellulose protofibrils are arranged to form what appear to be split lamellae.

The tortuosity of such a wall could be divided into three components. The product of these components yields the total tortuosity, $\tau = (\prod_{i=1}^{n} \tau_i)$. These components are:

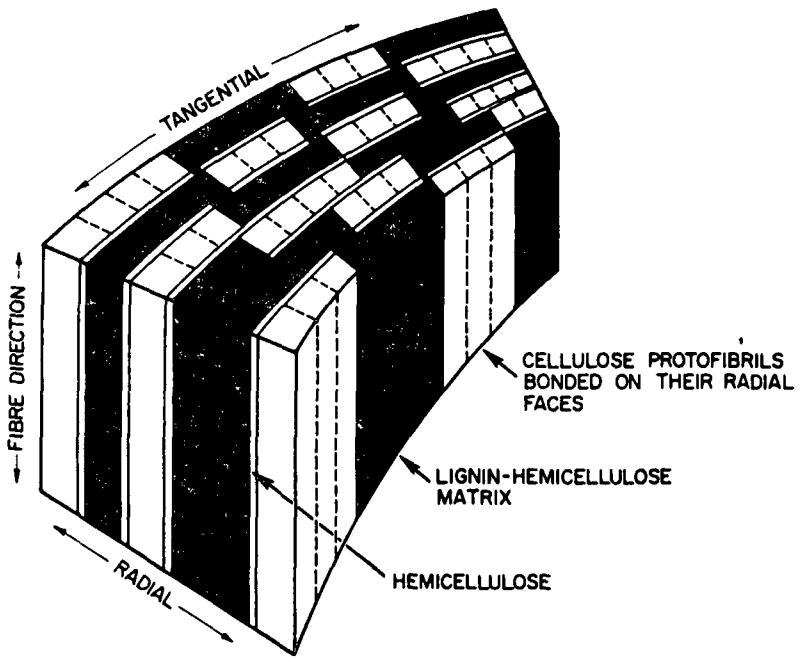

Figure 34. Model for cell wall ultrastructure from Kerr and Goring (63).

τ_m, the tortuosity within the matrix
τ_c, the effect of the protofibrils on tortuosity
τ_d, the effect of dead-ends or obstructed pores on tortuosity.

The determination of τ_m assumes the pores to be randomly aligned within the cell wall. This would give the pores an equal probability of winding in the radial, tangential, and longitudinal directions. In other words, the solute molecules will probably migrate one step in each of the three directions in order to move one step radially across the wall. This would give τ_m a value of three.

For the determination of the second component, τ_c, we assume the crystalline portion of the cellulose protofibrils are impenetrable; therefore, the solute molecules must diffuse around the cellulose crystals. Assuming the cellulose to be totally crystalline, Favis and Goring (64) determined a tortuosity of two for diffusion around the cellulose. If we give the cellulose a crystallinity of 67% and assume the tortuosity through the amorphous cellulose is comparable to that in the matrix, this factor, τ_c, is reduced to 1.67.

The final component, τ_d, accounts for dead-ends or impassable pores in the porous passageways through the cell wall. Stamm (65) used the pore-size distribution data in Table 19a to make such a determination. He assumed the pore walls to be lined with a monomolecular layer of firmly bound water (4 Å thick). This resulted in total blockage of any pores less than 8 Å in diameter. Such pores represented 92% of the pore length within the cell wall. This, in turn, reduced the diffusion coefficient by a factor of 1/(1-0.92) or 12.5.

This treatment of pore blockage was applied to this work after making two changes. First, although the presence of a firmly bound water monolayer is

Table 19. Pore-size distribution data; a). Stamm's data obtained through sorption techniques (65). Corrected data based on a 4 Å monolayer of water lining the pore wall; b). Stone and Scallan's data obtained through a solute exclusion technique (68). Corrected data based on a 2.8 Å monolayer of water lining the pore wall and a solute molecule diameter of 7.8 Å.

a).

Pore radius range (Å)	Avg. pore radius(Å)	Volume (cm^3)	Corrected[a] Volume(cm^3)	Pore Length[b] (cm x 10^{-12})
0-2	1	.012	-	38.217
2-4	3	.012	-	4.240
4-6	5	.012	.00048	1.529
6-8	7	.012	.00221	.779
8-10	9	.012	.00371	.472
10-12	11	.012	.00486	.316
12-20	16	.031	.01750	.386
20-30	25	.022	.01550	.112
30-40	35	.017	.01330	.044
40-140	90	.071	.06480	.028
140-1140	640	.071	.07010	.001

b).

Pore radius range (Å)	Avg. pore radius(Å)	Volume (cm^3)	Corrected[a] Volume(cm^3)	Pore Length[b] (cm x 10^{-12})
2-5	3.5	.14	-	3.638
5-7.5	6.3	.09	.010[c]	.733
7.5-10	8.8	.08	.037	.333
10-12.5	11.3	.08	.045	.201

[a] corrected volume = volume X $[(r - w)/r]^2$, where r is the pore radius and w is the diameter of a water molecule (4 Å for Stamm's data and 2.8 Å for Stone and Scallan's data.

[b] pore length = volume/πr^2.

[c] pores below 6.7 Å in radius are considered impassable for for Stone and Scallan's data due to the monolayer of water along the pore wall and the size of the solute molecule. The corrected volume for the 5-7.5 Å range represents that for those pores with radii between 6.7 Å and 7.5 Å.

well accepted (66), the diameter of the water molecules have, more recently, been determined to be 2.82 Å (67). Second, this work is concerned with diffusion of hydrated sulfite ions, so this analysis must account for the diameter of these molecules (7.8 Å). The determination of this diameter is shown in Appendix 5. Combining these two corrections yields a minimum effective pore diameter of 13.4 Å. Applying this to Stamm's pore-size distribution data yields a τ_d of 25.1.

Applying this same reasoning to Stone and Scallan's pore-size distribution data from spruce (68) yields a τ_d of 6.9. See Table 19b. The difference between these two values could be attributed to the higher percentage of smaller pores in Stamm's data.

Combination of the three tortuosity components yields:

$$\begin{aligned} \tau &= \tau_m \tau_c \tau_d \\ &= 125.8 \quad \text{(Stamm's data)} \\ &= 34.5 \quad \text{(Stone and Scallan's data).} \end{aligned} \tag{21}$$

The application of this technique to the determination of tortuosity in wood cell walls has little theoretical basis, especially since we know very little about cell wall structure. Because of this, the more conservative of the estimates, that from Stone and Scallan's data, seems more suitable.

Hindered diffusion in pores

Within the narrow pores in the cell wall, a number of forces or restrictions which hinder diffusion are acting on the diffusing sulfite ion. These are listed in Table 18. The magnitude of a number of these restrictions is influenced by the ratio of the solute radius (r_s) to that of the pore (r_p). This ratio is often represented by (69). The best way to apply many of these restrictions is through the various pore-size ranges provided by pore-size

distribution data. Once correction values are calculated for each range of pore sizes, they can be combined to give a single correction term.

The first restriction is the presence of a monomolecular layer of water on the pore walls. In addition to making a number of pores inaccessible, this layer will reduce the effective pore radius of the remaining pores. This layer could be viewed as a rigidly bound layer of water through which no diffusion occurs or a high viscosity layer through which the rate of diffusion is drastically reduced. In the former case, diffusion through the pore is reduced by a factor,

$$(r_p - d_w)^2/r_p^2 \qquad (22)$$

where d_w is the diameter of a water molecule and r_p is the pore radius. If water is viewed as a highly viscous layer, the correction takes the form of

$$1/(1 + \lambda P) \qquad (23)$$

where P is a term incorporating λ, d_w, and the enhanced viscosity of the water monolayer (69). Since the exact nature of this enhanced viscosity is not known, it is often simpler to assume that no diffusion occurs through this monolayer.

Steric or concentration effects arise from the inability of a solute molecule to occupy the entire diameter of the pore (69). This occurs because the center of the solute molecule cannot occupy the volume within a distance of r_s, the solute radius, from the pore wall. See figure 35. As a result, the solute concentration in the pore is lower than that in the bulk solution. This effect can be described by the relationship,

$$D_{eff} \propto (1 - \lambda)^2 \qquad (24)$$

As the ratio of solute radius to wall radius increases, the relative pore concentration and D_{eff} are reduced.

In narrow pores, hydrodynamic effects can cause substantial reductions in solute diffusivity. A number of relationships which attempt to describe this phenomenon have been developed (70). All describe these effects as a function of λ. For this work, the data of Wang and Shalak (71) will be used.

A number of studies have shown that electrostatic effects also influence diffusion in porous media (70,72,73). Although these effects are generally more pronounced at lower electrolyte concentrations, they can still be significant at the concentrations used in this study, especially in narrow pores (70,72). Studies using cellulose acetate and other synthetic membranes

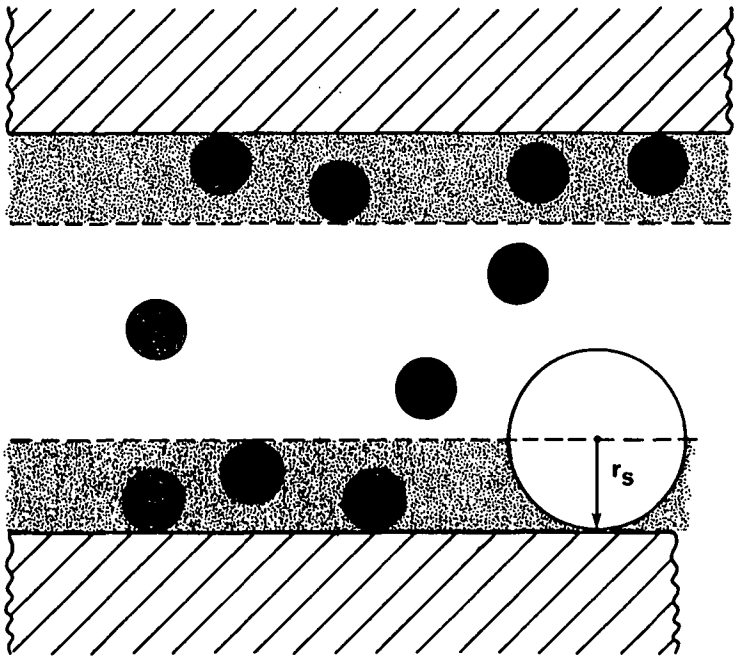

Figure 35. The origin of steric effects within the pore wall. The shaded region, of thickness r_s, is said to be unoccupied by the solute molecule since the center of the solute cannot occupy this area.

have shown the presence of anionic groups in the membrane to reduce diffusivity by a factor of around 25% at a concentration of 1 mole/liter (72,73). Such work has also shown this effect to vary with electrolyte concentration and surface charge (73).

In addition to the above factors, there are also other factors which influence diffusion which, at this point, are difficult to quantify. The first is enhanced viscosity within the pores. Studies using cellulose acetate and biological membranes have indicated that water within narrow pores has a viscosity which is as much as 39 times that in bulk solution (74). More recent studies (66) have suggested that such high viscosities were the result of contaminants and that any enhanced viscosity is only within one or two molecular layers from the pore surface (75). This is probably the result of bound water or counter-ions attracted to the pore wall. Since the above studies concluded that much of the observed enhanced viscosity was due to impurities and since wood chips are far from being pure, it is likely that the viscosity of the sulfite solution in the cell wall pores is enhanced to some extent. As the sulfonation reactions progress during the cooks, the introduction of degraded polymers into the pores should enhance pore viscosity, but the extent is not known.

Another factor affecting diffusion in the pores is adsorption of the sulfite ion onto the pore walls. So far no data is available for sulfite cooks, but studies using silica-alumina catalyst beads showed that diffusivities for preferentially adsorbed solutes in organic solvents were, on the average, reduced by a factor of four (76). Since this is a totally different system, it is difficult to apply these results to sodium sulfite diffusion through wood chips.

Calculation of D(eff)

The application of correction factors for many of the above phenomena to the bulk diffusivity will indicate the feasibility of attributing the observed sulfur distributions to diffusion limitations. The corrections can be applied through the following equation.

$$D_{eff} = D_B(C_T)(C_C)(\epsilon/\tau)(C_P)(C_E) \qquad (25)$$

The meaning of these correction factors and their values are shown in Table 20. The value of Deff represents vapor-phase cooking conditions at 140°C using 1.03 molar sodium sulfite. Stone and Scallan's (68) data in Table 19b were used to represent pore-size distribution. Combining all of these effects yields a value of 2.2×10^{-10} cm^2/sec for D_{eff}. Some of the above correction factors may be overestimates of their respective phenomena, but others, such as electrostatic effects, are probably underestimates. Some phenomena, such as adsorption and enhanced viscosity, are not included.

Model Results

The diffusion model was applied to a number of cooking conditions to evaluate the effects of lignin distribution, effective diffusivity, time, temperature, and sodium sulfite concentration. In addition to these variables, sulfonation during inpregnation and heat-up to final temperature can have a pronounced effect on the model results, especially sulfur content. During impregnation under the conditions used in this study, chip sulfur contents were estimated to reach values as high as 0.15%, as shown in Table 21. These data are based on data obtained by Engstrand, Hammer, and Htun (40), who found sulfonation to be extremely rapid up to sulfur contents of around 0.10% at temperatures as low as 80°C. The same activation energies are assumed to be in

Table 20. Correction factors for cell wall diffusion.

Factor	Definition	Value
D_B	Bulk diffusion coefficient at 25°C and infinite dilution (cm^2/sec)	1.23×10^{-5}
C_T	Correction factor for temperature	6.3
C_C	Correction factor for sodium sulfite concentration $[1 + c(\delta \ln(y)/\delta c)]$	0.57
ϵ	Cell wall porosity	0.282
τ	Cell wall tortuosity	34.5
C_E	Correction factor for electrostatic effects	0.75
C_P	Product of C_S, C_H, and C_M; these are applied through the pore-size distribution data. Calculated in Appendix 6.	0.000815
C_S	Correction factor for steric hindrances; $(1 - \lambda)^2$; $= r_{solute}/r_{pore}$	-
C_H	Correction factor for hydrodynamic effects	-
C_M	Correction factor for the presence of a water monolayer	-

effect at room temperature and would thus result in rapid sulfonation during impregnation. This assumption is supported by the bound sulfur contents of 0.19% obtained in this study after impregnation of latewood chips for 30 minutes followed by repeated soakings. Somewhere above 0.10%, the rate of sulfonation declines. This was demonstrated by Engstrand, Hammer, and Htun (40) at elevated temperatures and by Heitner, Beatson, and Atack (5) who obtained sulfur contents of 0.24% after a 24 hour impregnation in neutral sulfite liquor at room temperature.

Estimation of the degree of sulfonation during heat-up involved choosing one or more temperature intervals during the course of the heat-up. For each

interval, a representative or average temperature was chosen and the degree of sulfonation for each interval was calculated based on this temperature and the length of time spent in that temperature interval. The total change in sulfonation level during heat-up was added to that obtained after impregnation to yield the sulfur content at time, t=0, in Table 21.

Table 21. Initial Sulfur content data derived from data by Engstrand, et al. (40) after impregnation and impregnation plus heat-up (time = 0). Na_2SO_3 concentrations are those of the liquor.

Experiment	Na_2SO_3 conc., mole/l	Time, min.	Temp., degrees C	Length of impregnation min.	Sulfur content After impregnation	Sulfur content At time = 0
VP1	0.48	20	134	30	0.13	0.16
VP1	0.48	40	134	30	0.13	0.16
VP1	1.03	20	134	30	0.14	0.20
VP1	1.03	40	134	30	0.14	0.20
VP1	1.59	20	134	30	0.15	0.25
VP1	1.59	40	134	30	0.15	0.25
VP2	0.48	5	160	7	0.09	0.13
VP2	1.03	5	160	7	0.10	0.18
VP2	0.48	20	140	7	0.09	0.10
VP2	1.03	20	140	7	0.10	0.12

For each run, the model was started under the initial conditions of total and uniform impregnation of the liquor into the wall and no bound sulfur. For each set of conditions, a time of 0 minutes (t=0) was the time at which the cell wall sulfur content equalled that in Table 21. Timing of the cook started at this point. Under these circumstances, the cell wall would have a sulfite ion and bound sulfur gradient at time, t=0, which is a realistic situation given the sulfur gradients found in the chips which were impregnated but not cooked.

Such a gradient can be attributed to several factors. Several studies (42,43,44) have found the penetration of dry cell walls or wood with liquid to occur at rates which would require 2 to 5 minutes for the liquid to totally penetrate a 10 μm thick cell wall. This, combined with the rapid sulfonation which occurs during impregnation, may result in the formation of a bound sulfur and sulfite ion gradient during impregnation. Sulfonation during heat-up would enhance this gradient.

The DMU1 and DMS1 programs were used to evaluate the influence of time and effective diffusivity on sulfur distribution and sulfur content data for two different lignin distributions. These distributions were a uniform secondary wall lignin distribution (DMU1) and a similar lignin distribution with S3 lignin concentrations 1.4 times greater than those in the S2 layer (DMS1). The cooking conditions used to obtain the results were those of a 134^{o}C vapor-phase cook using 1.03 molar sodium sulfite. These results and a comparison of the results from the two lignin distributions are summarized in Table 22.

The data in Table 22 may be more easily interpreted if some of the actual distributions are seen first. Examples of some of the distributions obtained from the DMU1 program are shown for a time of 20 minutes in Figure 36. This figure demonstrates the influence of effective diffusivity on bound sulfite distribution. Within the range of effective diffusivities tested, gradients across the secondary wall vary in degree, with lower diffusivities giving more pronounced gradients. Of particular interest is the diffusivity of 1 X 10^{-10} cm^2/sec, which is very close to the estimated diffusivity and yields a fairly pronounced gradient. With a reasonable margin of error for the estimated D_{eff}, these results demonstrate that diffusion limitations could indeed influence the observed secondary wall sulfur gradients.

Table 22. Influence of diffusivity, time, and lignin distribution on sulfur distribution and sulfur content for a vapor-phase cook at 134°C using 1.03 molar Na_2SO_3. S = sulfur content (%OD treated wood).

D_{eff} cm^2/sec	Time, min.	Uniform secondary wall lignin (DMU1) A/B	CC/B	S	S3 lignin = 1.4 X S2 lignin (DMS1) A/B	CC/B	S	Comparison of lig. dists. (DMS1/DMU1) A/B	CC/B	S
1X10-10	0	1.14	2.74	0.21	1.60	2.73	0.21	1.40	1.00	1.00
1X10-10	20	1.25	2.90	0.40	1.75	2.89	0.40	1.40	1.00	1.00
1X10-10	40	1.26	3.01	0.51	1.76	3.01	0.51	1.40	1.00	1.00
5X10-10	0	1.12	2.81	0.21	1.57	2.79	0.21	1.40	0.99	1.00
5X10-10	20	1.15	2.99	0.42	1.61	2.99	0.42	1.40	1.00	1.00
5X10-10	40	1.14	3.16	0.54	1.59	3.16	0.54	1.39	1.00	1.00
1X10-9	0	1.09	2.82	0.21	1.53	2.82	0.22	1.40	1.00	1.05
1X10-9	20	1.10	3.02	0.43	1.55	3.02	0.43	1.41	1.00	1.00
1X10-9	40	1.10	3.20	0.55	1.54	3.20	0.55	1.40	1.00	1.00

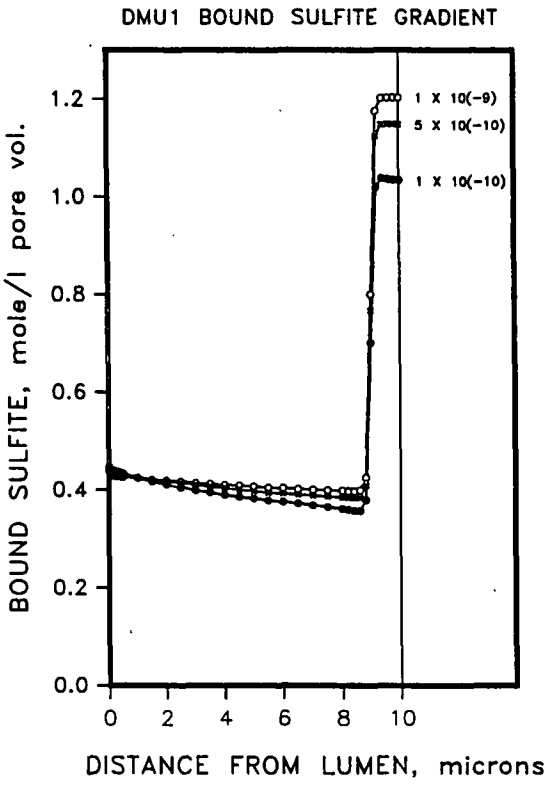

Figure 36. Bound sulfur distribution at different D_{eff} values. Data generated from program DMU1 for a 20-minute 134°C vapor-phase cook using 1.03 molar sodium sulfite. D_{eff} in cm^2/sec.

The corresponding A/B ratio data in Table 22 (DMU1; 20 minutes) reveals the same trends; the A/B ratio decreases as the diffusivity increases. The CC/B ratio and sulfur content data, on the other hand, increase slightly with increased diffusivity. This is due to the more rapid diffusion of sulfite ions into the cell wall from the lumen and into the middle lamella from the secondary wall.

When the lignin concentration in the S3 layer is higher than that in the S2 layer by a factor of 1.4, the gradients are even more pronounced, as shown in figure 37. These data, which were generated by program DMS1, are more reminiscent of some of the linescans than those in figure 36. Comparison of the DMS1 A/B ratio data in Table 22 with the corresponding DMU1 results demonstrates that the higher S3 lignin content had little effect on diffusion across the wall; the difference between the DMU1 and DMS1 generated A/B ratios was a factor of 1.4, which is the difference between the S3 and S2 lignin concentrations. Enhanced lignin levels in the S3 layer had no effect on the CC/B ratio and caused only a minute increase in sulfur content, which is proportional to the increase in overall lignin content or S_p.

In addition to effective diffusivity, the DMU1 and DMS1 data in Table 22 also demonstrates a pronounced effect of time on A/B ratio, CC/B ratio and sulfur content. As the cook progresses, the A/B ratio increases to a maximum and then remains constant or begins to decline. On the other hand, the CC/B ratio and chip sulfur content continue to increase with time.

A scheme based on the kinetics of the sulfonation reactions can explain the presence of the bound sulfur gradients as well as the effects of time on the magnitude of the gradient. In the early stages of the cook, reactions of the sulfite ions with the lignin will establish a concentration difference

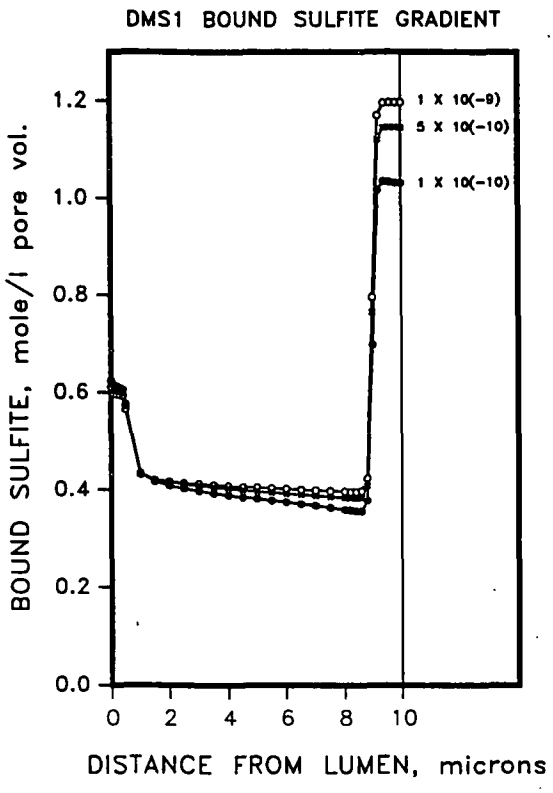

Figure 37. Bound sulfur distribution at different D_{eff} values. Data generated from program DMS1 for a 20 minute 134°C vapor-phase cook using 1.03 molar sodium sulfite. D_{eff} in cm^2/sec.

between wall and lumen, which initiates diffusion of sulfite ions into the wall. If diffusion is slow enough or the diffusing species is reacting fast enough as it diffuses across the wall, a sulfite ion gradient will form, as shown in Figure 38, and intensify during the early stages of the cook. A bound sulfur gradient will form and begin to mimic this gradient and the lignin distribution, giving the observed increase in A/B ratio with time. At some point during the course of the cook, the number of available sulfonation sites on the lignin will become limiting, thus allowing sulfite ions to diffuse further into the cell wall without reacting. This will halt or reverse the increase in sulfite ion and bound sulfur gradients, as observed in the model results. The extent to which the cell wall is uniformly impregnated at the

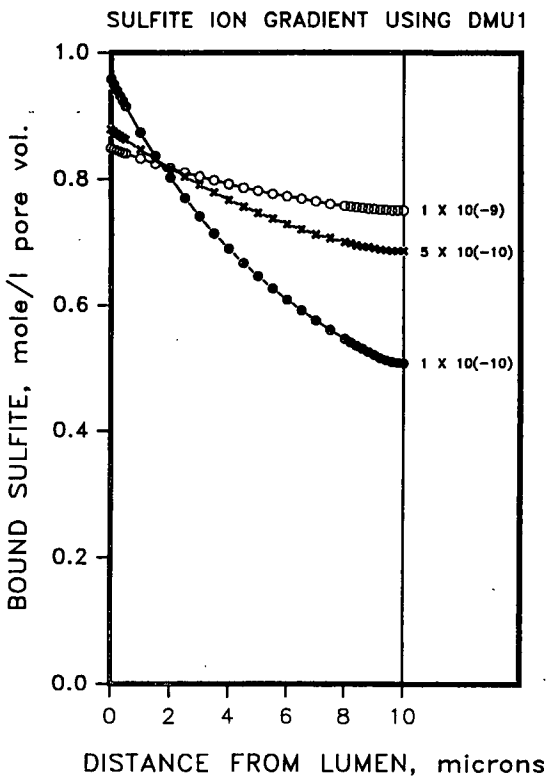

Figure 38. Sulfite ion distribution at different D_{eff} values. Data generated from program DMU1 for a 20 minute, 134°C vapor-phase cook using 1.03 molar sodium sulfite. D_{eff} in cm^2/sec. These data correspond to the data in Figure 36.

beginning of the cook should not affect this general scheme, but should influence the magnitude of the gradients obtained.

The vapor-phase conditions used in the VP1 and VP2 cooks were evaluated using programs DMU1 and DMS1 at a diffusivity of 5×10^{-10}. The results are shown in Figures 39 to 44 with the corresponding results from the linescan or sulfur content data. The data are shown in tabular form in Appendix 7. When comparing the model results with the experimental results, the agreement between the two sets of data should be viewed in two ways: agreement with respect to the overall magnitude of the values in the two sets of data, and agreement with respect to trends in the data.

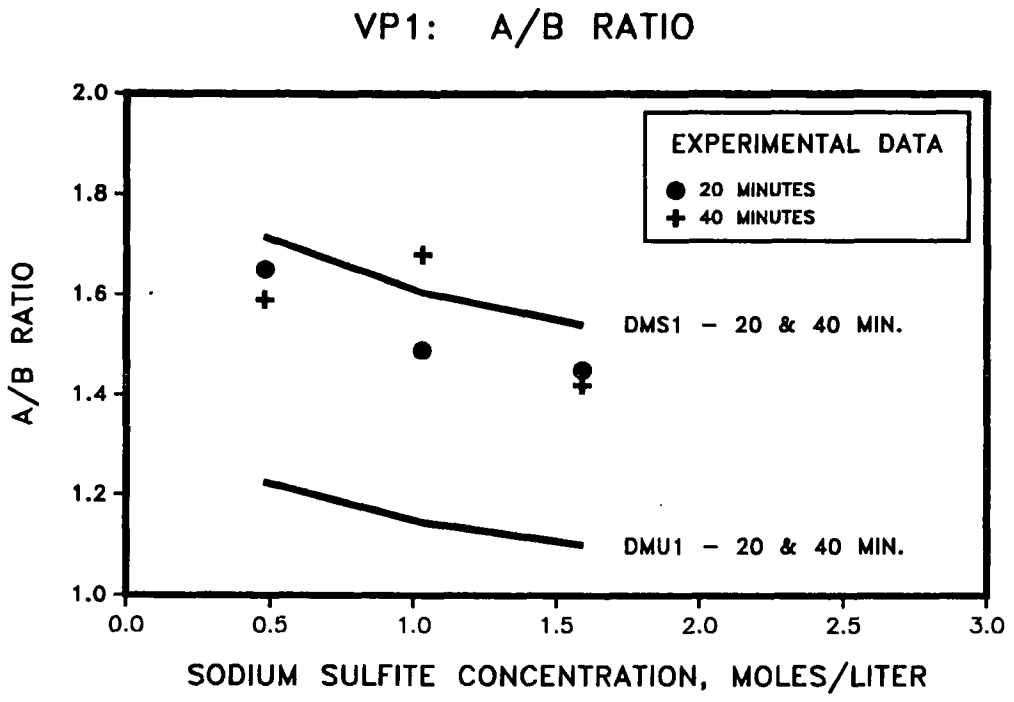

Figure 39. Comparison of experimental and generated A/B ratios for the VP1 cooks. Points represent experimental data. Solid lines represent generated data.

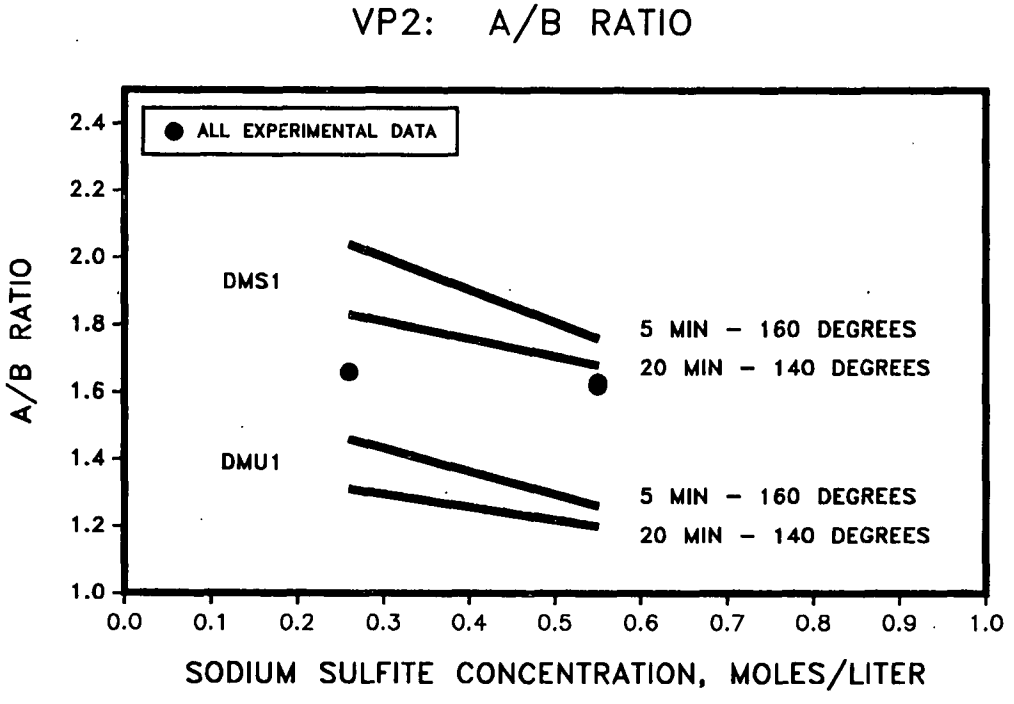

Figure 40. Comparison of experimental and generated A/B ratios for the VP2 cooks. Points represent experimental data. Solid lines represent generated data.

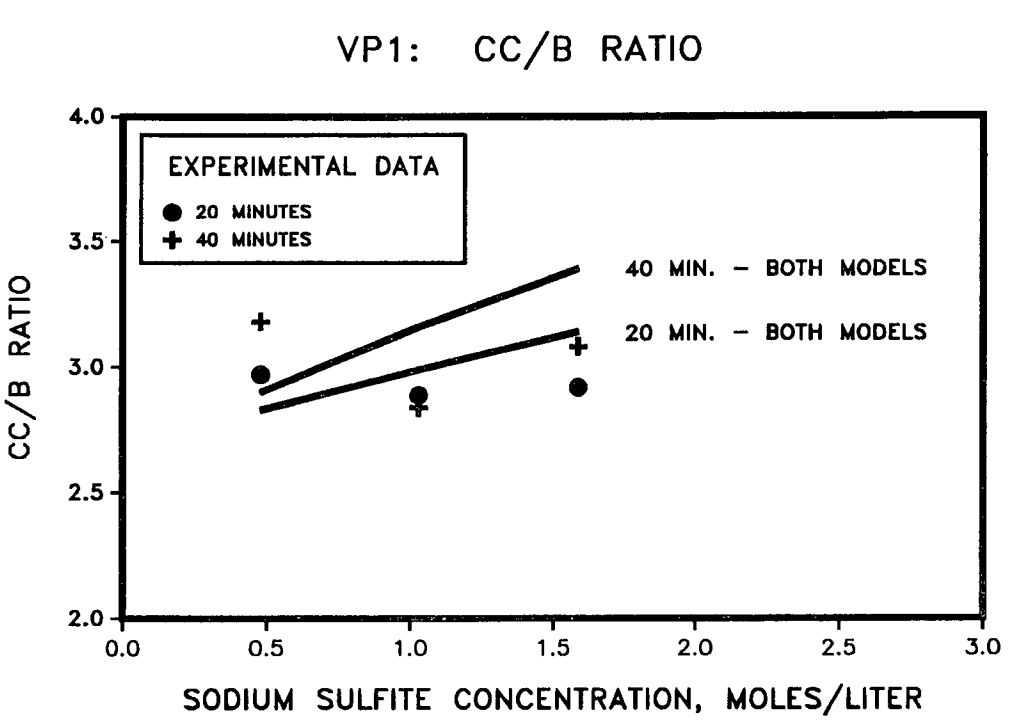

Figure 41. Comparison of experimental and generated CC/B ratios for the VP1 cooks. Points represent experimental data. Solid lines represent generated data.

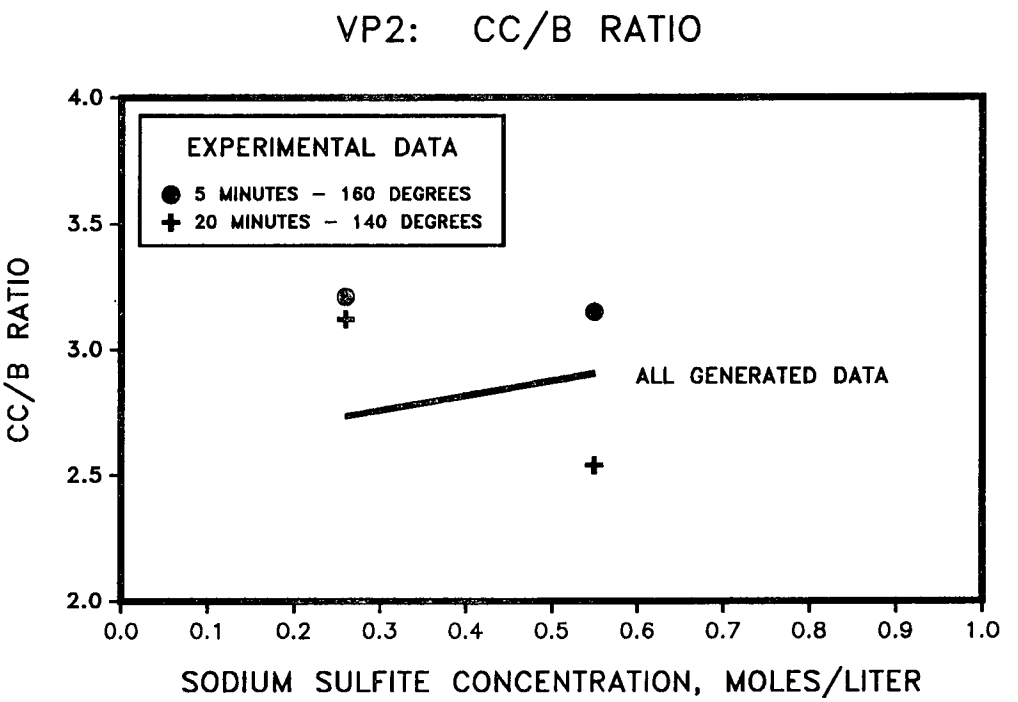

Figure 42. Comparison of experimental and generated CC/B ratios for the VP2 cooks. Points represent experimental data. Solid lines represent generated data.

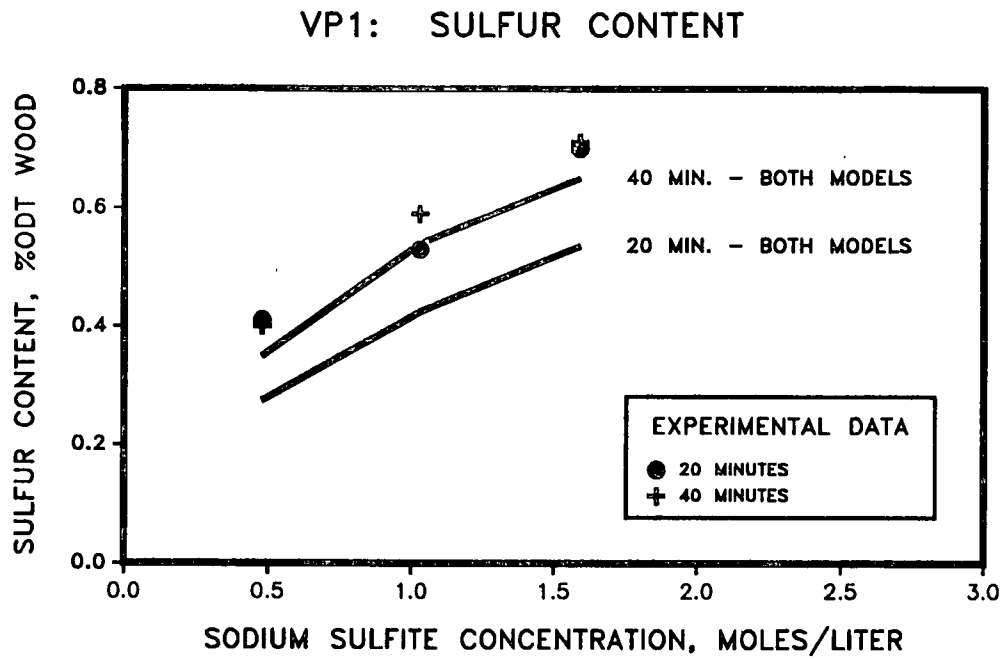

Figure 43. Comparison of experimental and generated sulfur contents (S) for the VP1 cooks. Points represent experimental data. Solid lines represent generated data.

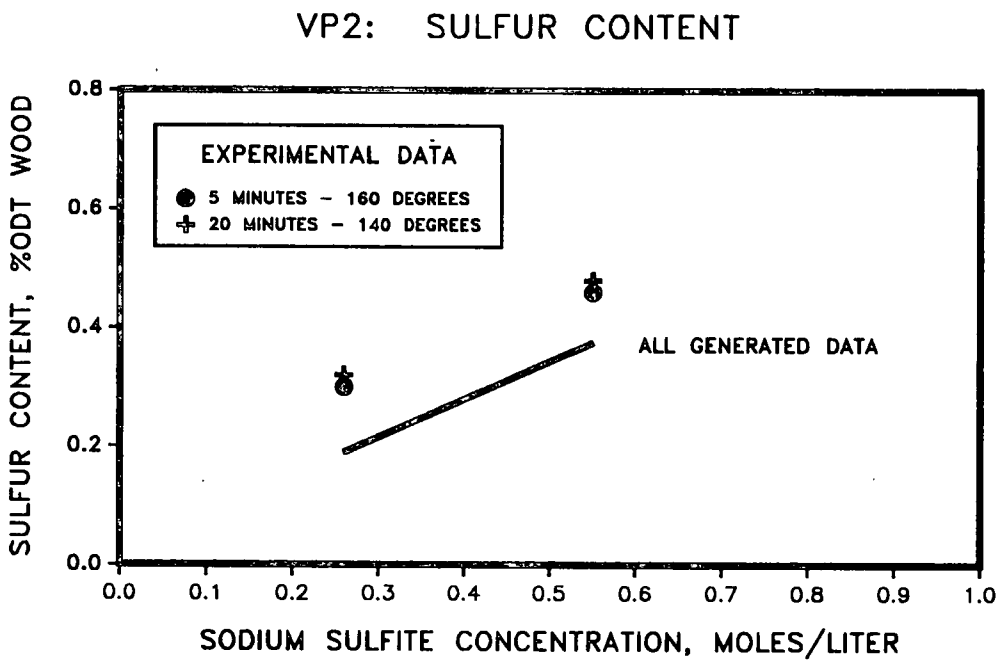

Figure 44. Comparison of experimental and generated sulfur contents (S) for the VP2 cooks. Points represent experimental data. Solid lines represent generated data.

Agreement with respect to the overall magnitudes of the experimental and generated results could be considered quite good. In the case of the A/B ratio data from both sets of cooks (Figures 39 and 40), the DMU1 program (S3/S2 lignin ratio = 1.0) gave A/B ratios which were consistently lower than those of the experimental data, while the DMS1 program (S3/S2 lignin ratio = 1.4) gave A/B ratios which were usually higher than those of the experimental data. These displacements of the model results from the experimental results do not represent an inherent flaw in the models, but simply reflect the choice of S3/S2 lignin ratio. Figures 39 and 40 indicate that the proper choice for the S3/S2 lignin ratio lies somewhere between the values of 1.0 and 1.4 used by the two programs. The CC/B ratio data in Figures 41 and 42 exhibit generated CC/B ratios which were comparable in magnitude to those obtained experimentally.

The generated sulfur content data in Figures 43 and 44 consistently gave lower sulfur contents than those obtained experimentally. These lower sulfur contents may be the result of an underestimation of the maximum attainable sulfur content (S_p = 0.8%). Since the kinetics of sulfonation are second order with respect to S_p and sodium sulfite concentration (5), a low S_p will give lower sulfur contents for a given time. An increase in S_p from 0.8% to 1.0% would probably compensate for much of the observed discrepancy.

Figures 39 to 44 also demonstrate that the agreement between the trends observed in the experimental and generated data was good; although some differences existed. In the case of the VP1 cooks, both the generated and experimental A/B ratio data showed a decline with increased sodium sulfite concentration. Although the analysis of variance results in Table 9a did not find a significant trend in the VP1 data alone, the regression analysis in Figure 24 did find such a trend when all of the cooks were combined. Neither the experimental nor the generated data demonstrated a time effect.

As demonstrated in Figure 40, the influence of sodium sulfite concentration on the generated A/B ratio data in the VP2 cooks is the same as that observed in the VP1 cooks, although the trend was not obvious in the linescan results. Figure 40 also demonstrates no significant time effect for both types of data at high sodium sulfite concentrations, but demonstrates a pronounced effect at the lower sodium sulfite concentration.

The generated CC/B data in Figures 41 and 42 show slight increases with sodium sulfite concentration. These trends are not obvious in the experimental results, probably a result of the weakness of the trends.

The VP1 sulfur content data in Figure 43 demonstrated an increase with increased sodium sulfite concentration in both the experimental and generated data. On the other hand, while time had little effect in the experimental data, it had a substantial effect in the generated results. One explanation is the lower sulfur contents obtained with the model after 20 minutes. At these lower sulfur contents, sulfite depletion was less limiting, allowing sulfur contents to increase at the longer simulated cooking times. This time effect in the generated data may also be attributed to phenomena which reduce the sulfonation rate with time during the cooks, but are not accounted for by the models. One such factor is a reduction in liquor pH during the course of the cook. This has been discussed previously. The experimental and generated sulfur content data from the VP2 cooks yielded comparable trends, as shown in Figure 44.

This diffusion study has demonstrated that diffusion limitations in the cell wall could very easily account for the observed secondary wall sulfur gradients in the sulfonated southern pine latewood chips. The mathematical model for diffusion across the cell wall predicted sulfur distributions which

were very similar to those obtained through STEM-EDS analysis. Based on current knowledge in the areas of diffusion in porous solids and cell wall structure, the cell wall diffusivities used in the modelling were realistic. Considering this study applied a relatively simple model to such an unstable situation as a vapor-phase cook, the agreement between the experimental and generated results was good. A greater understanding of sulfite pulping chemistry would improve the predictability of the diffusion model.

An increased understanding of the effects of pH would be particularly helpful. The effects of liquor pH on cell wall sulfur distribution were not dealt with by the diffusion model. Higher pH levels are likely to increase cell wall diffusivity by swelling the cell wall and otherwise softening its structure. The flatter distributions obtained at higher pH levels could be attributed to increased diffusivity.

While the observed pH effects in the liquid-phase cooks are real, those observed in the vapor-phase cooks may be related to sodium sulfite concentration. Those cooks using higher sodium sulfite concentrations are better buffered against a drop in pH during the cook, so the higher sulfite ion concentrations yield higher final pH levels. The model demonstrates that sodium sulfite concentration can influence the A/B ratio independently, while the corresponding effect on pH may or may not influence sulfonation and cell wall sulfur distribution.

CONCLUSIONS

The work presented in this thesis represents a significant contribution to our understanding of cell wall sulfur distribution in sulfonated wood. This work has provided unique findings concerning the nature of these distributions and how they can be manipulated. A fundamental knowledge of the origins of the observed distributions was also acquired.

The observed bound sulfur distributions across the cell wall were characterized by a nonuniform secondary wall distribution and considerably higher levels in the middle lamella. The secondary wall distribution consisted of relatively high sulfur levels toward the lumen and a decline in sulfur levels across the cell wall to a minimum near the S1 layer. Statistical analysis established the existence of this gradient with a high degree of confidence; although its extent varied from very pronounced to virtually flat, depending on liquor pH and sodium sulfite concentration. The sulfur levels in the cell corner were generally three times greater than those at the minimum in the outer secondary wall, which is in agreement with the findings of Beatson, et al. (19).

The influence of liquor pH and sodium sulfite concentration on the extent of the secondary wall sulfur gradient was established by statistical analysis of the linescan data. The results demonstrated that higher pH levels and sodium sulfite concentrations yielded flatter secondary wall sulfur profiles. These effects can be explained in terms of limited diffusion across the cell wall.

The three most likely sources of the observed distributions are lignin distribution, lignin reactivity differences, and diffusion limitations.

Evaluation of these three phenomena has led to the conclusion that the observed sulfur distributions are most likely the result of lignin distribution and diffusion limitations. Lignin reactivity may also be a factor, but too little is known about it to draw any conclusions. The observed lignin distributions across the secondary wall were generally flat with frequent peaks in the S3 layer. These higher lignin levels in the S3 layer may account for some of the non-uniformity in cell wall sulfonation, but certainly cannot account for the observed S2 sulfur gradients.

The presence of this gradient can be attributed to diffusion limitations. From what is known about cell wall structure and diffusion in porous solids, it appears that the diffusivity of the sodium sulfite in the cell wall is low enough to inhibit diffusion from the lumen into the cell wall, resulting in a gradient in bound sulfur. This was demonstrated by mathematical modelling of sodium sulfite diffusion across the cell wall in vapor-phase cooks.

The observed secondary wall sulfur distributions are quite different from flat distributions obtained by Beatson, et al (19). The difference can be explained in terms of lignin distribution, possible differences in lignin reactivity, and diffusion limitations. One primary difference between Beatson's experiments and those presented here is the manner in which the chips were impregnated. In this study, chips which had been air-dried were impregnated for 7 to 30 minutes and then cooked. Beatson and co-workers soaked their chips in water for 7 days, and then soaked them in liquor for 24 hours before cooking. This treatment may be more effective in swelling the wood than rapid impregnation of air-dried chips. In addition, the long exposure to the liquor could result in some degradation of the wood components and induce added swelling, resulting in the removal of some diffusion barriers.

Another primary difference is the wood source; Beatson used spruce while this study used southern pine juvenile wood. This difference could result in lignin distribution differences, especially with regard to the S3 layer, and possibly, lignin reactivity differences.

RECOMMENDATIONS FOR FUTURE WORK

The work presented in this thesis has pursued an area where there are still many unknowns, such as cell wall diffusivity, and x-ray microanalysis. As would be expected from this type of work, many questions and ideas for future work have arisen.

The sulfur distribution and modelling work have laid a broad foundation on which future studies on sulfonation variables can be based. The evaluation of a wider range of pH levels would contribute a better understanding of the pH effect and its origin. The results from the sulfur distribution work and modelling also suggest that sodium sulfite concentration and temperature effects deserve further study. In order to obtain a more fundamental understanding of these effects, the performance of these studies under more highly buffered conditions is suggested. Once the fundamentals are better understood, they can be applied to the less stable environment of the vapor-phase cook, where this instability is likely to serve a purpose.

In terms of diffusion modelling, there are many unknowns. The most prominent unknown is the cell wall diffusivity. Techniques for direct measurement of cell wall diffusivity need to be tested. In order to study possible diffusion limitations and other aspects of sulfonation further, more information concerning sulfonation kinetics, especially in the early stages of the cook or at room temperature, is needed.

The use of STEM-EDS for this kind of work also presents questions which need to be addressed. Of primary concern is the matter of mass loss. This study has measured mass loss and sulfur loss in the wood sections, but their origin is not well understood. The sulfur loss is most likely from the

lignin, but the percentage of mass loss from the lignin, carbohydrates, or resin is not known.

By understanding mass loss, it may be possible to reduce its occurrence. This study has shown that initial exposure to a moderate electron dose will reduce overall mass loss, but other measures, such as use of a cryostage to cool the sample, should also be tested. As with any work dealing with thin sections, new procedures for embedding and sectioning latewood to improve section quality would be helpful.

ACKNOWLEDGEMENTS

I would like to thank my advisor, Dr. Thomas J. McDonough, for his advice and encouragement throughout the course of this work. I would also like to thank Bill Whitsitt and John Litvay for many helpful discussions.

I thank the Institute of Paper Chemistry and its member companies for supporting this work and for providing funds for living expenses. A number of Institute staff members contributed their talents to this work. Special thanks go to Terry Conners, Mary Block, Ellen Foxgrover, and Hilkka Kaustinen for their assistance with the electron microscopy.

Finally, I would like to thank my family, especially my wife, Mary, and my daughters, Clota and Melanie, for their love and support throughout the course of this work.

SYMBOLS

A	Atomic weight; or maximum sulfur counts near the lumen in a secondary wall sulfur distribution
AOV	Analysis of variance
A_x	UV absorbance of a cell wall layer, x
A/B	Ratio of points A and B in a secondary wall sulfur distribution
b	Electron beam broadening within a sample in an electron microscope. Also used as an exponent.
B	Minimum sulfur counts near the middle lamella in a secondary wall sulfur distribution
BG	Background
C	Lignin concentration
c	Solution molarity
CC	Cell corner; or STEM-EDS cell corner sulfur counts
CC/B	Ratio of cell corner sulfur counts and point B from a cell wall sulfur distribution
CF_i	Generic correction factor for cell wall diffusion
CML	Compound middle lamella
C_1	C_1 lens (#1 condenser lens) in an a TEM or STEM
CMP	Chemimechanical Pulp
CTMP	Chemithermomechanical Pulp
d	Section thickness
D_{eff}	Effective diffusion coefficient (in the cell wall)
d_p	Pore diameter in cell wall
d_w	Diameter of water molecule
D_x	Density of colloidal silver on an area of film imaging cell wall layer, x
E_o	Electron energy in an electron microscope
EDS	Energy Dispersive Spectrometry

F	Faraday constant
I_o	Initial UV light intensity used for UV microscopy
I_x	UV light intensity after passing through wall layer, x
k, k_1, k_{-1}, k_2	Kinetic rate constants
k_B	Boltzmann's constant
KV	Accelerating potential in an electron microscope
K_α, K_β	Transitions from the L and M-shell atomic orbitals to a K-shell. These produce peaks in a STEM-EDS x-ray spectrum.
L, l	Lumen
LP1	Set of high-yield sulfite cooks; defined in Table 3
L_x	Lignin concentration in a wall layer, x
l_+, l_-	Cationic and anionic conductivities
ML	Mass loss or middle lamella
Na_2SO_3	Sodium sulfite
NS	Net sulfur
n_+, n_-	Cationic and anionic valences
R	Gas constant
RMP	Refiner Mechanical Pulp
r_p	Pore radius
r_s	Solute molecule radius
S	Sulfite ion concentration; or net secondary wall sulfur counts
S_L	Sodium sulfite concentration in the lumen
S_o	Initial sodium sulfite concentration
S_p	Maximum possible bound sulfite concentration
S_{wall}	Sodium sulfite concentration in the cell wall
S1	S1 wall layer of secondary wall
S2	S2 wall layer of secondary wall
S3	S3 wall layer of secondary wall

S^*	Total bound sulfonate (sulfite) content of a substrate
SEM	Scanning Electron Microscope (Microscopy)
$SO_3^=$	sulfite ion
STEM	Scanning Transmission Electron Microscope (Microscopy)
t	Thickness
T_g	Glass transition temperature
TEM	Transmission Electron Microscope (Microscopy)
TMP	Thermomechanical Pulp
TS	Total sulfur
UV	Ultraviolet
V_l	Volume of lumen used for diffusion modeling
V_w	Volume of cell wall used for diffusion modeling
V_x	Volume fraction of a wall layer, x
VP1	Set of high-yield sulfite cooks; defined in Table 3
VP2	Set of high-yield sulfite cooks; defined in Table 3
x	Subscript designating a wall layer; S2, S3, S1, CC, CML, L
y	Solute molar activity coefficient
ϵ	Extinction coefficient (l/(g cm)).
γ	Film constant for UV microscopy
λ	Ratio of solute to pore radius (r_s/r_p)
μ	Viscosity
τ	Tortuosity
τ_c	The effect of cellulose protofibrils on tortuosity
τ_d	The effect of obstructed pores or dead ends on tortuosity
τ_m	Tortuosity within the cell wall matrix material

REFERENCES

1. Gellerstedt, G. The reactions of lignin during sulfite pulping. Svensk Papperstidning 79(16):537 (1976).

2. Gierer, J. The chemistry of delignification - a general concept, part 1. Holzforschung 36(1):43 (1982).

3. Gellerstedt, G.; Gierer, J. The reactions of lignin during neutral sulfite pulping. Part V. The reactions of α-(4-hydroxy-3-methoxyphenyl)-glycerol-β-guaiacyl ether with sulfite and their dependence on pH. Acta Chemica Scandinavica B 29(5):3 (1975).

4. Morrison, R. T.; Boyd, R. N. Organic Chemistry, 3rd edition. Boston, Allyn and Bacon, Inc., 1973.

5. Beatson, R. P.; Heitner, C.; Atack, D. Sulphonation of eastern black spruce chips, part 2. Journal of Wood Chemistry and Technology 4(4): 439 (1984).

6. Atack, D.; Heitner, C. Dynamic mechanical properties of sulphonated eastern black spruce. Pulp and Paper Magazine of Canada 80(12):TR99 (1979).

7. Heitner, C.; Beatson, R. P.; Atack, D. Factors affecting sulphonation eastern black spruce wood chips. in Proceedings of the International Symposium on Wood and Pulping Chemistry, Stockholm, June 9-12, 1981. Vol. 2:145.

8. Gardner, P. E.; Tyminski, A. The SCMP chemimechanical pulping process, part II: Chip sulfonation studies. in Canadian Wood Chemistry Symposium, Niagara Falls, September 13-15, 1982, p. 85.

9. Axelson, P.; Simonson, R. Thermomechanical pulping with low addition of sulfite. Svensk Papperstidning 86(3):R17 (1983).

10. Vikstrom, B.; Nelson, P. Mechanical properties of chemically treated wood and chemimechanical pulps. Tappi 63(3):87 (1980).

11. Axelson, P.; Simonson, R. Thermomechanical pulping with low addition of sulfite: influence of the preheating temperature at mild sulfite treatment of spruce chips prior to defibration. Paperi Ja Puu 64(11):729 (1982).

12. Vikstrom, B.; Hammar, L. -A. Softening of spruce wood during sulphite pulping and its relevance for the character of high-yield pulps. in Proceedings of the International Symposium on Wood and Pulping Chemistry, Stockholm, June 9-12, 1981, Vol. 5:112.

13. Iwamida, T.; Sumi, Y.; Nakano, J. Mechanisms of softening and refining in high-yield sulfite pulping processes. Cellulose Chemistry and Technology 14:253 (1980).

14. Atack, D.; Heitner, C.; Karnis, A. Ultra-high yield pulping of eastern black spruce, part 2. Svensk Papperstidning 83(5):133 (1980).

15. Mutton, D. B.; Tombler, G.; Gardner, P. E.; Ford, M. J. Sulfonated chemimechanical pulping process. Pulp and Paper Magazine of Canada 83(6):120 (1982).

16. Dines, R. E.; Tyminski, A. The vapour-phase SCMP process. Journal of Pulp and Paper Science 10(1):J17 (1984).

17. Gancet, C.; Heitner, C.; Beatson, R. P.; Gray, D. G. Analysis of a sulfonated wood cross-section by Auger electron spectroscopy. Tappi 63(10):139 (1980)

18. Kolar, J. J.; Lindgren, B. O.; Treiber, E. The distribution of lignin between fiber wall and middle lamella. Svensk Papperstidning 85(3):R21 (1982).

19. Beatson, R. P.; Gancet, C.; Heitner, C. The topochemistry of black spruce sulfonation. Tappi Journal 63(3):82 (1984).

20. Saka, S.; Whiting, P.; Fukazawa, K.; Goring, D. A. I. Comparative studies of lignin distribution by UV microscopy and bromination combined with EDXA. Wood Science and Technology 16(4):269 (1982).

21. Whiting, P.; Goring, D. A. I. Relative reactivities of middle lamella and secondary wall lignin of black spruce. Holzforschung 36:303 (1982).

22. Hardell, H-L; Leary, G. J.; Stoll, M.; Westermark, U. Variations in lignin structure in defined morphological parts of spruce. Svensk Papperstidning 83(2):44 (1980).

23. Whiting, P.; Goring, D. A. I. Phenolic hydroxyl analysis of lignin by pyrolytic gas chromatography. Paperi ja Puu 64(10):592 (1982).

24. Williams, D. B. Practical Analytical Electron Microscopy in Materials Science. Mahwah, NJ, Phillips Electronic Instruments, Inc., 1984.

25. Goldstein, J. I.; Costley, J. L.; Lorimer, G. W.; Reed, S. J. B. Quantitative x-ray analysis in the electron microscope. in Scanning Electron Microscopy/1977, Vol I.

26. Hren, J. J.; Goldstein, J. I.; Joy, D. C. Introduction to Analytical Electron Microscopy. New York, Plenum Press, 1979.

27. Jeol, Inc. Personal Communication.

28. Hall, T. A.; Gupta, B. L. Beam-induced mass loss of organic mass under electron-microprobe conditions. Journal of Microscopy 100(2):177 (1974).

29. Cosslett, V. E. Radiation damage in the high resolution electron microscopy of biological materials: a review. Journal of Microscopy 113(2):113 (1978).

30. Mary, M.; Revol, J. -F.; Goring, D. A. I. Mass loss of wood and its components during transmission electron microscopy. Journal of Applied Polymer Science 31:957 (1986).

31. Sarkanen, K. V.; Ludwig, C. H. Lignins: Occurrence, Formation, Structure, and Reactions. New York, Wiley-Interscience, 1971.

32. Scott, J. A. N.; Procter, A. R.; Fergus, B. J.; Goring, D. A. I. The application of ultraviolet microscopy to the distribution of lignin in wood: description and validity of the technique. Wood Science and Technology 3:73 (1969).

33. Plouff, M. T. analysis of brominated loblolly pine by STEM-EDS. A-190 Independent Study report, Appleton, WI, The Institute of Paper Chemistry. March 23, 1987.

34. French, R. J. The examination of lignin distribution in loblolly pine tracheids via SEM-EDS. A-291 Project Report, Appleton, WI, The Institute of Paper Chemistry, 1984.

35. Parham, R. A.; Cote, W. A. Distribution of lignin in normal and compression wood of Pinus taeda L. Wood Science and Technology 5:49 (1971).

36. Colaruotolo, J. F.; Eddy, R. S. Determination of Chlorine, Bromine, Phosphorus, and Sulfur in organic molecules by ion chromatography. Analytical Chemistry 49(6):884 (1977).

37. TAPPI Standard No. 699.

38. Spurr, A. R. A low-viscosity epoxy resin embedding medium for electron microscopy. Journal of Ultrastructure Research 26:31 (1969).

39. Erickson, R. W. Computer Programming of X-ray Linescan Data for Application in the Pulp and Paper Industry. A291 Research Project. Appleton, WI, The Institute of Paper Chemistry, 1985.

40. Engstrand, P.; Hammar, L. -A.; Htun, M. The kinetics of sulphonation reactions on Norwegian spruce. in Proceedings of the International Symposium on Wood and Pulping Chemistry, Vancouver, Canada, 1985, p. 275.

41. Wenneras, S. On sulfonation of undissolved lignin in sprucewood and birchwood. Trondheim, Norway, Technical University of Norway.

42. Stamm, A. J. Bound-water diffusion into wood in the fiber direction. Forest Products Journal 9(1):27 (1959).

43. Yata, S.; Mukudai, J.; Kajita, H. Morphological studies on the movement of substances into the cell wall of wood. II. Diffusion of copper compounds into the cell wall. Mokuzai Gakkaishi 25(3):171 (1979).

44. Yata, S.; Mukudai, J.; Kajita, H. Morphological studies on the movement of substances into the cell wall of wood. III. Diffusion of zinc compounds into the cell wall. Mokuzai Gakkaishi 27(11):761 (1981).

45. Egerton, R. F. Measurement of radiation damage by electron energy-loss spectroscopy. Journal of Microscopy 118(4):389 (1980).

46. Sachs, I. B.; Clark, I. T.; Pew, J. C. Investigation of lignin distribution in the cell wall of certain woods. Journal of Polymer Science: Part C 2:203 (1963).

47. Scott, J. A. N.; Goring, D. A. I. Lignin concentration in the S3 layer of softwoods. Cellulose Chemistry and Technology 4:83 (1970).

48. Saka, S.; Thomas, R. J.; Gratzl, J. S. Lignin distribution in Douglas-fir and loblolly pine as determined by energy dispersive x-ray analysis. in Proceedings of the International Symposium on Wood and Pulping Chemistry, Stockholm, June 9-12, 1981, p. 35.

49. Saka, S.; Thomas, R. J. A study of lignification in loblolly pine tracheids by the SEM-EDXA technique. Wood Science and Technology 16:167 (1982).

50. Yang, J.-M.; Yean, W. Q.; Goring, D. A. I. The phenolic hydroxyl content of the lignin residual in spruce wood cooked by sulphite and kraft. Cellulose Chemistry and Technology 15:337 (1981).

51. Berry, R; Bolker, H. I. The topochemical effect in acid-sulphite delignification: a theoretical analysis. in Canadian Wood Chemistry Symposium, Niagara Falls, September 13-15, 1982, p. 137.

52. Westermark, U. The occurrence of p-hydroxyphenylpropane units in the middle-lamella lignin of spruce (Picea abies). Wood Science and Technology 19:223 (1985).

53. Terashima, N. Cell wall formation in tree xylem. Journal of the Japanese Wood Research Society. 33(8):615 (1987).

54. Terashima, N.; Seguchi, Y. Factors affecting the formation of condensed structures in lignin. in Proceedings of the Fourth International Symposium on Wood and Pulping Chemistry, Paris, April 27-30, 1987, Vol.II:1.

55. Beatson, R. P. The topochemistry of aspen sulphonation. Holzforschung 40(Suppl.):11 (1986).

56. Cussler, E. L. Diffusion: Mass Transfer in Fluid Systems. Cambridge, Cambridge University Press, 1984.

57. Rice, J. R. Numerical Methods, Software, and Analysis, IMSL Reference Edition. New York, McGraw-Hill, 1983.

58. Boutelje, J.; Eriksson, I. Analysis of lignin in fragments from thermomechanical spruce pulp by ultraviolet microscopy. Holzforschung 38:249 (1984).

59. CRC Handbook of Chemistry and Physics, 65th edition. Boca Raton, Fla., Chemical Rubber Company Press, 1984.

60. Reid, R. C.; Prausnitz, J. M.; Sherwood, T. K. The Properties of Gases and Liquids, 3rd edition. New York, McGraw-Hill, 1977.

61. Burazin, M. A. A Dynamic Model of Kraft-anthraquinone Pulping. Ph.D. Thesis, Appleton, Wis., The Institute of Paper Chemistry, 1986.

62. Robinson, R. A.; Stokes, R. H. Electrolyte Solutions, 2nd edition. London, Butterworths Scientific Publications, 1959.

63. Kerr, A. J.; Goring, D. A. I. Ultrastructural arrangement of the wood cell wall. Cellulose Chemistry and Technology 9(6):563 (1975).

64. Favis, B. D.; Goring, D. A. I. A model for the leaching of lignin macromolecules from pulp fibres. Journal of Pulp and Paper Science 10(5):J139 (1984).

65. Stamm, A. J. Passage of Liquids, Vapors, and Dissolved Materials Through Softwoods. U.S.D.A. Technical Bulletin No. 929, 1946.

66. Clifford, J. Properties of water in capillaries and thin films. in Water: A Comprehensive Treatise, Vol. 5 (F Franks, ed.), 1975.

67. Franks, F. Water. London, The Royal Society of Chemistry, 1984.

68. Stone, J. E.; Scallan, A. M. A structural model for the cell wall of water swollen wood pulp fibers based on their accessibility to macromolecules. Cellulose Chemistry and Technology 2(3):343 (1968).

69. Ternan, M. The diffusion of liquids in pores. The Canadian Journal of Chemical Engineering 65(2):244 (1987).

70. Deen, W. M. Hindered transport of large molecules in liquid-filled pores. AIChE Journal 33(9):1409 (1987).

71. Wang, H.; Shalak, R. Viscous flow in a cylindrical tube containing a line of spherical particles. Journal of Fluid Mechanics 38(1):75 (1969).

72. Takigami, S.; Nakamura, Y. Permeability of solutes through cellophanes grafted with vinyl monomers, II. Diffusion of potassium chloride through cellophanes grafted with acrylic acid. Journal of Applied Polymer Science 24(6):1429 (1979).

73. Ueda, T.; Kamo, N.; Ishida, N.; Kobatake, Y. Effective fixed charge density governing membrane phenomena. IV. Further study of activity coefficients and mobilities of small ions in charged membranes. The Journal of Physical Chemistry 76(17):2447 (1972).

74. Schultz, R. D.; Asunmaa, S. K. Ordered water and ultrastructure of cellular plasma membrane. in Progress in Surface and Membrane Science, Vol. 3 (J.F. Danielli, A.C. Riddiford, M.D. Rosenberg, eds.). New York, Academic Press, 1970.

75. Israelachvili, J. N. Measurement of viscosity in very thin films. Journal of Colloid and Interface Science 110(1):263 (1986).

76. Satterfield, C. N.; Colton, C. K.; Pitcher, W. H. Restricted diffusion in liquids within fine pores. AIChE Journal 19(3):628 (1973).

77. Hayduk, W.; Minhas, B. S. Correlations for prediction of molecular diffusivities in liquids. Canadian Journal of Chemical Engineering 60:295 (1982).

78. Stamm, A. J. Wood and Cellulose Science. New York, The Ronald Press Company, 1964.

APPENDIX 1: DATA TRANSFER PROGRAM (DTP)

```
1,5 %% DATA TRANSFER PROGRAM (DTP)

2,5 %% READ AND DISPLAY DATA
2,10 >WT 4

5,1 M 15000;>+DV 0
5,5 A KQ(4351),IG:KQ,JR(7):KQ(1),NP:KQ(9),IX:KQ(10),LY:KQ(11),IN:KQ(12),
IM:KQ(13),AM(40):KQ(14),AB(50):KQ(35),AE(2,7):KQ(61),KR(7):KQ(73),
KP(4096):KQ(148),AK(8192):KP
5,7 A NS:KQ:(1172),JS(49):KQ(1173),MT:KQ(1223),ID,IF,M(@36-1):@@34,LC(24),
Y,N,Q,QA,LS
5,10 L>AA(11) 0 10 1;>CD>(11);*0;$LI 0,17,10,42,38;$CC('4000');$CC('7200',
7,2,7,7,0,0,0);$CC('7209',255,0);$CC('7218',0,0,255,255);>OP 1
5,15 S ID=!"DISKETTE NO.="?;S IF=-1;S IF=!"FILE NO.="?;D 7,5
5,25 I IF>,[;P !"INVALID FILE NO.";G 5,15
5,30 I $UM(4,IF)>,[;P !!"FILE DOES NOT EXIST!"?;D 7,5
5,35 $UM(4,IF,1,1,KQ,1280);$YA(@36,KP,M,M);$CC('5300');S MT=KQ(1223);
*11;G 10

7,5 *0;S AC ==IR=NR=SR=ER=RR=TR= R=DR=IR=SR=KR=ER=TR=TR=ER= R=&R= R=pR=
RR=ER=SR=SR= R=RR=UR=NR0;$VC(24,28,C512*10+18,AC);>WT 0;*11

10,10 S LS=1024/IG-1;S LC=1;S LC(NS)=NP+1;I NS<=1 [;D 10,15;F I=1,NS-1;
I SL=0 S LC(I)=JS(I*2)-IX)/IN+2;I SL=0 [;S PB=JS(I*2+1)+JS(I*2)/SL;S PX=
(PB-SI)/(SL+1/SL);S LC(I)=(PX-IX)IN+2
10,12 G 15
10,15 S SL=(JS(NS*2+1)-JS(1)))/(JS(NS*2)-JS);S SI=JS(1)-SL*JS

15,5 $VC(21);$VC(22);$VC(23);I NS=1 [;$CC('5421',IG*(NS-1),0);F I=0,IG-1;
F J=1,NS-1;$CC(1023,I*LS+LC(J)-1)
15,10 $CC('5622',IG);F I=0,IG-1;$CC(I*LS+NP+16,(AE(0,I)),(AE(1,I)))
15,15 $VC(23,20,C8197,AB)
15,20 >WT 0

19,1 %%; OPTION TO ALTER SECTION BOUNDARY MARKERS

20,5 S Y=1;S N=0;S QA=!!"CHANGE MARKERS (Y/N) "?;I QA=1 [;G 40
20,10 S L=!"MARKER NO.="?;I L<=NS-1 [;P !"INVALID MARKER NUMBER";D 20,10
20,15 P <F2>!"MARKER "L," IS AT PIXEL "LC(L),;S LC(L)=!"NEW POSITION FOR
MARKER IS"?
20,20 D 5,10;$YA(@36,KP,M,M);$CC('5300');*11;D 15
20,25 S Q=!"CHANGE ANOTHER MARKER? (Y/N)"?;I Q=1 GO 20,10

40,1 %%;PUSH RUN TO TRANSFER DATA

41,5 >WT 0;>+DV 1;P <F4>!"DISKETTE:  "ID;P <F4>!"FILE NO.:  "IF;
$IO(!0,AB);$IC(!0,AM(10));P <F6,3>!"SECONDS/PIXEL= "MT/100;D 45,15
41,10 P <F3>!!"            *   COUNTS FOR"IG," ELEMENT(S)"!
"CHANNEL     * ";F I=0,IG-1;$IO("    "0,AE(,I))
41,15 F I=0,NS-1;D 45,15;P <F3>!"SECTION"I+1,"  *";F J=LC(I),LC(I+1)-1;
P<F3>!"   "J,"      * ";F K=0,IG-1;P <F6>KQ(147+J+K*LS)
41,20 D 45L,15
```

```
45,5 P !!"          NUMBER OF *  SECTION AVERAGES"!"SECTION   CHANNELS
* ";F I=0,IG-1;$IO("    "0,AE(,I))
45,10 D 45,15;F I=1,NS;P <F4>!I,"       "LC(I)-LC(I-1),"     * ";F J=0,
IG-1;D 46;P <F6>SA/(LC(I)-LC(I-1))+.5
45,15 P <H18>!42,42,42,42
45,20 G 50

46,5 S SA=0;F K=LC(I-1),LC(I)-1;S SA SA+KQ(147+K+J*LS)

50,1 >+DV 0
50,5 S Y=1;S N=0;S Q=!"TRANSFER MORE DATA? (Y/N)"?;I Q=1 G 5,10;E

100,1 V NS,!NP,!JS(NS*2+1),!JS(1),!JS(0),!JS(SN*2),!PB,!PX,!SL,!SI
100,2 F I=0,19;V !JS(I)
100,3 F I=1,8;V !LC(I)

240,5 >OP 0;$LIB 40;>OP 1;$SA(14,DTP14,_)
```

APPENDIX 2: RESULTS FROM UV MICROSCOPY/DENSITOMETRY

UV photographs of the cell walls evaluated and the resulting density distributions are shown on the following pages. Comparison of the non-treated and treated sample results, at first glance, indicates a more pronounced gradient across the secondary walls for the treated samples. Since the two samples were photographed at different exposures, the apparent differences in distributions may simply reflect differences in contrast obtained at the two exposures (32). Such differences in contrast are apparent when comparing the cell corner peaks in figures A1 and A2 with that in figure A4. The samples are described in Table 6.

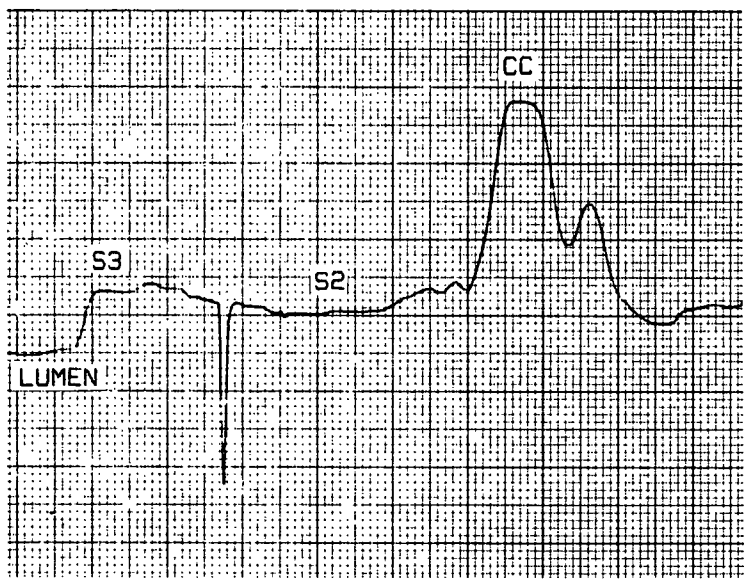

Figure A1. Sample 1.

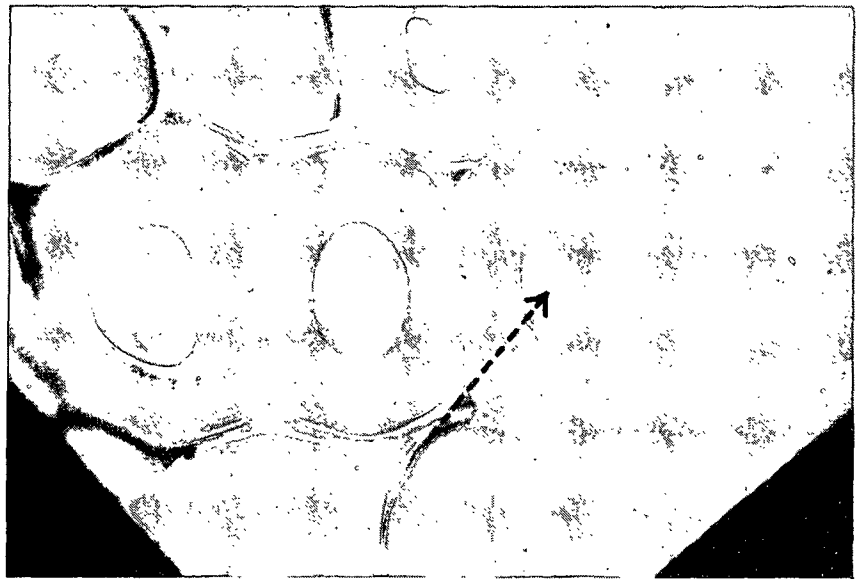

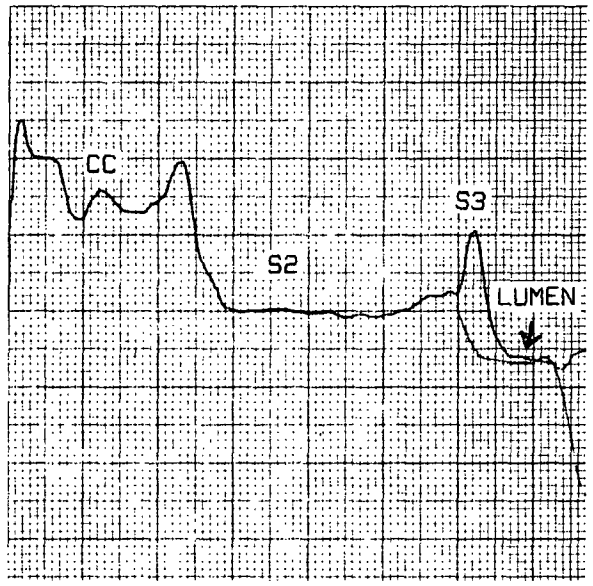

Figure A2. Sample 1. The two peaks surrounding the cell corner (CC) are artifacts.

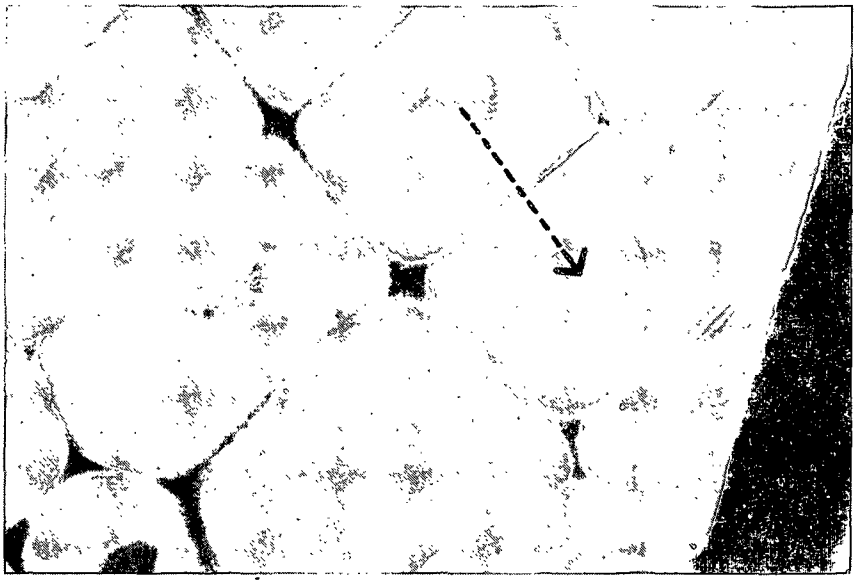

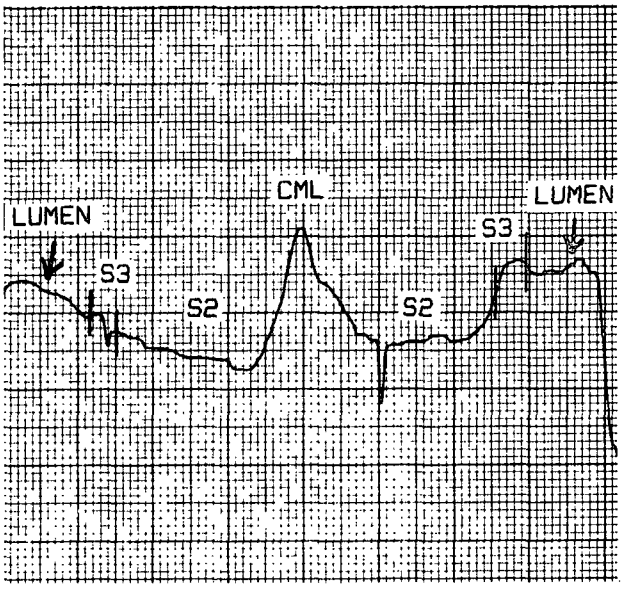

Figure A4. Sample 3-EM.

APPENDIX 3: UV MICROSPECTROPHOTOMETER LIGNIN DISTRIBUTION DATA (Figures A5 - A9)

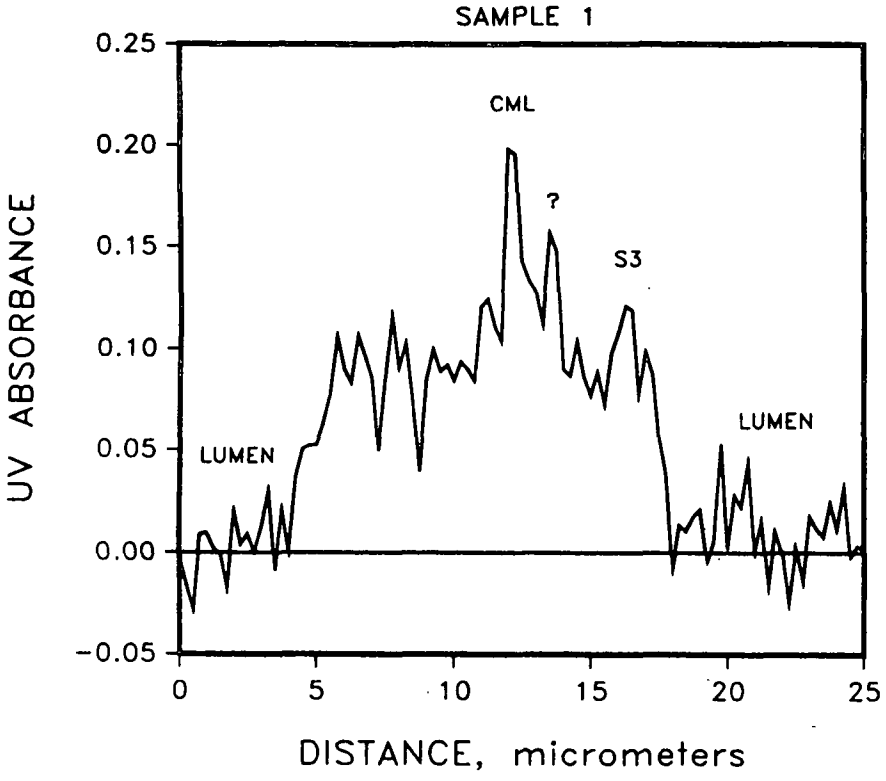

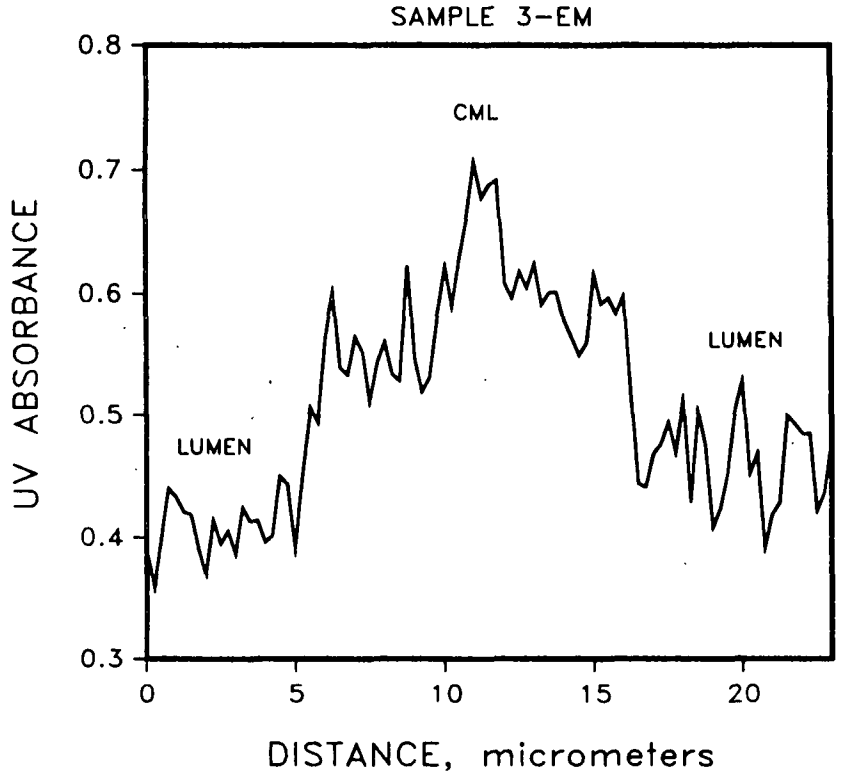

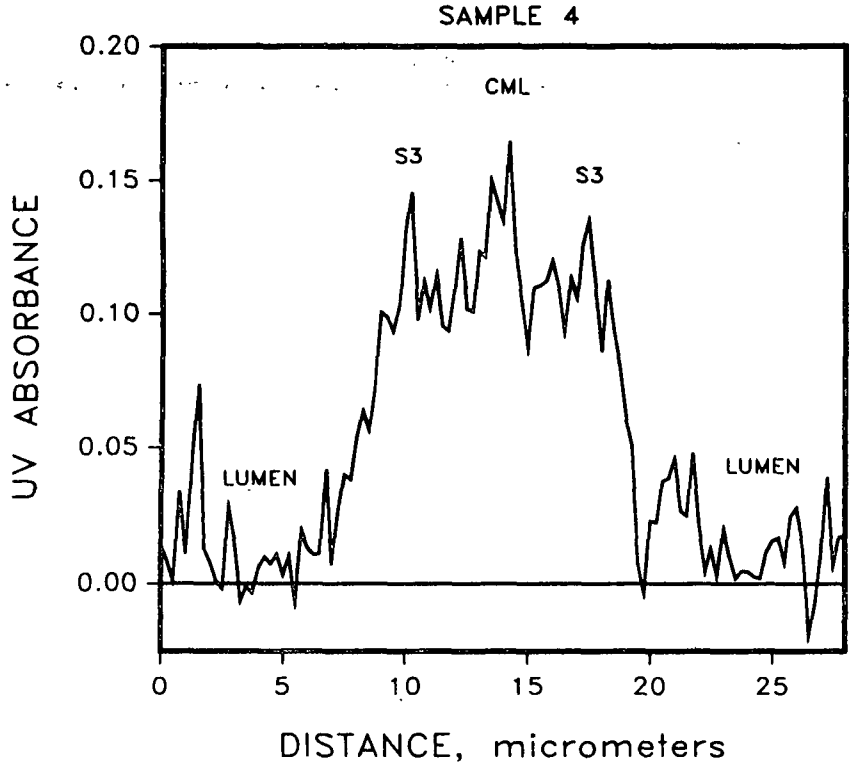
SAMPLE 4
0.20
0.15
0.10
0.05
0.00
UV ABSORBANCE
CML
S3
S3
LUMEN
LUMEN
0
5
10
15
20
25
DISTANCE, micrometers

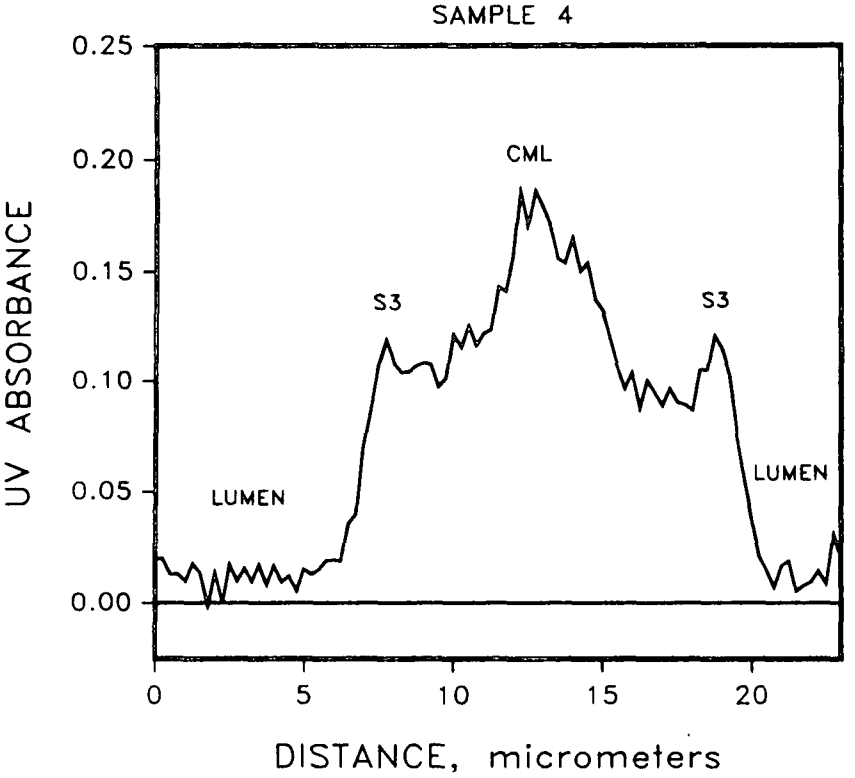
SAMPLE 4
0.25
0.20
0.15
0.10
0.05
0.00
UV ABSORBANCE
CML
S3
S3
LUMEN
LUMEN
0
5
10
15
20
DISTANCE, micrometers

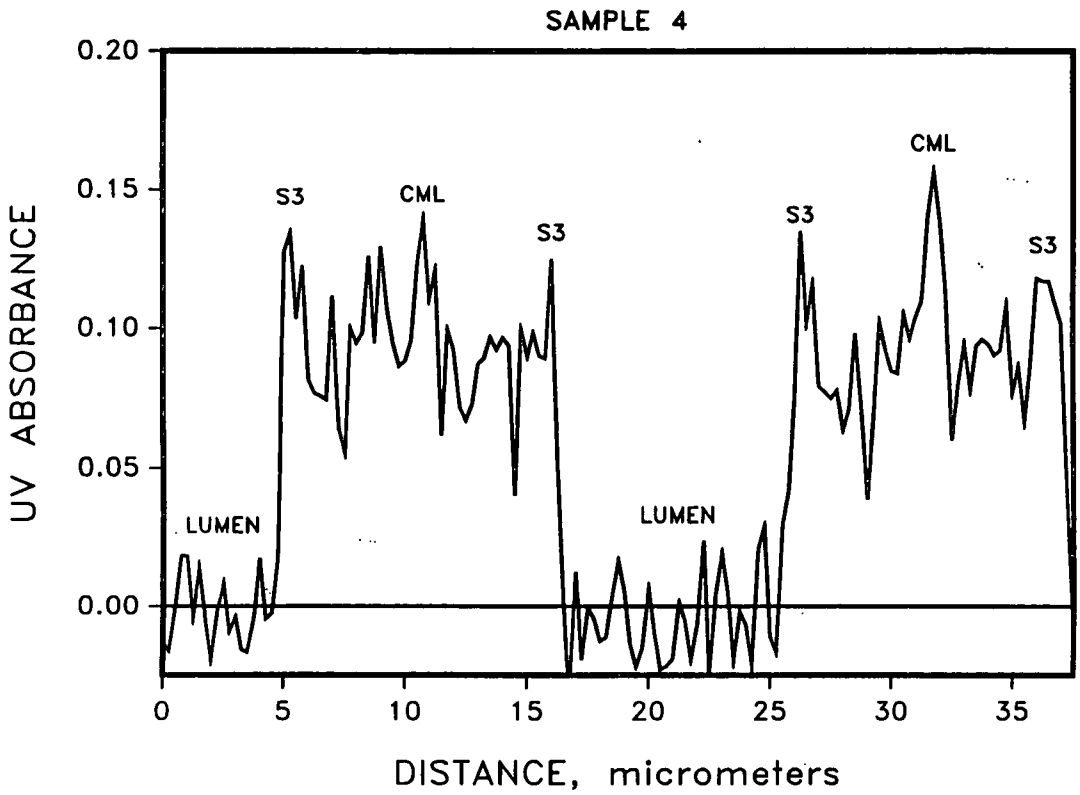
SAMPLE 4
0.20
0.15
0.10
0.05
0.00
UV ABSORBANCE
LUMEN
S3
CML
S3
LUMEN
S3
CML
S3
0
5
10
15
20
25
30
35
DISTANCE, micrometers

APPENDIX 4: DMU1 AND DMS1 PROGRAMS

DMU1

```
$RESET FREE
C     MODEL FOR DIFFUSION WITH REACTION ACROSS THE CELL WALL DURING A
C     VAPOR-PHASE SCMP COOK.  DIFFERENCES IN LIGNIN CONTENT AND
C     REACTIVITY BETWEEN THE S2 AND ML ARE ACCOUNTED FOR.  S3 LAYER HAS
C     SAME LIG CONTENT AS S2.  ML WIDTH CAN BE UP TO 20% OF WALL.
C     SECONDARY WALL ASSUMED TO HAVE 1.5 TIMES AS MANY PHENOLIC
C     HYDROXYLS AS THE MIDDLE LAMELLA.  ANY TEMPERATURE ABOVE 80 DEGREES
C     CENTIGRADE CAN BE EVALUATED.
C
FILE  5(KIND=REMOTE)
FILE  6(KIND=REMOTE)
FILE  7(KIND=DISK,TITLE='MODELDAT',FILETYPE=8)
FILE  11(KIND=DISK,TITLE='U1/4B5E0',PROTECTION=SAVE,NEWFILE=TRUE,
     1FILETYPE=0)
$INCLUDE "*IMSL/DPDES"
$INCLUDE "*IMSL/DGRCS"
$INCLUDE "*IMSL/DGRIN"
$INCLUDE "*IMSL/DPDET"
$INCLUDE "*IMSL/DPDEU"
$INCLUDE "*IMSL/DPDEV"
$INCLUDE "*IMSL/DPDEW"
$INCLUDE "*IMSL/DPDEX"
$INCLUDE "*IMSL/LEQT1B"
$INCLUDE "*IMSL/UERTST"
$INCLUDE "*IMSL/UGETIO"
$INCLUDE "*IMSL/USPKD"
$INCLUDE "*IMSL/VMULBF"
C
C
C SUBROUTINE SUPPLYING THE PARTIAL DIFFERENTIAL EQUATIONS AND THE VALUES
C FOR THE RATE CONSTANT (K) AND SP.
C
      SUBROUTINE FCN(NPDES,X,T,U,UX,UXX,UT)
      INTEGER    NPDES
      REAL       X,T,U(2),UX(2),UXX(2),UT(2),W
      COMMON /KINET/ SRK,RK
      COMMON /LUMEN/ SL,RN,SP,DC,SMX
      W=10000*X
      IF(W.GE.SMX) GO TO 30
   20 RK=SRK
      SP=0.000685
      GO TO 40
   30 RK=0.67*SRK
      SP=0.00274
   40 CONTINUE
      UT(1) =    RK*SL*U(2)*(SP-U(1))
      UT(2) =    DC*UXX(2)-UT(1)/SL
      RETURN
      END
```

```
C
C
C SUBROUTINE SUPPLYING THE BOUNDARY CONDITIONS.
C
      SUBROUTINE BNDRY(NPDES,X,T,ALP,BET,GAMP)
      INTEGER NPDES
      REAL X,T,ALP(2),BET(2),GAMP(2)
      COMMON /KINET/ SRK,RK
      COMMON /LUMEN/ SL,RN,SP,DC,SMX
      IF (X.GT..0005) GO TO 30
      ALP(1) = 1.0
      BET(1) = 0.0
      GAMP(1) = RK*SL*EXP(-1*RK*SL*T+ALOG(SP))
      ALP(2) = 1.0
      BET(2) = 0.0
      GAMP (2) = 0.0
      RETURN
   30 ALP(1) = 0.0
      BET(1) = 1.0
      GAMP(1) = 0.0
      ALP(2) = 0.0
      BET(2) = 1.0
      GAMP(2) = 0.0
      RETURN
      END
C
C
C MAIN PROGRAM.
C
      COMMON /KINET/ SRK,RK
      COMMON /LUMEN/ SL,RN,SP,DC,SMX
      DIMENSION Y(2,2,40),WK(7000),X(40),S(40)
      EXTERNAL FCN,BNDRY
      INTEGER     IER,K,INDEX,I,J,NIN,NOUT,NPDES,NX,IY,SM,L
      REAL        H,TEND,TOL,T,WK,X,Y,RI,RN,TRA1,TRA2,TRB1,TRB2,TRC1,
     *         TRC2,WC1,WC2,SL,SO,U,UX,S,RK,SP,DC,WL,SMX,HL,TC,MT,
     *         TK,SRK,BS
C
C INPUT DATA.
C
      DO 5 I=1,1
    5 READ(7,100) DC,WL,SMX,SO,MT,TK
  100 FORMAT(E8.1,F6.2,F5.1,E11.3,I5,I6)
      WRITE(11,850) DC,WL,SMX,SO,MT,TK
  850 FORMAT("DC = ",E9.2,/"WL = ",F6.2,/"SMX = ",F5.1,/"SO = ",E11.3,
     */"MT = ",I5,/"TEMP (TK) = ",I6)
      NX = 31
      SL=SO
      NPDES = 2
      SM = 21 + (SMX-8)*5
      IY = 2
      RN = NX-1
      SRK = EXP(-3.348-7280*(1/TK-0.00283))
C
```

```
C SET INITIAL CONDITIONS.
C
      DO 10 I=1,6
      RI = I-1
      X(I) = RI*.00001
   10 CONTINUE
      DO 11 I=7,21
      RI = I-1
      X(I) = (RI-5)*.00005 + .00005
   11 CONTINUE
      DO 12 I=22,31
      RI = I-1
      X(I) = (RI-20)*.00002 + .0008
   12 CONTINUE
      DO 13 I=1,31
      Y(1,1,I) = 0.0
      Y(1,2,I) = 0.0
      Y(2,1,I) = 1.0
      Y(2,2,I) = 0.0
   13 CONTINUE
      H = .01
      TOL = .001
      T = 0.000
      INDEX = 1
      WRITE(11,1000)
 1000 FORMAT (50H T (SEC)  X (CM)  S/SL     SL          S          SB/)
      DO 15 M=1,NX
   15 WRITE(11,1100)T,X(M),Y(2,1,M),SO,SO,Y(1,1,M)
 1100 FORMAT (F7.2,E9.2,F7.3,3E11.4)
      WRITE(11,1200)
 1200 FORMAT (/)
C
C BEGINNING OF CALCULATIONS AT SELECTED TIME INTERVALS.
C
      TC = 18 + (MT-20)/2.5
      DO 60 J=1,TC
      IF(J .GT. 10) GO TO 20
      TEND = J*30.000
      GO TO 24
   20 IF(J .GT. 18) GO TO 21
      TEND = 120*(J-8)
      GO TO 24
   21 TEND = 150*(J-10)
   24 CALL DPDES(NPDES,FCN,BNDRY,T,H,TEND,X,Y,IY,NX,TOL,INDEX,WK,IER)
      TRA1=0
      TRA2=0
      TRB1=0
      TRB2=0
      TRC1=0
      TRC2=0
C
C CALCULATION OF S AND S* INTEGRALS ACROSS THE WALL USING A TAYLOR SERIES.
C
      DO 25 M=2,5
      TRA1=TRA1+2*Y(1,1,M)
```

```
   25 TRA2=TRA2+2*Y(2,1,M)
      WCA1=(.00005/(2*5))*(Y(1,1,1)+TRA1+Y(1,1,6)
      WCA2=(.00005/(2*5))*(Y(2,1,1)+TRA2+Y(2,1,6)
C
      DO 30 M=7,20
      TRB1=TRB1+2*Y(1,1,M)
   30 TRB2=TRB2+2*Y(2,1,M)
      WCB1=(.00075/(2*15))*(Y(1,1,6)+TRB1+Y(1,1,21))
      WCB2=(.00075/(2*15))*(Y(2,1,6)+TRB2+Y(2,1,21))
C
      DO 35 M=22,30
      TRC1=TRC1+2*Y(1,1,M)
   35 TRC2=TRC2+2*Y(2,1,M)
      WCC1=(.0002/(2*10))*(Y(1,1,21)+TRC1+Y(1,1,31))
      WCC2=(.0002/(2*10))*(Y(2,1,21)+TRC2+Y(2,1,31))
C
      WC1 = WCA1 + WCB1 + WCC1
      WC2 = WCA2 = WCB2 + WCC2
      BS = WC1*1000
C
C CALCULATION OF SL.
C
      SL=((1.0+0.282*WL)*SO-282*WL*WC1)/(1.0+282*WL*WC2)
      L = J/2
      HL = (FLOAT(J)/2)
   40 DO 50 M=1,NX
      S(M) = Y(2,1,M)*SL
   50 WRITE (11,1300)T,X(M),Y(2,1,M),SL,S(M),Y(1,1,M)
 1300 FORMAT (F7.2,E9.2,F7.3,3E11.4)
      WRITE (11,1400) BS,IER
 1400 FORMAT (" BS = ",F10.7,/" IER = ",I3)
      WRITE (11,1200)
   60 CONTINUE
      STOP
      END
```

DMS1

```
$RESET FREE
C     MODEL FOR DIFFUSION WITH REACTION ACROSS THE CELL WALL DURING A
C     VAPOR-PHASE SCMP COOK.  DIFFERENCES IN LIGNIN CONTENT AND
C     REACTIVITY BETWEEN THE S3, S2 AND ML ARE ACCOUNTED FOR.
C     S3 WIDTH FIXED AT 0.5 MICRONS.  ML WIDTH CAN BE UP TO 20% OF WALL.
C     SECONDARY WALL ASSUMED TO HAVE 1.5 TIMES AS MANY PHENOLIC
C     HYDROXYLS AS THE MIDDLE LAMELLA.  ANY TEMPERATURE ABOVE 80 DEGREES
C     CENTIGRADE CAN BE EVALUATED.
C
FILE  5(KIND=REMOTE)
FILE  6(KIND=REMOTE)
FILE  7(KIND=DISK,TITLE='MODELDAT',FILETYPE=8)
FILE  11(KIND=DISK,TITLE='S1/B1E9',PROTECTION=SAVE,NEWFILE=TRUE,
     1FILETYPE=0)
$INCLUDE "*IMSL/DPDES"
$INCLUDE "*IMSL/DGRCS"
$INCLUDE "*IMSL/DGRIN"
$INCLUDE "*IMSL/DPDET"
$INCLUDE "*IMSL/DPDEU"
$INCLUDE "*IMSL/DPDEV"
$INCLUDE "*IMSL/DPDEW"
$INCLUDE "*IMSL/DPDEX"
$INCLUDE "*IMSL/LEQT1B"
$INCLUDE "*IMSL/UERTST"
$INCLUDE "*IMSL/UGETIO"
$INCLUDE "*IMSL/USPKD"
$INCLUDE "*IMSL/VMULBF"
C
C
C SUBROUTINE SUPPLYING THE PARTIAL DIFFERENTIAL EQUATIONS AND THE VALUES
C FOR THE RATE CONSTANT (K) AND SP.
C
      SUBROUTINE FCN(NPDES,X,T,U,UX,UXX,UT)
      INTEGER    NPDES
      REAL       X,T,U(2),UX(2),UXX(2),UT(2),W
      COMMON /KINET/ SRK,RK
      COMMON /LUMEN/ SL,RN,SP,DC,SMX
      W=10000*X
      IF(W.GT.0.5 .AND. W.LT.SMX) GO TO 20
      IF(W.GE.SMX) GO TO 30
   10 RK=SRK
      SP=0.000959
      GO TO 40
   20 RK=SRK
      SP=0.000685
      GO TO 40
   30 RK=0.67*SRK
      SP=0.00274
   40 CONTINUE
      UT(1) =    RK*SL*U(2)*(SP-U(1))
      UT(2) =    DC*UXX(2)-UT(1)/SL
      RETURN
      END
```

```
C
C
C SUBROUTINE SUPPLYING THE BOUNDARY CONDITIONS.
C
      SUBROUTINE BNDRY(NPDES,X,T,ALP,BET,GAMP)
      INTEGER NPDES
      REAL X,T,ALP(2),BET(2),GAMP(2)
      COMMON /KINET/ SRK,RK
      COMMON /LUMEN/ SL,RN,SP,DC,SMX
      IF (X.GT..0005) GO TO 30
      ALP(1) = 1.0
      BET(1) = 0.0
      GAMP(1) = RK*SL*EXP(-1*RK*SL*T+ALOG(SP))
      ALP(2) = 1.0
      BET(2) = 0.0
      GAMP (2) = 0.0
      RETURN
   30 ALP(1) = 0.0
      BET(1) = 1.0
      GAMP(1) = 0.0
      ALP(2) = 0.0
      BET(2) = 1.0
      GAMP(2) = 0.0
      RETURN
      END
C
C
C MAIN PROGRAM.
C
      COMMON /KINET/ SRK,RK
      COMMON /LUMEN/ SL,RN,SP,DC,SMX
      DIMENSION Y(2,2,40),WK(7000),X(40),S(40)
      EXTERNAL FCN,BNDRY
      INTEGER     IER,K,INDEX,I,J,NIN,NOUT,NPDES,NX,IY,SM,L
      REAL        H,TEND,TOL,T,WK,X,Y,RI,RN,TRA1,TRA2,TRB1,TRB2,TRC1,
     *            TRC2,WC1,WC2,SL,SO,U,UX,S,RK,SP,DC,WL,SMX,HL,TC,MT,
     *            TK,SRK,BS
C
C INPUT DATA.
C
      DO 5 I=1,1
    5 READ(7,100) DC,WL,SMX,SO,MT,TK
  100 FORMAT(E8.1,F6.2,F5.1,E11.3,I5,I6)
      WRITE(11,850) DC,WL,SMX,SO,MT,TK
  850 FORMAT("DC = ",E9.2,/"WL = ",F6.2,/"SMX = ",F5.1,/"SO = ",E11.3,
     */"MT = ",I5,/"TEMP (TK) = ",I6)
      NX = 31
      SL=SO
      NPDES = 2
      SM = 21 + (SMX-8)*5
      IY = 2
      RN = NX-1
      SRK = EXP(-3.348-7280*(1/TK-0.00283))
C
```

```
C SET INITIAL CONDITIONS.
C
      DO 10 I=1,6
      RI = I-1
      X(I) = RI*.00001
   10 CONTINUE
      DO 11 I=7,21
      RI = I-1
      X(I) = (RI-5)*.00005 + .00005
   11 CONTINUE
      DO 12 I=22,31
      RI = I-1
      X(I) = (RI-20)*.00002 + .0008
   12 CONTINUE
      DO 13 I=1,31
      Y(1,1,I) = 0.0
      Y(1,2,I) = 0.0
      Y(2,1,I) = 1.0
      Y(2,2,I) = 0.0
   13 CONTINUE
      H = .01
      TOL = .001
      T = 0.000
      INDEX = 1
      WRITE(11,1000)
 1000 FORMAT (50H T (SEC)  X (CM)  S/SL     SL          S          SB/)
      DO 15 M=1,NX
   15 WRITE(11,1100)T,X(M),Y(2,1,M),SO,SO,Y(1,1,M)
 1100 FORMAT (F7.2,E9.2,F7.3,3E11.4)
      WRITE(11,1200)
 1200 FORMAT (/)
C
C BEGINNING OF CALCULATIONS AT SELECTED TIME INTERVALS.
C
      TC = 18 + (MT-20)/2.5
      DO 60 J=1,TC
      IF(J .GT. 10) GO TO 20
      TEND = J*30.000
      GO TO 24
   20 IF(J .GT. 18) GO TO 21
      TEND = 120*(J-8)
      GO TO 24
   21 TEND = 150*(J-10)
   24 CALL DPDES(NPDES,FCN,BNDRY,T,H,TEND,X,Y,IY,NX,TOL,INDEX,WK,IER)
      TRA1=0
      TRA2=0
      TRB1=0
      TRB2=0
      TRC1=0
      TRC2=0
C
C CALCULATION OF S AND S* INTEGRALS ACROSS THE WALL USING A TAYLOR SERIES.
C
      DO 25 M=2,5
      TRA1=TRA1+2*Y(1,1,M)
```

```
   25 TRA2=TRA2+2*Y(2,1,M)
      WCA1=(.00005/(2*5))*(Y(1,1,1)+TRA1+Y(1,1,6)
      WCA2=(.00005/(2*5))*(Y(2,1,1)+TRA2+Y(2,1,6)
C
      DO 30 M=7,20
      TRB1=TRB1+2*Y(1,1,M)
   30 TRB2=TRB2+2*Y(2,1,M)
      WCB1=(.00075/(2*15))*(Y(1,1,6)+TRB1+Y(1,1,21))
      WCB2=(.00075/(2*15))*(Y(2,1,6)+TRB2+Y(2,1,21))
C
      DO 35 M=22,30
      TRC1=TRC1+2*Y(1,1,M)
   35 TRC2=TRC2+2*Y(2,1,M)
      WCC1=(.0002/(2*10))*(Y(1,1,21)+TRC1+Y(1,1,31))
      WCC2=(.0002/(2*10))*(Y(2,1,21)+TRC2+Y(2,1,31))
C
      WC1 = WCA1 + WCB1 + WCC1
      WC2 = WCA2 = WCB2 + WCC2
      BS = WC1*1000
C
C CALCULATION OF SL.
C
      SL=((1.0+0.282*WL)*SO-282*WL*WC1)/(1.0+282*WL*WC2)
      L = J/2
      HL = (FLOAT(J)/2)
   40 DO 50 M=1,NX
      S(M) = Y(2,1,M)*SL
   50 WRITE (11,1300)T,X(M),Y(2,1,M),SL,S(M),Y(1,1,M)
 1300 FORMAT (F7.2,E9.2,F7.3,3E11.4)
      WRITE (11,1400) BS,IER
 1400 FORMAT (" BS = ",F10.7,/" IER = ",I3)
      WRITE (11,1200)
   60 CONTINUE
      STOP
      END
```

APPENDIX 5: CALCULATION OF SULFITE ION RADIUS

The radii of diffusing species (r) are generally calculated using the Stokes-Einstein equation,

$$D_B = \frac{k_B T}{6\pi\mu r}$$

However, this relationship does not hold when the solute radius is less than five times that of the solvent (56). In this case, some authors have suggested replacing 6π with 4π or 2 (56). An alternative is to use a relationship which accounts for the solvent molecular radius. Such a relationship is that proposed by Hayduk and Minhas (77).

$$D_B = 6.916 \times 10^{-10} \left[\frac{(T)^{1.7}\ (R_B)^{0.2}}{(\mu)^{0.8}\ (R_A)^{0.4}}\right]$$

R_B = radius of gyration of the solvent, water = 1.41 Å

R_A = radius of gyration of the sulfite ion

Solving for R_A at 25°C yields a radius of 3.90 Å. Based on molecular geometry, the radius of a sulfite ion would be expected to be in the range of 2 to 2.5 Å. The difference can be attributed hydration of the sulfite ion, which dictates the effective radius of the sulfite in diffusion processes (62). It is worth noting that the result obtained from the Hayduk and Minhas equation is comparable to that obtained from the Stokes-Einstein equation when 6π is replaced with 3.6π.

APPENDIX 6: CALCULATION OF C_P USING A RESISTORS-IN-SERIES ANALOGY

C_P is obtained by applying the effects of steric hinderances (C_S), hydrodynamic forces (C_H), and the monomolecular layer of water (C_M) to each size range of pore-size distribution data. The pore-size distribution data to be used will be an expanded version of Stone and Scallan's data, shown below. Here the 5 to 7.5 Å range is divided into two components: that with a pore radius below 6.7 Å, and that with a pore radius above 6.7 Å. This cut-off point (6.7 Å) is the sum of the radius of a hydrated sulfite ion (3.9 Å) and the diameter of a water molecule in the monolayer (2.8 Å). Any pore with a radius below 6.7 Å cannot effectively transport the sulfite ion due to size limitations.

Table A1. Expanded version of Stone and Scallan's data (68) with and without corrections for the water monolayer.

Original data					Corrected data				
r	V	XS	L	S	r	V	XS	L	H
3.5	.14	.038	3.638	-	-	-	-	-	-
5.95	.062	.111	.557	-	-	-	-	-	-
7.11	.028	.159	.176	.203	4.29	.010	.058	.176	434.8
8.75	.08	.241	.333	.303	5.93	.037	.110	.333	19.2
11.25	.08	.398	.201	.423	8.43	.045	.223	.201	5.0
TOTAL	.39		4.905			.092		.710	

r = average pore radius for the size range in question.
V = the incremental pore volume fraction; the total V for the original data is the cell wall porosity; the total V for the corrected data is the effective porosity for diffusion.
XS = pore cross-sectional area.
L = pore length (V/XS) in 10^{12} cm.
S = steric correction factor for the individual pore-size range, $(1 - \lambda)^2$.
H = hydrodynamic correction factor for the individual pore-size range.

The data in the above table is divided into sections: the original, and corrected data. The original data includes steric correction factors based on the original pore radius. The corrected data is that which is obtained after the diameter of a water molecule (from the monolayer) is subtracted from each pore radius. The correction for hydrodynamic effects (H) will be applied through the corrected data, while the steric correction will be applied through the original data. It is assumed that the sulfite ions can penetrate the monolayer between bound water molecules, but cannot move along the length of the pore within the monolayer.

Diffusion through pores of various sizes in the cell wall can be viewed as several resistors in series, with each resistor representing a range of pore radii. The total resistance (R) is given by

$$R = R_1 + R_2 + R_3$$
$$R = rL/A = L/(cA)$$

where r is the resistivity, L is the length, A is the average cross-sectional area, and c is the conductivity (= 1/r). Since diffusivity can also be expressed as a conductivity,

$$R = L/(D_{eff}A_c)$$
$$R_i = L_i/[(1/H_i)(A_i)(S_i)(D)(C_M)]$$

where i represents a pore-size range and L_i, H_i, and A_i can be obtained from the right-hand side of Table A1 for each pore-size range. S_i can be obtained from the left-hand side of Table A1 for each pore-size range. L is the total pore length for the corrected data and A_c is the average pore cross-sectional area for the corrected data.

$$A_C = V/L = .092/.71 = .130 \qquad \text{(corrected data)}$$

From the definition of R above,

$$\frac{L}{D_{eff}\ A_C} = \left(\frac{1}{D'}\right)\left[\sum_{i=1}^{n} \frac{L_i}{(1/H_i)(A_i)(S_i)}\right] \quad \text{where } D' = D_{eff}/C_P$$

$$D_{eff} = (L)(1/A_C)(D') \Big/ \left[\sum_{i=1}^{n} \frac{L_i}{(1/H_i)(A_i)(S_i)}\right]$$

$$D_{eff} = (.710)(1/.130)[1/(6499+192+11)](D')$$

$$D_{eff} = .000815\ D'$$

$$C_P = .000815$$

APPENDIX 7: EXPERIMENTAL AND GENERATED DATA USED FOR FIGURES 39 TO 44

Time, min.	Temp., °C	Na_2SO_3 conc., mole/l[c]	Experimental results			DMU1			DMS1		
			A/B	CC/B	S	A/B	CC/B	S	A/B	CC/B	S
20[a]	134	0.48	1.65	2.97	0.41	1.22	2.83	0.27	1.71	2.83	0.28
20[a]	134	1.03	1.49	2.89	0.53	1.15	2.99	0.42	1.61	2.99	0.43
20[a]	134	1.59	1.45	2.92	0.70	1.11	3.14	0.53	1.55	3.14	0.54
40[a]	134	0.48	1.59	3.18	0.40	1.23	2.90	0.35	1.72	2.90	0.36
40[a]	134	1.03	1.68	2.84	0.59	1.14	3.16	0.54	1.60	3.16	0.55
40[a]	134	1.59	1.42	3.08	0.71	1.09	3.39	0.65	1.53	3.39	0.66
5[b]	160	0.26	1.66	3.21	0.30	1.46	2.71	0.19	2.04	2.71	0.19
5[b]	160	0.55	1.62	3.15	0.46	1.26	2.88	0.36	1.76	2.88	0.37
20[b]	140	0.26	1.66	3.12	0.32	1.31	2.76	0.19	1.83	2.76	0.19
20[b]	140	0.55	1.63	2.54	0.48	1.20	2.93	0.38	1.68	2.93	0.39

[a] VP1 cooks
[b] VP2 cooks
[c] Effective Na_2SO_3 concentration